The Complex Dendroclimatology of Pinus aristata

THE COMPLEX DENDROCLIMATOLOGY OF *PINUS ARISTATA*

by

William Lazar Tintor

———————————————

A Dissertation Submitted to the Faculty of the

SCHOOL OF GEOGRAPHY, DEVELOPMENT & ENVIRONMENT

In Partial Fulfillment of the Requirements

For the Degree of
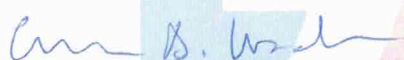
DOCTOR OF PHILOSOPHY

In the Graduate College
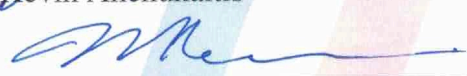
THE UNIVERSITY OF ARIZONA

2021

THE UNIVERSITY OF ARIZONA
GRADUATE COLLEGE

As members of the Dissertation Committee, we certify that we have read the dissertation prepared by William Lazar Tintor, titled: *The Complex Dendroclimatology of Pinus aristata*

and recommend that it be accepted as fulfilling the dissertation requirement for the Degree of Doctor of Philosophy.

_____   Date: 11/19/21
Connie A. Woodhouse

_____   Date: 11/19/21
Kevin Anchukaitis

_____   Date: 11/19/21
Michael Crimmins

_____   Date: 11/19/21
Gregg Garfin

Final approval and acceptance of this dissertation is contingent upon the candidate's submission of the final copies of the dissertation to the Graduate College.

I hereby certify that I have read this dissertation prepared under my direction and recommend that it be accepted as fulfilling the dissertation requirement.

_____   Date: 11/19/21
Connie A. Woodhouse
Dissertation Committee Chair
School of Geography, Development and Environment

ACKNOWLEDGEMENTS

I would like to thank my advisor Connie Woodhouse, who encouraged my application to the University of Arizona and first suggested I investigate Rocky Mountain bristlecone pine. I genuinely appreciate her unwavering commitment to my research, tireless help during fieldwork, and ability to pare down my loquacious writing to more cogent thoughts. Over the past four years she taught through example, helping me develop as a scientist and as a critical thinker. I am also grateful to the members of my dissertation committee, Kevin Anchukaitis, Michael Crimmins, and Gregg Garfin, who were always willing to generously offer their time and help.

This dissertation would not have been possible without all of the help I had scouting, collecting, and lugging down hundreds of bristlecone pine samples from the high peaks of Colorado and New Mexico. To those who willingly followed me up deer paths and old cowboy trails, I want to thank you: Mark Losleben, Soumaya Belmecheri, Matt Meko, Jonathan King, Tom de Mil, Trevor Birt, Flavio Lehner, Angeline Pendergrass, Andy Wood, and Sean Fleming. In particular, Kyler McNeely deserves recognition for his work preparing and measuring nearly all of the bristlecone samples used in my work. His patience to look through a microscope for hours on end is the reason my research exists today.

Beyond my research, I want to thank my colleagues in the Laboratory of Tree-Ring Research whose conversations and support helped me throughout this process: Amy Hudson, Jessie Pearl, Talia Anderson, Julie Edwards, Dave Meko, David Frank, and Bethany Coulthard. Additionally, I would like to thank those at the LTRR who helped track down old bristlecone collections and taught me the fundamentals of field work: Rex Adams, Chris Baisan, Peter Brewer, and Matt Salzer. Finally, I want to thank John Fleck and Paul Tashjian who encouraged me to seek a PhD when I worked in Albuquerque and who continued to provide support when I moved back to New Mexico.

I want to also thank the support of my family. Thank you to my Mom who taught me to always value education and who has consistently supported my academic work, even after the math became too new. Thanks to my Dad who provided an example of perseverance and taught me to always take pride in my handiwork. And last but not least, I want to thank Lindsay, without whom none of this would have been possible. Her unwavering encouragement and support helped me throughout this process and for that I will be forever grateful.

DEDICATION

To my dad, Mike Tintor, who taught me to value the past,
and to my grandpa, Bill Reedy, who taught me to value the land.

TABLE OF CONTENTS

APPENDIX B: IN PREP - UTILIZING THE VAGANOV-SHASHKIN MODEL TO SIMULATE CLIMATE SENSITIVITY IN ROCKY MOUNTAIN BRISTLECONE PINE (*PINUS ARISTATA* ENGELM.)

APPENDIX C: IN PREP - THE INFLUENCE OF RECENT AND RECONSTRUCTED SPRING HYDROCLIMATE CONDITIONS ON THE RIO GRANDE HEADWATERS

LIST OF TABLES

LIST OF FIGURES

ABSTRACT

In the southwestern United States persistent aridity has led to the development of a system of institutions to manage and distribute limited water resources. The management of such systems was based on an imperfect understanding of potential variability in the region's climate. With anthropogenic warming already altering the Southwest's climate, understanding the past potential for extreme drought and the role temperature played during drought will provide a baseline for water managers to anticipate risks to this system. Tree-ring reconstructions of climate provide a useful metric for assessing past shifts in precipitation, streamflow, and temperature. Despite an abundance of multimillennial hydroclimate reconstructions for the Southwest, few contemporaneous, skillful tree-ring reconstructions of temperature are similarly available. In an attempt to address this gap, I evaluate the complex climate sensitivity of Rocky Mountain bristlecone pine (*Pinus aristata* Engelm.), a long-lived, climatically sensitive proxy with the potential to be utilized in temperature and hydroclimate reconstructions.

The first study of the dissertation begins with an extensive evaluation of climate sensitivity across ten new and previously sampled collection sites. I identified a robust spring hydroclimate response throughout the lower elevation collections and a weaker but still significant late summer temperature response intermixed with hydroclimate sensitivity in the upper elevation collections. In the second study, I utilized the Vaganov-Shashkin proxy system model to simulate tree-ring growth in *P. aristata*, identifying temperature thresholds controlling climate sensitivity. My results provided further confirmation of the late-spring/early-summer

hydroclimate response in low elevation *P. aristata*. The upper elevation *P. aristata* were found to respond to temperature variability under cooler pre-anthropogenic warming conditions. This provides a direction for future research to investigate past temperature sensitivity at sites that no longer contain a clear temperature response or to aid in the identification of locations where cooler growing season conditions may still produce a temperature sensitivity in *P. aristata* growth.

For the final study, I used the results from the climate sensitivity analysis and proxy system modeling to develop the first April-June drought index reconstruction for the Southern Rockies. I utilized this reconstruction to evaluate the multi-century relationship between winter snowpack and spring drought conditions in the Rio Grande headwaters. Initial analysis of the observed relationship between winter snowpack and spring hydroclimate conditions indicated the potential, albeit rare, for extreme spring conditions to ameliorate or exacerbate winter moisture conditions and alter streamflows. I found no consistent multi-year relationship between the new spring drought index reconstruction and an existing snowpack reconstruction, but did identify periods of simultaneous fluctuations that coincided with extreme drought and pluvial events, and provided evidence that during major drought events dry spring conditions may have exacerbated the severity of winter moisture deficits. Overall, the findings in this body of research confirm that *P. aristata* is a climatically sensitive species, capable of providing sufficient growth response to construct a hydroclimate reconstruction. Additionally, the identification of a late summer temperature response using both climate sensitivity analysis and proxy system modeling

provides a solid foundation to pursue the development of a skillful, multi-millennial

reconstruction of temperature using *P. aristata*.

CHAPTER 1: INTRODUCTION

1.1 STATEMENT OF PROBLEM

The aridity that defines the climate of the southwestern United States (hereafter Southwest) is also a perpetual risk to the region. The ever-present threat of water scarcity led to the development of a complex network of inter-state agreements, international treaties, physical infrastructure, and political institutions that distribute the limited water supply and provide a buffer during scarcity (Stegner, 1992). Unfortunately, it was a system built with a limited understanding (or, in part, a willful ignorance) of the potential for extreme multi-decadal drought (Kuhn and Fleck, 2019; Reisner, 1993) and under the assumption of hydrologic stationarity that anthropogenic climate change is likely to alter (Milly et al., 2008). Without a baseline understanding of past droughts, the managers of this complex water network are using an incomplete framework to anticipate not only the risk of extreme drought, but the risk of extreme drought with the added impact of climate change.

Fortunately, the science of dendrochronology provides a way to reconstruct past climate variability. During the period when the Southwest's water management system was under development, scientists began to recognize many of the region's tree species responded to fluctuations in hydroclimatic variability with corresponding variations in ring widths (Douglass, 1920, 1919; Schulman, 1938). Employing the analysis of tree-ring widths led to the development of multi-century precipitation (e.g., D'Arrigo and Jacoby, 1991; Knight et al., 2010; Stahle et al., 2009), soil moisture (e.g., Cook et al., 2004, 1999), and streamflow reconstructions (e.g., Meko

et al., 2007; Stockton and Jacoby, 1976; Woodhouse et al., 2006) for the Southwest. These

reconstructions provided context for the instrumental records, identifying past drought conditions

much more severe than those seen since European settlement (Cook et al., 2010; Douglass, 1929;

Woodhouse et al., 2010; Woodhouse and Overpeck, 1998). In recent years there has been an

increasing recognition of the role higher temperatures play in exacerbating drought severity and

reducing the volume of snowpack-derived streamflow (Lehner et al., 2017; Udall and Overpeck,

2017; Williams et al., 2020; Woodhouse et al., 2016). With earth system models projecting a

2.7°C increase in regional temperatures by 2100 (Gonzalez et al., 2018), it is even more crucial

to understand the role temperature played during past megadroughts. Despite the plethora of tree-

ring derived hydroclimatic reconstructions (Ljungqvist et al., 2020; Stahle et al., 2020), the

Southwest has a limited number of temperature sensitive tree-ring chronologies of similar length

or coverage (PAGES2k Consortium, 2017; Wilson et al., 2016).

To address the knowledge gap of how temperature interacts with the Southwest's hydroclimate,

this study examines the complex climate sensitivity of Rocky Mountain bristlecone pine (*Pinus

aristata* Englem.) and the potential for climate reconstruction using this long-lived species.

Found among the highest mountains in Arizona, Colorado, and New Mexico (Schoettle and

Coop, 2017), *P. aristata* has long been considered a candidate species for climate reconstruction

(Schulman, 1956). However, limited published research and an intermixture of temperature and

precipitation signals contained in the tree-ring measurements (LaMarche Jr and Stockton, 1974)

have limited its utilization. New methodologies developed for Great Basin bristlecone pine

(*Pinus longaeva* D.K. Bailey), a sister taxa of *P. aristata*, have led to breakthroughs in

disentangling climatic responses (Bruening et al., 2017; Bunn et al., 2018; Tran et al., 2017), promising higher quality multi-millennia temperature reconstructions. This study applies the lessons learned from *P. longaeva* to unravel the complex climate sensitivity in *P. aristata*. First, an extensive evaluation of new and existing *P. aristata* tree-ring collections identified regional and site-specific climate sensitivities found in the ring-width measurements. Next, proxy system modeling of *P. aristata* growth mechanistically assessed the type and seasonality of climate responses. Finally, leveraging the conclusions of the first two studies, a reconstruction of the strongest climate signal contained within the ring widths of *P. aristata* was developed and utilized to evaluate the relationship between winter snowpack and spring hydroclimate in the headwaters of the Rio Grande.

The findings of this study provide a solid foundation to pursue the development of a multimillennial summer temperature reconstruction using *P. aristata*. The presence of a late summer temperature response previously identified by LaMarche Jr. and Stockton (1974) was confirmed at upper elevation sites in Colorado and New Mexico, while proxy system modeling demonstrated that *P. aristata* climate sensitivity is determined by a threshold value of growing season mean temperature similar to *P. longaeva* (Bunn et al., 2018; Tran et al., 2017). The present intermixture of temperature and moisture response in *P. aristata* growth is likely caused by an increase in growing season mean temperature that has approached the threshold determining climate response. Sensitivity testing using the proxy system model, run under cooler, pre-industrial conditions, simulated a robust temperature response at high elevation, even under extreme drought scenarios. This suggests that the upper elevation *P. aristata* may have

been more reliably temperature limited prior to the 20th century increase in temperature. These

findings may allow the evaluation of past temperature sensitivity at *P. aristata* sites that

currently contain a weak or mixed temperature signal and aid future efforts to develop new

temperature reconstructions using *P. aristata*. If successfully produced, these temperature

reconstructions could improve our understanding of the role temperature played in the

Southwest's hydroclimate variability and give a broader context for the increasing temperatures

in the region (Lukas and Payton, 2020).

1.2   BACKGROUND

1.2.1   Climate of the Southern Rockies

The primary habitat for P. aristata is the Southern Rocky Mountains (or Southern Rockies)

(Bailey, 1970), a region of central and southern Colorado and northern New Mexico. Two

factors exert spatial control on precipitation in the Southern Rockies, the topography of the

mountain ranges and interaction of subtropical and mid-latitude circulation regimes throughout

the year (Sheppard et al., 2002). The steep topography of the Southern Rockies produces extreme

orographic effects, resulting in annual precipitation rates above 1500 mm on the high, windward

side of mountains, that drop to below 200 mm in valleys located leeward of nearby mountains

(Daly et al., 1994). Located between 35°N and 40°N, the Southern Rockies are on the boundary

between mid-latitude circulation to the north and the descending limb of the Hadley cell to the

south. In the winter, the majority of precipitation is derived from mid-latitude cyclones moving

east across the region, with orographic lift resulting in high precipitation totals and deep

snowpacks throughout the upper elevations of the Southern Rockies, with the highest totals on

the western slopes of range (Lukas et al., 2014). This snowpack is the primary source of water for riparian systems, contributing to more than 70% of total streamflow for the Southern Rockies (Li et al., 2017).

By the onset of the warm season (e.g., May), the upper-level westerly flow has moved north, and the sinking limb of the Hadley Cell circulation suppresses convective processes over the region leading to the development of high pressure ridge, low cloud cover, and increasing solar insolation (Adams and Comrie, 1997). By July, the heated air induces convection that counters the subtropical circulation, producing a thermal low over northern Mexico that draws moisture northward from the Gulf of California and westward from the Gulf of Mexico, producing the North American Monsoon (NAM, Adams and Comrie, 1997). The NAM exhibits much more temporal and spatial variability than the winter synoptic storms, but the generally southerly winds of the NAM consistently result in higher precipitation totals on the south facing slopes of the Southern Rockies (Sheppard et al., 2002).

Daytime temperatures in the Southern Rockies are largely driven by solar insolation and lapse rate, with low elevation, south-facing slopes having the highest mean maximum temperatures and high elevation, north-facing slopes having the lowest mean maximum temperatures (Daly et al., 1994). At night, cold-air inversions may develop in closed basins resulting in cooler temperatures relative to the surrounding ranges (Reeves and Stensrud, 2009). Known as cold air pooling, this effect occurs during periods of atmospheric stability and low humidity (Lundquist and Cayan, 2007). These conditions allow shallow surface air layers to cool quickly, become

denser, and then descend downslope, collecting in topographic depressions in a manner similar to water runoff. In the Southern Rockies, this effect can occur at a regional scale producing significant temperature inversions in the intermontane valleys and at a local scale, influencing vegetation growth by inhibiting the survival of trees in topographic depressions subject to frequent cold air pooling (Coop and Givnish, 2007).

1.2.2   Paleoclimate Reconstructions in the Southwest United States

In the early 20th century, Andrew Ellicott Douglass founded the science of dendrochronology at the University of Arizona. Initially developed as a system to study sunspot cycles and date archaeological sites in the Southwest, Douglass recognized that the annual variability in tree-ring widths could also reconstruct hydroclimatic fluctuations in the region (Douglass, 1920, 1919, 1914). Douglass's student Edmund Schulman continued this investigation, developing tree-ring variability indices that corresponded to climate fluctuations throughout the Southwest (Schulman, 1956, 1942, 1938). Following the development of new statistical techniques allowing the production of climate reconstructions (Fritts, 1976; Fritts et al., 1971) the first streamflow reconstruction in the Southwest was completed for the Colorado River (Stockton and Jacoby, 1976). Further advancements in chronology construction, signal identification in tree rings, and reconstruction methods (Cook and Kairiukstis, 2013; Meko, 1997) led to the prolific development of hydroclimate reconstructions throughout the Southwest, including multi-century reconstructions of precipitation (D'Arrigo and Jacoby, 1991; Knight et al., 2010; Stahle et al., 2009), soil moisture (e.g., Cook et al., 2004, 1999), and streamflow (Meko et al., 2007; Woodhouse et al., 2006; Woodhouse et al., 2012).

The large collection of hydroclimate reconstructions in the Southwest has contributed to the

recognition of 'megadroughts' with durations and magnitudes not seen in droughts observed in

the modern instrumental period (Woodhouse and Overpeck, 1998). The late 13th century "Great

Drought" was the first multi-decadal drought identified using tree-rings and was discovered

during the archaeological research on the Colorado Plateau (Douglass, 1929). Further studies

identified a late 16th century drought that was the most severe event in a 1000 year tree-ring

record from New Mexico (D'Arrigo and Jacoby, 1991; Stahle et al., 2000), a mid-12th century

drought, coinciding with lowest reconstructed streamflow volumes for the Colorado River (Meko

et al., 2007; Woodhouse et al., 2010), and a 2nd century drought that was unsurpassed in

intensity and duration in a 2000 year tree-ring record from southwestern Colorado (Routson et

al., 2011). Evidence suggests the occurrence of North American megadroughts is the result of

internal climate variability of the atmosphere-ocean system (Coats et al., 2015), although

persistent periods of recurring megadrought, such as the Medieval Climate Anomaly (800-1300

CE), may result from external forcing mechanisms, such as changes in solar insolation, or from

internal variability not well sampled in the current instrumental record (Ault et al., 2018).

With anthropogenic climate change already increasing temperatures in the Southwest (Vose et

al., 2017), higher temperatures have been identified as reducing effective streamflow derived

from snowpack (Lehner et al., 2017; Udall and Overpeck, 2017; Woodhouse et al., 2016).

Evidence also suggests that the severity of the early twenty-first century drought is the result of a

moderate drought pushed into extreme conditions by anthropogenic warming (Williams et al.,

2020). Climate modeling suggests that even if precipitation totals were to remain fixed, increased warming will drive a significant increase in the risk of megadrought in the Southwest (Ault et al., 2016). Despite the likely importance of temperature in past hydroclimate variability, recent compilations of tree-ring chronologies highlight the relative paucity in the spatial and temporal coverage of temperature sensitive tree-rings relative to that of hydroclimate sensitive tree-rings. In the Southwest, 11 of the 12 temperature sensitive tree-ring chronologies with at least 1000 years of record are located either in California or Nevada (PAGES2k Consortium, 2017). In contrast the states of Colorado, New Mexico, and Utah have 23 hydroclimate sensitive tree-ring chronologies over 1000 years in length but not a single temperature sensitive tree-ring chronology covering a comparable time span (PAGES2k Consortium, 2017; Stahle et al., 2020).

Temperature sensitivity in Southwest tree-ring widths was first analyzed in the 1970s with the application of empirical orthogonal functions (EOF) to isolate temperature responses (Blasing and Fritts, 1976) and the use of frequency analysis to isolate multi-year temperature sensitivity from the annual hydroclimate variability (LaMarche, 1974). The first regional temperature reconstruction with tree-ring widths was an extension of earlier EOF analysis producing an annual (December to November) reconstruction of temperature (Fritts and Lough, 1985). Temperature reconstructions soon shifted towards the use of maximum latewood density rather than ring-width due to a stronger temperature response. Extensive sampling for maximum latewood density was done throughout western North America in the 1980s (Schweingruber, 1988) which resulted in a set of western North America temperature reconstructions (Briffa et al., 1992; Schweingruber et al., 1991). Several localized temperature reconstructions using tree-

ring widths were still constructed after the introduction of maximum latewood density

methodologies. These included a summer temperature reconstruction using foxtail pine (*Pinus*

balfouriana Balf.) in the Sierra Nevada (Graumlich, 1993), a mean-maximum annual

temperature reconstruction using *P. aristata* in the southern Colorado Plateau (Salzer and

Kipfmueller, 2005), and a summer temperature reconstruction using the *P. longaeva* in the Great

Basin (Salzer et al., 2014a). The Great Basin and southern Colorado Plateau reconstructions were

notable for their multi-millennia time span, but recent efforts to develop summer temperature

reconstructions for the Northern Hemisphere have not incorporated either set of chronologies due

to their relatively weak temperature sensitivity (Büntgen et al., 2020; Wilson et al., 2016).

The relatively weak climate sensitivities of the bristlecone chronologies may be explained by the

intermixture of temperature and hydroclimate growth signals at upper-elevation bristlecone sites.

Evidence suggests that the inter-mixture of climate sensitivities in *P. longaeva* are the result of

topographically induced microclimates (topoclimate) resulting in highly localized and variable

growing season conditions (Bunn et al., 2011). Additional research suggests that *P. longaeva* are

temperature sensitive only within a narrow elevational band below upper tree line, and the recent

increases in temperature may have moved *P. longaeva* on south facing slopes out of this band

and into hydroclimate sensitivity (Salzer et al., 2014b). Efforts to counteract these complicating

factors and determine temperature thresholds controlling climate sensitivity have included the

use of cluster analyses on *P. longaeva* ring-width growth signals and fine-scale topoclimate

modeling (Bruening et al., 2017; Tran et al., 2017). This work led to the simulation of *P.*

longaeva tree-ring growth using proxy system models to determine the timing of changing

climate responses (Bunn et al., 2018) and the development of multimillennial tree-line position mapping to determine proximity to upper tree line during the establishment of now remnant *P. longaeva* samples (Bruening et al., 2018).

1.2.3   A History of Pinus aristata Dendrochronology

P. aristata grows primarily at high elevation in central and southern Colorado and northern New Mexico, with an isolated stand present at tree line in the San Francisco Peaks of northern Arizona (Gilbert et al., 2019). *P. aristata* is typically found on steep, south-facing slopes at elevations ranging from 2750 m to 3650 m (Baker, 1992). *P. aristata* experiences cambial dieback after several centuries of growth, resulting in the formation of "strip-bark" growth (Brunstein, 1996). The dense and resinous wood of *P. aristata* is extremely resistant to decay and deterioration, resulting in the preservation of remnants hundreds of years after the death of the tree (Carrara and McGeehin, 2015).

The first recorded dendrochronologic investigation of *P. aristata* was in 1944 by Edmund Schulman in Arizona and Colorado (Schulman, 1956). His *P. aristata* collection in central Colorado "indicated maximum ages of the order of 700-800 years," while a sample in northern Arizona contained over 1200 rings; however, he did not determine absolute ages for either site (Schulman, 1956). Until 1970, both Great Basin (*P. longaeva*) and Rocky Mountain bristlecone pine (*P. aristata*) were assumed to be the same species (Bailey, 1970); therefore, Schulman assumed the *P. aristata* were part of a continuum of a single bristlecone species which attained increasingly older ages from east to west (Schulman, 1956). Further investigations therefore

focused on the older and more charismatic western bristlecones (*P. longaeva*), with researchers developing multi-millennial chronologies (Ferguson, 1969) and identifying individual *P. longaeva* approaching 5000 years in age (Currey, 1965; Schulman, 1958, 1954).

It was not until 1973 that Pauline Krebs re-evaluated the dendrochronological potential of *P. aristata*, constructing the first cross-dated chronologies of *P. aristata* and identified living trees over 1,500 years in age (Krebs, 1973). Unfortunately, this investigation did not extend beyond constructing chronologies. The following year, a climatic response analysis of both *P. aristata* and *P. longaeva* was conducted, using chronologies from throughout the Southwest. The results indicated both temperature and precipitation sensitivity in the *P. aristata* collection, although the precipitation sensitive *P. aristata* sites were highlighted as having the greatest reconstruction potential (LaMarche Jr and Stockton, 1974). Samples from this investigation were also used to date frost rings formed during extremely cool periods caused by volcanic eruptions (LaMarche and Hirschboeck, 1984). Work with *P. aristata* continued sporadically with a technical report on increasing carbon dioxide levels and tree growth (Graybill, 1985), a fire history in northern New Mexico (Touchan and Swetnam, 1995), and a second *P. aristata*-specific frost ring reconstruction in Colorado (Brunstein, 1996). One of the researchers during this period, Craig Brunstein, was notable for identifying the oldest living *P. aristata* in Colorado (Brunstein and Yamaguchi, 1992) and developing a detailed guide to bristlecone growth and morphology (Brunstein, 2006) all while pursuing this work as an amateur dendrochronologist.

The first climate reconstruction using *P. aristata* tree-ring chronologies as proxies was developed in 2005. Samples from the isolated San Francisco Peak stand in Arizona were used in a 2262-year temperature reconstruction for the Colorado Plateau (Salzer and Kipfmueller, 2005). This was followed by the development of two new moisture sensitive chronologies in Colorado, a 2200-year chronology indicating an extreme 2nd century megadrought (Routson et al., 2011) and an 1800-year chronology used to evaluate decadal-scale moisture variability in the upper Arkansas River basin (Woodhouse et al., 2011). Additional recent work with *P. aristata* includes a localized temperature reconstruction, using oxygen isotopes, at one sampling site on the Front Range of Colorado (Berkelhammer and Stott, 2012), an annual precipitation reconstruction at Black Mountain, Colorado, the site of the oldest living *P. aristata* (Miller, 2014), and a radiocarbon-dated (not dendrochronologically cross-dated) assessment of remnant *P. aristata* indicating trees growing above the present tree line in central Colorado between 700 BCE and 1200 CE years (Carrara and McGeehin, 2015).

1.3   ORGANIZATION OF DISSERTATION

Until this study, only individual (or a limited set of) *P. aristata* chronologies have been evaluated for climate sensitivity, with no comprehensive investigation conducted to identify the type and seasonality of the *P. aristata* climate response across its range. Furthermore, no attempt has been made to disentangle potential mixed climate responses at *P. aristata* collection sites in a manner similar to the proxy system modeling conducted with *P. longaeva*. Finally, only one reconstruction of hydroclimate (Miller, 2014) and no reconstructions of temperature have been developed with the *P. aristata* chronologies from Colorado or New Mexico, despite the extreme

longevity of *P. aristata* and the potential for both temperature and hydroclimate sensitivity. In this dissertation, I address these deficits in our understanding of *P. aristata* through the studies described below.

In my first study, I conduct an extensive evaluation of climate sensitivity across ten *P. aristata* collection sites, assessing common growth signals between chronologies and individual trees within collection sites. I identify a robust annual late spring/early summer hydroclimate growth response in low elevation collections, and at upper elevation sites I identify a weaker but still significant low-frequency, summer temperature response overlain with an annual early summer hydroclimate sensitivity. In my second study, I utilize the Vaganov-Shashkin proxy system model to simulate *P. aristata* tree-ring growth at an upper and a lower elevation sampling site. Sensitivity testing using pre-industrial temperature and moisture conditions is applied to simulate growth prior the modern observed record. The results provide further confirmation of the late spring/early summer hydroclimate sensitivity in lower elevation *P. aristata*, while identifying a positive temperature response in upper elevation trees when grown under cooler, pre-anthropogenic warming conditions. The simulation of temperature response in upper elevation *P. aristata* provides a direction for future research to investigate this past temperature sensitivity at sites that no longer contain a clear temperature response or in locations where cooler growing season conditions may still provide a temperature limitation to growth.

For the final study, I used the results from the climate sensitivity analysis and proxy system modeling to develop the first April-June drought index reconstruction for the Southern Rockies.

Initial analysis of the observational relationship between winter snowpack and spring hydroclimate conditions indicated the potential, albeit rare, for extreme spring conditions to ameliorate or exacerbate winter moisture conditions and alter streamflow totals beyond that predicted by prior winter's snowpack. I utilized the April-June drought index reconstruction and a previously produced reconstruction of snowpack (Pederson et al., 2011) to evaluate the multi-century relationship between winter snowpack and spring hydroclimate conditions in the Rio Grande headwaters. I found no consistent multi-year relationship between the two reconstructed indices, but did identify periods of simultaneous fluctuations that coincided with extreme drought and pluvial events, and provided evidence that during the major drought events, spring deficits may have exceeded the severity of winter deficits.

This dissertation is formatted per University of Arizona Graduate College guidelines as a Manuscript/Article Dissertation with three research projects described in three appendices. Each appendix is formatted as a publishable manuscript complete with detailed methods, findings, and conclusions. I am the lead author for each manuscript, with my advisor Dr. Connie Woodhouse as my co-author. Chapter 2 contains a summary of the major objectives and findings for each of the three studies that comprise my dissertation research. The first study was submitted and published in Dendrochronologia in 2021 and is included as Appendix A (Tintor and Woodhouse, 2021). The second study was written and prepared as a manuscript suitable for submission to Environmental Research Letters and is included as Appendix B. The third, and final, study was written and prepared as a manuscript suitable for submission to Water Resources Research and is included as Appendix C.

CHAPTER 2: PRESENT STUDY

2.1   PRESENT STUDY

The present study is focused on disentangling the complex climate response of *P. aristata* by

identifying the type and seasonality of climate sensitivity contained within the tree-ring widths of

this species. Initially motivated by the potential development of a temperature reconstruction,

this study uncovered a robust spring hydroclimate sensitivity in *P. aristata* suitable for the

production of a novel multi-century reconstruction. The study did identify a positive, multi-year

response to late summer temperatures in upper elevation *P. aristata* and simulated tree-growth

modeling similarly showed a strong, positive temperature response at high elevation sites prior to

late 20th century warming. Additional work is needed to fully isolate the temperature signal

contained with *P. aristata*, but this study presents a foundation to pursue the development of a

skillful temperature reconstruction for the Southern Rockies using *P. aristata*. The following

sections summarize the major objectives and findings for the three studies that comprise my

dissertation research.

2.2   APPENDIX A - THE VARIABLE CLIMATE RESPONSE OF ROCKY MOUNTAIN BRISTLECONE
    PINE (*PINUS ARISTATA* ENGELM.)

The semi-arid western United States has numerous tree-ring proxies of moisture that capture

extreme droughts with magnitudes of severity greater than those captured by instrumental

records. Recent increases in temperature have been shown to exacerbate drought and reduce

streamflow, but our understanding of the role temperature played in past droughts is limited due

to the low number of tree-ring based temperature proxies for the region. The goal of this study is to evaluate the climate sensitivity of Rocky Mountain bristlecone pine (*P. aristata*) and evaluate its potential for developing new multi-century proxy records of both temperature and precipitation in an effort to fill this gap. To do this, we used five new and five previously collected *P. aristata* ring-width chronologies to answer the following research questions:

- What do the regional set of chronologies tell us about *P. aristata* response to climate and how it varies by location and site characteristics?
- Within each sampling site, is the climate sensitivity consistent among trees that make up the site chronology, or is there intra-site variability as documented in previous *P. longaeva* studies?
- What is the potential for developing long moisture and/or temperature reconstructions from this set of data?

To answer these questions, I isolated the dominant patterns of growth variability in the *P. aristata* ring-width datasets using empirical orthogonal function (EOF) analysis (Preisendorfer and Mobley, 1988) on chronologies and on individual trees. I also used a modified form of hierarchical cluster analysis (Kipfmueller and Salzer, 2010) applied to a matrix of simple correlations between individual tree samples and local climate data to isolate a third set of tree growth patterns. Following the isolation of growth patterns, I constructed time series using the strongest common growth signals and correlated each with a regional gridded climate dataset to

assess the spatial relationship between the *P. aristata* data and regional climate over the 20th century.

The results showed evidence of a mixed climate response within high elevation, upper-tree line sampling sites as previously observed with *P. longaeva* collections. The strongest climatic signal identified was a June drought stress signal (growth corresponded positively to precipitation and negatively to maximum temperature), which was present at multiple sampling sites. A low frequency positive correlation with late summer temperatures was also found among trees that simultaneously contained a weak June drought stress signal at higher frequencies. The June drought stress signal contained within the ring-width data was identified as having the strongest potential for reconstruction. Remnants collected for this study are the oldest crossdated remnants identified in Colorado and New Mexico with respective start dates of 847 BCE and 778 BCE.

2.3   APPENDIX B - UTILIZING THE VAGANOV-SHASHKIN MODEL TO SIMULATE CLIMATE

SENSITIVITY IN ROCKY MOUNTAIN BRISTLECONE PINE (*PINUS ARISTATA* ENGELM.)

Trees growing at the elevational or latitudinal limits of growth have long been utilized as high resolution proxies of past temperature variability. Recent studies of *P. longaeva* have highlighted the co-occurrence of a moisture growth signal alongside elevation driven temperature sensitivity producing weak correlations with both climate parameters (Bunn et al., 2011; Salzer et al., 2014b). Similar mixed temperature and moisture signals have also been identified in high elevation, tree-line *P. aristata* (Tintor and Woodhouse, 2021). Building on the work with *P. longaeva*, this study seeks to disentangle the mixed climate signals and determine if *P. aristata*

located at tree line are currently temperature limited or were limited in the past under cooler

general conditions. Two objectives were developed to answer this question:

- Develop an understanding of the current dynamics of growth limitation related to climate in *P. aristata*, determining their utility as temperature or moisture proxies.
- Evaluate changes in *P. aristata* climate sensitivity during cooler climates observed in paleoclimate records, thereby determining the stability of their climate sensitivity.

To address the first objective, I used the Vaganov-Shaskin Model (VSM) (Anchukaitis et al.,

2020; Vaganov et al., 2011, 2006) to simulate 28 years (1989-2016 CE) of *P. aristata* tree-ring

growth at two locations in New Mexico, an upper elevation tree-line site and a lower elevation

site. I used a series of temperature sensors placed at each sampling site to modify a multi-decade

temperature record to represent temperature variability more accurately at each sampling

location. These two daily temperature datasets and daily PRISM precipitation data (Daly et al.,

1994) were used to simulate tree-ring growth in the VSM. I addressed the second objective by

developing daily climate datasets adjusted to simulate cooler and drier conditions during the late

16th century Southwest megadrought and then ran the VSM with these adjusted datasets to

identify climate sensitivity under the adjusted conditions.

The results showed the lower elevation *P. aristata* were consistently moisture limited during the

late spring/early summer period throughout the 28 year simulation. The upper elevation trees

were not robustly temperature limited and were shown to vary in strength and timing of moisture

limitation depending on the annual growing season temperature. Sensitivity tests did not change the moisture response in the lower elevation trees, but did induce temperature limitation in the upper elevation trees, suggesting that upper elevation tree growth was previously temperature limited even during periods of extreme drought. Evidence suggests that at some point prior to modern VSM run the upper elevation site passed a seasonal growing temperature threshold similar to the one identified in *P. longaeva* (Tran et al., 2017) resulting in a shift from temperature to moisture sensitivity. These results show the robustness of the late spring/early summer drought signal in *P. aristata* at lower elevation while also highlighting the current instability of the climate response at upper elevation. The findings do provide evidence of past temperature sensitivity under cooler conditions and the potential for *P. aristata* temperature sensitivity at locations where cooler growing season temperatures currently occur.

2.4   APPENDIX C - THE INFLUENCE OF RECENT AND RECONSTRUCTED SPRING HYDROCLIMATE
         CONDITIONS ON THE RIO GRANDE HEADWATERS

The headwaters of the Rio Grande in Colorado are the primary source of streamflow for the upper Rio Grande, despite constituting a relatively small portion of the full watershed (Blythe and Schmidt, 2018). The majority of spring and summer streamflow originating in the headwaters is produced by melting snowpack, allowing annual prediction of streamflow using systematized measurements of snowpack (Pagano et al., 2009). Despite this close relationship, recent years have seen a decline in the power of snowpack to predict streamflow (Pagano et al., 2004) and an increasing influence of spring hydroclimate conditions on streamflow totals in the Rio Grande (Chavarria and Gutzler, 2018). For example, in 2021 it appeared that wetter, cooler

conditions during the months of April through June were responsible for an increase in spring

streamflow totals above that predicted by snowpack measurements. Given the potential for

spring conditions to influence seasonal streamflow totals in an already stressed and over-

apportioned hydrologic system, a better understanding is needed of the relationship between

winter snowpack and spring hydroclimate conditions and associated impacts on streamflow.

Therefore, in an effort to improve this understanding, two objectives were developed for this

study:

- Evaluate the relationship between snowpack, spring hydroclimate conditions, and streamflow volumes of the Rio Grande, identifying years when spring hydroclimate conditions coincide with spring streamflow volumes that are outside anticipated streamflows based on preceding winter snowpack.
- Assess the pre-instrumental period relationship between snowpack and spring conditions over the past centuries in order to situate the observed relationship between snowpack and spring hydroclimate conditions within a broader historic context.

To address the first objective, I used an April 1 snow water equivalent (SWE) index from

Pederson et al. (2011), an April-June standardized precipitation evapotranspiration index (SPEI)

from Vicente-Serrano et al. (2010), and April-June stream gage measurements from the Del

Norte gage along the Rio Grande to represent, respectively, snowpack, spring hydroclimate

conditions, and spring streamflow from 1937-2004 CE. Converting the datasets to percentiles, I

first identified years when there was a significant difference (one quintile or more) between

spring hydroclimate and snowpack. Within the years with a significant difference between spring

conditions and snowpack, I identified the years with a significant difference between spring

streamflow and snowpack percentiles. There were only 16% of years where a significant

difference between snowpack and spring hydroclimate conditions coincided with streamflow

totals beyond the magnitude of snowpack-based predicted volumes.

To address the second objective, I used the evidence gained from previous research on *P.

aristata* to produce a new April-June spring hydroclimate (SPEI) reconstruction for the Rio

Grande headwaters from 445-2004 CE. This reconstruction was compared with a previous

reconstruction of snowpack (Pederson et al., 2011), giving a long-term context to the

instrumental relationship between snowpack and spring hydroclimate. The percentile comparison

process used for the observed datasets was also applied to the reconstruction datasets. The

comparison results for the full reconstruction show the percent of years with significant

differences between spring hydroclimate and snowpack was similar to the percent seen in the

observed data. Breaking down the reconstruction comparisons by century indicated slight

variability in relationship between snowpack and spring hydroclimate. Still, the magnitude of

this variability was not large enough to indicate an increase in the influence of spring

hydroclimate conditions on streamflow totals during past periods. When multi-decadal

fluctuations in the two reconstructions are compared, the relationship is highly stochastic,

indicating that there was no stable long-term relationship between snowpack variability and

spring hydroclimate in the past.

Finally, the relationship between snowpack and spring hydroclimate reconstructions was analyzed during the top five megadroughts and extreme pluvials during the reconstruction interval (445-2005). The extreme events were identified using North American Drought Atlas (NADA) Palmer drought severity index (PDSI) reconstruction data for the Rio Grande headwaters (Cook et al., 2004). The results suggest the pluvials coincided almost entirely with large winter snowpacks, not spring hydroclimate conditions, while megadroughts occurred during periods that experienced both snowpack deficits and dry springs. The full set of findings have implications for water managers in the upper Rio Grande basin. With increasing temperatures expected to decrease snowpack contribution to streamflow (Llewellyn and Vaddey, 2013) the occurrence of cool, wet springs which increase streamflows relative to the snowpack-based predictions will become increasingly important. Unfortunately, both the observed datasets and the reconstructed indices suggest that the occurrence of such cool, wet springs is rare and should not be expected to regularly supplement Rio Grande streamflow.

WORKS CITED

Adams, D.K., Comrie, A.C., 1997. The North American Monsoon. *Bull. Amer. Meteor. Soc.* 78, 2197–2213. https://doi.org/10.1175/1520-0477(1997)078<2197:TNAM>2.0.CO;2

Anchukaitis, K.J., Evans, M.N., Hughes, M.K., Vaganov, E.A., 2020. An interpreted language implementation of the Vaganov–Shashkin tree-ring proxy system model. *Dendrochronologia* 60, 125677. https://doi.org/10.1016/j.dendro.2020.125677

Ault, T.R., Mankin, J.S., Cook, B.I., Smerdon, J.E., 2016. Relative impacts of mitigation, temperature, and precipitation on 21st-century megadrought risk in the American Southwest. *Sci. Adv.* 2, e1600873. https://doi.org/10.1126/sciadv.1600873

Ault, T.R., St. George, S., Smerdon, J.E., Coats, S., Mankin, J.S., Carrillo, C.M., Cook, B.I., Stevenson, S., 2018. A Robust Null Hypothesis for the Potential Causes of Megadrought in Western North America. *Journal of Climate* 31, 3–24. https://doi.org/10.1175/JCLI-D-17-0154.1

Bailey, D.K., 1970. Phytogeography and Taxonomy of Pinus Subsection Balfourianae. *Annals of the Missouri Botanical Garden* 57, 210. https://doi.org/10.2307/2395110

Baker, W.L., 1992. Structure, Disturbance, and Change in the Bristlecone Pine Forests of Colorado, U.S.A. *Arctic and Alpine Research* 24, 17. https://doi.org/10.2307/1551316

Berkelhammer, M., Stott, L.D., 2012. Secular temperature trends for the southern Rocky Mountains over the last five centuries: ROCKY MOUNTAIN TEMPERATURE TRENDS. *Geophys. Res. Lett.* 39, n/a-n/a. https://doi.org/10.1029/2012GL052447

Blasing, T.J., Fritts, H.C., 1976. Reconstructing Past Climatic Anomalies in the North Pacific and Western North America from Tree-Ring Data. *Quat. res.* 6, 563–579. https://doi.org/10.1016/0033-5894(76)90027-2

Blythe, T.L., Schmidt, J.C., 2018. Estimating the Natural Flow Regime of Rivers With Long-Standing Development: The Northern Branch of the Rio Grande. *Water Resour. Res.* 54, 1212–1236. https://doi.org/10.1002/2017WR021919

Briffa, K.R., Jones, P.D., Schweingruber, F.H., 1992. Tree-Ring Density Reconstructions of Summer Temperature Patterns across Western North America since 1600. *J. Climate* 5, 735–754. https://doi.org/10.1175/1520-0442(1992)005<0735:TRDROS>2.0.CO;2

Bruening, J.M., Bunn, A.G., Salzer, M.W., 2018. A climate-driven tree line position model in the White Mountains of California over the past six millennia. *J Biogeogr* 45, 1067–1076. https://doi.org/10.1111/jbi.13191

Bruening, J.M., Tran, T.J., Bunn, A.G., Weiss, S.B., Salzer, M.W., 2017. Fine-scale modeling of bristlecone pine treeline position in the Great Basin, USA. *Environ. Res. Lett.* 12, 014008. https://doi.org/10.1088/1748-9326/aa5432

Brunstein, F.C., 2006. Growth-Form Characteristics of Ancient Rocky Mountain Bristlecone Pines (*Pinus aristata*), Colorado. *U.S. Geological Survey.*

Brunstein, F.C., 1996. Climatic Significance of the Bristlecone Pine Latewood Frost-Ring Record at Almagre Mountain, Colorado, U.S.A. *Arctic and Alpine Research* 28, 65. https://doi.org/10.2307/1552087

Brunstein, F.C., Yamaguchi, D.K., 1992. The Oldest Known Rocky Mountain Bristlecone Pines (*Pinus aristata* Engelm.). *Arctic and Alpine Research* 24, 253. https://doi.org/10.2307/1551666

Bunn, A.G., Hughes, M.K., Salzer, M.W., 2011. Topographically modified tree-ring chronologies as a potential means to improve paleoclimate inference: A letter. *Climatic Change* 105, 627–634. https://doi.org/10.1007/s10584-010-0005-5

Bunn, A.G., Salzer, M.W., Anchukaitis, K.J., Bruening, J.M., Hughes, M.K., 2018. Spatiotemporal Variability in the Climate Growth Response of High Elevation Bristlecone Pine in the White Mountains of California. *Geophys. Res. Lett.* 45. https://doi.org/10.1029/2018GL080981

Büntgen, U., Arseneault, D., Boucher, É., Churakova (Sidorova), O.V., Gennaretti, F., Crivellaro, A., Hughes, M.K., Kirdyanov, A.V., Klippel, L., Krusic, P.J., Linderholm, H.W., Ljungqvist, F.C., Ludescher, J., McCormick, M., Myglan, V.S., Nicolussi, K., Piermattei, A., Oppenheimer, C., Reinig, F., Sigl, M., Vaganov, E.A., Esper, J., 2020. Prominent role of volcanism in Common Era climate variability and human history. *Dendrochronologia* 64, 125757. https://doi.org/10.1016/j.dendro.2020.125757

Carrara, P.E., McGeehin, J.P., 2015. Evidence of a higher late-Holocene treeline along the Continental Divide in central Colorado. *The Holocene* 25, 1829–1837. https://doi.org/10.1177/0959683615591353

Chavarria, S.B., Gutzler, D.S., 2018. Observed Changes in Climate and Streamflow in the Upper Rio Grande Basin. *J Am Water Resour Assoc* 54, 644–659. https://doi.org/10.1111/1752-1688.12640

Coats, S., Smerdon, J.E., Cook, B.I., Seager, R., 2015. Are Simulated Megadroughts in the North American Southwest Forced?. *Journal of Climate* 28, 124–142. https://doi.org/10.1175/JCLI-D-14-00071.1

Cook, E.R., Kairiukstis, L.A., 2013. *Methods of dendrochronology: applications in the environmental sciences.* Springer Science & Business Media.

Cook, E.R., Meko, D.M., Stahle, D.W., Cleaveland, M.K., 1999. Drought reconstructions for the continental United States. Journal of Climate 12, 1145–1162.

Cook, E.R., Seager, R., Heim, R.R., Vose, R.S., Herweijer, C., Woodhouse, C., 2010. Megadroughts in North America: placing IPCC projections of hydroclimatic change in a long-term palaeoclimate context: MEGADROUGHTS IN NORTH AMERICA. *J. Quaternary Sci.* 25, 48–61. https://doi.org/10.1002/jqs.1303

Cook, E.R., Woodhouse, C.A., Eakin, C.M., Meko, D.M., Stahle, D.W., 2004. Long-Term Aridity Changes in the Western United States. *Science* 306, 1015–1018. https://doi.org/10.1126/science.1102586

Coop, J.D., Givnish, T.J., 2007. Spatial and temporal patterns of recent forest encroachment in montane grasslands of the Valles Caldera, New Mexico, USA: Valles Caldera tree-line shift. *Journal of Biogeography* 34, 914–927. https://doi.org/10.1111/j.1365-2699.2006.01660.x

Currey, D.R., 1965. An Ancient Bristlecone Pine Stand in Eastern Nevada. *Ecology* 46, 564–566. https://doi.org/10.2307/1934900

Daly, C., Neilson, R.P., Phillips, D.L., 1994. A Statistical-Topographic Model for Mapping Climatological Precipitation over Mountainous Terrain. *J. Appl. Meteor.* 33, 140–158. https://doi.org/10.1175/1520-0450(1994)033<0140:ASTMFM>2.0.CO;2

D'Arrigo, R.D., Jacoby, G.C., 1991. A 1000-year record of winter precipitation from northwestern New Mexico, USA: a reconstruction from tree-rings and its relation to El Niño and the Southern Oscillation. *The Holocene* 1, 95–101. https://doi.org/10.1177/095968369100100201

Douglass, A.E., 1929. The secret of the Southwest solved by talkative tree rings. *National Geographic* 56, 737–770.

Douglass, A.E., 1920. Evidence of Climatic Effects in the Annual Rings of Trees. *Ecology* 1, 24–32. https://doi.org/10.2307/1929253

Douglass, A.E., 1919. Climatic cycles and tree-growth. *Carnegie Institution of Washington.*

Douglass, A.E., 1914. A method of estimating rainfall by the growth of trees. *Bulletin of the American Geographical Society* 46, 321–335.

Ferguson, C.W., 1969. A 7104-year annual tree-ring chronology for bristlecone pine, *Pinus aristata*, from the White Mountains, California.

Fritts, H., 1976. *Tree rings and climate*. Elsevier.

Fritts, H.C., Blasing, T.J., Hayden, B.P., Kutzbach, J.E., 1971. Multivariate Techniques for Specifying Tree-Growth and Climate Relationships and for Reconstructing Anomalies in Paleoclimate. *J. Appl. Meteor.* 10, 845–864. https://doi.org/10.1175/1520-0450(1971)010<0845:MTFSTG>2.0.CO;2

Fritts, H.C., Lough, J.M., 1985. An estimate of average annual temperature variations for North America, 1602 to 1961. *Climatic Change* 7, 203–224. https://doi.org/10.1007/BF00140506

Gilbert, E., Gries, C., Franz, N., Landrum, L.R., Nash III, T.H., 2019. SEINet: A Centralized Specimen Resource Managed by a Distributed Network of Researchers. Biodiversity Information Science and Standards.

Gonzalez, P., Breshears, D., Brooks, K., Brown, H.E., Elias, E., Gunasekara, A., Huntly, N., Maldonado, J.K., Mantua, N.J., Margolis, H.G., McAfee, S., Middleton, B.R., Udall, B., 2018. *Chapter 25 : Southwest. Impacts, Risks, and Adaptation in the United States: The Fourth National Climate Assessment, Volume II.* U.S. Global Change Research Program. https://doi.org/10.7930/NCA4.2018.CH25

Graumlich, L.J., 1993. A 1000-Year Record of Temperature and Precipitation in the Sierra Nevada. *Quat. res.* 39, 249–255. https://doi.org/10.1006/qres.1993.1029

Graybill, D.A., 1985. Western US tree-ring index chronology data for detection of arboreal response to increasing carbon dioxide.

Hidalgo, H.G., Dracup, J.A., 2003. ENSO and PDO Effects on Hydroclimatic Variations of the Upper Colorado River Basin. *J. Hydrometeor* 4, 5–23. https://doi.org/10.1175/1525-7541(2003)004<0005:EAPEOH>2.0.CO;2

Kipfmueller, K.F., Salzer, M.W., 2010. Linear trend and climate response of five-needle pines in the western United States related to treeline proximity. *Can. J. For. Res.* 40, 134–142. https://doi.org/10.1139/X09-187

Knight, T.A., Meko, D.M., Baisan, C.H., 2010. A Bimillennial-Length Tree-Ring Reconstruction of Precipitation for the Tavaputs Plateau, Northeastern Utah. *Quat. res.* 73, 107–117. https://doi.org/10.1016/j.yqres.2009.08.002

Krebs, P.V., 1973. Dendrochronology of bristlecone pine (*Pinus aristata* Engelm.) in Colorado. *Arctic and Alpine Research* 5, 149–150.

Kuhn, E., Fleck, J., 2019. *Science be dammed: how ignoring inconvenient science drained the Colorado River.* University of Arizona Press.

LaMarche Jr, V.C., Stockton, C.W., 1974. Chronologies from temperature-sensitive bristlecone pines at upper treeline in Western United States. *Tree-Ring Bulletin*.

LaMarche, V.C., 1974. Frequency-dependent relationships between tree-ring series along an ecological gradient and some dendroclimatic implications. *Tree-Ring Bulletin*.

LaMarche, V.C., Hirschboeck, K.K., 1984. Frost rings in trees as records of major volcanic eruptions. *Nature* 307, 121–126. https://doi.org/10.1038/307121a0

Lehner, F., Wahl, E.R., Wood, A.W., Blatchford, D.B., Llewellyn, D., 2017. Assessing recent declines in Upper Rio Grande runoff efficiency from a paleoclimate perspective. *Geophys. Res. Lett.* 44, 4124–4133. https://doi.org/10.1002/2017GL073253

Li, D., Wrzesien, M.L., Durand, M., Adam, J., Lettenmaier, D.P., 2017. How much runoff originates as snow in the western United States, and how will that change in the future? *Geophys. Res. Lett.* 44, 6163–6172. https://doi.org/10.1002/2017GL073551

Ljungqvist, F.C., Piermattei, A., Seim, A., Krusic, P.J., Büntgen, U., He, M., Kirdyanov, A.V., Luterbacher, J., Schneider, L., Seftigen, K., Stahle, D.W., Villalba, R., Yang, B., Esper, J., 2020. Ranking of tree-ring based hydroclimate reconstructions of the past millennium. *Quaternary Science Reviews* 230, 106074. https://doi.org/10.1016/j.quascirev.2019.106074

Llewellyn, D., Vaddey, S., 2013. West-Wide Climate Risk Assessment: Upper Rio Grande Impact Assessment: Report. US Department of the Interior, Bureau of Reclamation, Upper Colorado Region.

Lukas, J., Barsugli, J., Wolter, K., Rangwala, I., Doesken, N., 2014. *Climate Change in Colorado: A Synthesis to Support Water Resources Management and Adaptation.* https://doi.org/10.13140/RG.2.2.36741.35043

Lukas, J., Payton, E., 2020. *Colorado River Basin Climate and Hydrology: State of the Science.* https://doi.org/10.25810/3HCV-W477

Lundquist, J.D., Cayan, D.R., 2007. Surface temperature patterns in complex terrain: Daily variations and long-term change in the central Sierra Nevada, California. *J. Geophys. Res.* 112, D11124. https://doi.org/10.1029/2006JD007561

Meko, D., 1997. Dendroclimatic Reconstruction with Time Varying Predictor Subsets of Tree Indices. *J. Climate* 10, 687–696. https://doi.org/10.1175/1520-0442(1997)010<0687:DRWTVP>2.0.CO;2

Meko, D.M., Woodhouse, C.A., Baisan, C.A., Knight, T., Lukas, J.J., Hughes, M.K., Salzer, M.W., 2007. Medieval drought in the upper Colorado River Basin. *Geophys. Res. Lett.* 34, L10705. https://doi.org/10.1029/2007GL029988

Miller, K., 2014. 2,462 Years of Upper Arkansas River Basin Precipitation Reconstructed from Tree-Rings at Black Mountain (Thesis). University of Arizona, Tucson, AZ.

Milly, P.C.D., Betancourt, J., Falkenmark, M., Hirsch, R.M., Kundzewicz, Z.W., Lettenmaier, D.P., Stouffer, R.J., 2008. Stationarity Is Dead: Whither Water Management? *Science* 319, 573–574. https://doi.org/10.1126/science.1151915

Pagano, T., Garen, D., Sorooshian, S., 2004. Evaluation of Official Western U.S. Seasonal Water Supply Outlooks, 1922–2002. *J. Hydrometeor* 5, 896–909. https://doi.org/10.1175/1525-7541(2004)005<0896:EOOWUS>2.0.CO;2

Pagano, T.C., Garen, D.C., Perkins, T.R., Pasteris, P.A., 2009. Daily Updating of Operational Statistical Seasonal Water Supply Forecasts for the western U.S. *JAWRA Journal of the American Water Resources Association* 45, 767–778. https://doi.org/10.1111/j.1752-1688.2009.00321.x

PAGES2k Consortium, 2017. A global multiproxy database for temperature reconstructions of the Common Era. *Sci Data* 4, 170088. https://doi.org/10.1038/sdata.2017.88

Pederson, G.T., Gray, S.T., Woodhouse, C.A., Betancourt, J.L., Fagre, D.B., Littell, J.S., Watson, E., Luckman, B.H., Graumlich, L.J., 2011. The Unusual Nature of Recent Snowpack Declines in the North American Cordillera. *Science* 333, 332–335. https://doi.org/10.1126/science.1201570

Preisendorfer, R.W., Mobley, C.D., 1988. Principal component analysis in meteorology and oceanography. *Developments in atmospheric science* 17.

Reeves, H.D., Stensrud, D.J., 2009. Synoptic-Scale Flow and Valley Cold Pool Evolution in the Western United States. *Weather and Forecasting* 24, 1625–1643. https://doi.org/10.1175/2009WAF2222234.1

Reisner, M., 1993. *Cadillac desert: The American West and its disappearing water.* Penguin.

Routson, C.C., Woodhouse, C.A., Overpeck, J.T., 2011. Second century megadrought in the Rio Grande headwaters, Colorado: How unusual was medieval drought?: SECOND CENTURY MEGADROUGHT. *Geophys. Res. Lett.* 38, n/a-n/a. https://doi.org/10.1029/2011GL050015

Salzer, Matthew W., Bunn, A.G., Graham, N.E., Hughes, M.K., 2014a. Five millennia of paleotemperature from tree-rings in the Great Basin, USA. *Clim Dyn* 42, 1517–1526. https://doi.org/10.1007/s00382-013-1911-9

Salzer, M.W., Kipfmueller, K.F., 2005. Reconstructed Temperature And Precipitation On A Millennial Timescale From Tree-Rings In The Southern Colorado Plateau, U.S.A. *Climatic Change* 70, 465–487. https://doi.org/10.1007/s10584-005-5922-3

Salzer, Matthew W, Larson, E.R., Bunn, A.G., Hughes, M.K., 2014b. Changing climate response in near-treeline bristlecone pine with elevation and aspect. *Environ. Res. Lett.* 9, 114007. https://doi.org/10.1088/1748-9326/9/11/114007

Schoettle, A.W., Coop, J.D., 2017. Range-wide conservation of *Pinus aristata*: a genetic collection with ecological context for proactive management today and resources for tomorrow. *New Forests* 48, 181–199. https://doi.org/10.1007/s11056-017-9570-z

Schulman, E., 1958. Bristlecone Pine, Oldest Known Living Thing. *National Geographic* 113.

Schulman, E., 1956. *Dendroclimatic changes in semiarid America.* University of Arizona Press.

Schulman, E., 1954. Longevity under adversity in conifers. *Science* 119, 396–399.

Schulman, E., 1942. Centuries-long tree indices of precipitation in the southwest (I). *Bulletin of the American Meteorological Society* 148–161.

Schulman, E., 1938. Nineteen centuries of rainfall history in the southwest. *Bulletin of the American Meteorological Society* 19, 211–215.

Schweingruber, F., 1988. A new dendroclimatic network for western North America. *Dendrochronologia* 6, 171–180.

Schweingruber, F.H., Briffa, K.R., Jones, P., 1991. Yearly maps of summer temperatures in Western Europe from AD 1750 to 1975 and Western North America from 1600 to 1982. *Vegetatio* 92, 5–71.

Sheppard, P.R., Comrie, A.C., Packin, G.D., Angersbach, K., Hughes, M.K., 2002. The climate of the US Southwest. *Clim. Res.* 21, 219–238. https://doi.org/10.3354/cr021219

Stahle, D.W., Cleaveland, M.K., Grissino-Mayer, H.D., Griffin, R.D., Fye, F.K., Therrell, M.D., Burnette, D.J., Meko, D.M., Villanueva Diaz, J., 2009. Cool- and Warm-Season Precipitation Reconstructions over Western New Mexico. *Journal of Climate* 22, 3729–3750. https://doi.org/10.1175/2008JCLI2752.1

Stahle, D.W., Cook, E.R., Burnette, D.J., Torbenson, M.C.A., Howard, I.M., Griffin, D., Diaz, J.V., Cook, B.I., Williams, A.P., Watson, E., Sauchyn, D.J., Pederson, N., Woodhouse, C.A., Pederson, G.T., Meko, D., Coulthard, B., Crawford, C.J., 2020. Dynamics, Variability, and Change in Seasonal Precipitation Reconstructions for North America. *Journal of Climate* 33, 3173–3195. https://doi.org/10.1175/JCLI-D-19-0270.1

Stahle, D.W., Cook, E.R., Cleaveland, M.K., Therrell, M.D., Meko, D.M., Grissino-Mayer, H.D., Watson, E., Luckman, B.H., 2000. Tree-ring data document 16th century megadrought over North America. *Eos Trans. AGU* 81, 121. https://doi.org/10.1029/00EO00076

Stegner, W., 1992. *Beyond the hundredth meridian: John Wesley Powell and the second opening of the West.* Penguin.

Stockton, C.W., Jacoby, Gcj., 1976. Long-term surface-water supply and streamflow trends in the Upper Colorado River Basin. *Lake Powell Research Project Bulletin.*

Tintor, W.L., Woodhouse, C.A., 2021. The variable climate response of Rocky Mountain bristlecone pine (*Pinus aristata* Engelm.). *Dendrochronologia* 68, 125846. https://doi.org/10.1016/j.dendro.2021.125846

Touchan, R., Swetnam, T.W., 1995. Fire history in ponderosa pine and mixed-conifer forests of the Jemez Mountains, northern New Mexico.

Tran, T.J., Bruening, J.M., Bunn, A.G., Salzer, M.W., Weiss, S.B., 2017. Cluster analysis and topoclimate modeling to examine bristlecone pine tree-ring growth signals in the Great Basin, USA. *Environ. Res. Lett.* 12, 014007. https://doi.org/10.1088/1748-9326/aa5388

Udall, B., Overpeck, J., 2017. The twenty-first century Colorado River hot drought and implications for the future: COLORADO RIVER FLOW LOSS. *Water Resour. Res.* 53, 2404–2418. https://doi.org/10.1002/2016WR019638

Vaganov, E.A., Anchukaitis, K.J., Evans, M.N., 2011. How well understood are the processes that create dendroclimatic records? A mechanistic model of the climatic control on conifer tree-ring growth dynamics, in: *Dendroclimatology*. Springer, pp. 37–75.

Vaganov, E.A., Hughes, M.K., Shashkin, A.V., 2006. *Growth dynamics of conifer tree rings: images of past and future environments.* Springer Science & Business Media.

Vicente-Serrano, S.M., Beguería, S., López-Moreno, J.I., 2010. A Multiscalar Drought Index Sensitive to Global Warming: The Standardized Precipitation Evapotranspiration Index. *Journal of Climate* 23, 1696–1718. https://doi.org/10.1175/2009JCLI2909.1

Vose, R.S., Easterling, D.R., Kunkel, K.E., LeGrande, A.N., Wehner, M.F., 2017. Ch. 6: Temperature Changes in the United States. Climate Science Special Report: *Fourth National Climate Assessment, Volume I.* U.S. Global Change Research Program. https://doi.org/10.7930/J0N29V45

Williams, A.P., Cook, E.R., Smerdon, J.E., Cook, B.I., Abatzoglou, J.T., Bolles, K., Baek, S.H., Badger, A.M., Livneh, B., 2020. Large contribution from anthropogenic warming to an

emerging North American megadrought. *Science* 368, 314–318.
https://doi.org/10.1126/science.aaz9600

Wilson, R., Anchukaitis, K., Briffa, K.R., Büntgen, U., Cook, E., D'Arrigo, R., Davi, N., Esper, J., Frank, D., Gunnarson, B., Hegerl, G., Helama, S., Klesse, S., Krusic, P.J., Linderholm, H.W., Myglan, V., Osborn, T.J., Rydval, M., Schneider, L., Schurer, A., Wiles, G., Zhang, P., Zorita, E., 2016. Last millennium northern hemisphere summer temperatures from tree rings: Part I: The long term context. *Quaternary Science Reviews* 134, 1–18. https://doi.org/10.1016/j.quascirev.2015.12.005

Woodhouse, C., Stahle, D., Villanueva Díaz, J., 2012. Rio Grande and Rio Conchos water supply variability over the past 500 years. *Clim. Res.* 51, 147–158. https://doi.org/10.3354/cr01059

Woodhouse, C.A., Gray, S.T., Meko, D.M., 2006. Updated streamflow reconstructions for the Upper Colorado River Basin: UPDATED COLORADO RIVER RECONSTRUCTIONS. *Water Resour. Res.* 42. https://doi.org/10.1029/2005WR004455

Woodhouse, C.A., Meko, D.M., MacDonald, G.M., Stahle, D.W., Cook, E.R., 2010. A 1,200-year perspective of 21st century drought in southwestern North America. *Proceedings of the National Academy of Sciences* 107, 21283–21288. https://doi.org/10.1073/pnas.0911197107

Woodhouse, C.A., Overpeck, J.T., 1998. 2000 Years of Drought Variability in the Central United States. *Bull. Amer. Meteor. Soc.* 79, 2693–2714. https://doi.org/10.1175/1520-0477(1998)079<2693:YODVIT>2.0.CO;2

Woodhouse, C.A., Pederson, G.T., Gray, S.T., 2011. An 1800-yr record of decadal-scale hydroclimatic variability in the upper Arkansas River basin from bristlecone pine. *Quat. res.* 75, 483–490. https://doi.org/10.1016/j.yqres.2010.12.007

Woodhouse, C.A., Pederson, G.T., Morino, K., McAfee, S.A., McCabe, G.J., 2016. Increasing influence of air temperature on upper Colorado River streamflow: TEMPERATURE AND COLORADO STREAMFLOW. *Geophys. Res. Lett.* 43, 2174–2181. https://doi.org/10.1002/2015GL067613

APPENDIX A: THE VARIABLE CLIMATE RESPONSE OF ROCKY MOUNTAIN BRISTLECONE PINE (*PINUS ARISTATA* ENGELM.)

William Lazar Tintor [a, b, *], Connie Woodhouse [a, b]

Paper was published in the journal Dendrochronologia, 2021

[a] School of Geography, Development and Environment, University of Arizona, Tucson, AZ, 85721, USA
[b] Laboratory of Tree-Ring Research, University of Arizona, Tucson, AZ, 85721, USA

[*]Corresponding author: wtintor@email.arizona.edu (W. Tintor).

A.1 ABSTRACT

Recent increases in temperature over the semi-arid western United States have been shown to exacerbate drought, reducing streamflow, and increasing stress on ecosystems. Our understanding of the role temperature played during drought in the more distant past is far from complete. While numerous tree-ring proxy records of moisture provide evidence for past extreme droughts in this region, few contemporaneous tree-ring proxy records of temperatures exist. This limits our ability to evaluate the variable influence of temperature on drought over past centuries and to contextualize the present interplay of moisture and temperature during more recent drought events. It is also important to understand the complexity of climatic interactions that produced drought under natural variability prior to evaluating the potential impacts of future climate change. In response to this knowledge gap, we undertook the first extensive evaluation of climate sensitivity in Rocky Mountain bristlecone pine (*Pinus aristata* Engelm.), focusing on the potential for developing new multi-century proxy records of both temperature and precipitation. We isolated dominant patterns of growth variability among trees from ten ring-width datasets across the Southern Rocky Mountains of Colorado and New Mexico and assessed their response to climate. We utilized both an empirical orthogonal function (EOF) analysis and a modified form of hierarchical cluster analysis to produce time series representing growth patterns in *P. aristata*. The results indicate a widespread June drought stress signal with a high potential for multi-millennial reconstruction. We also found a positive minimum temperature response during late summer, evident only at lower frequency and co-occurring at locations with the June drought stress signal. The potential for temperature reconstruction will require further investigation into the physiological linkages between *P. aristata* and climate variability. The presence of multiple

climate responses within *P. aristata* sampling sites highlights the need for particular care when
including *P. aristata* in regional climate reconstructions.

A.2   INTRODUCTION

Tree-ring reconstructions of precipitation and streamflow in the semi-arid western U.S. provide
an expanded framework for contextualizing both the severity of current droughts and the impact
of predicted climate change over the next century (Meko and Woodhouse, 2011). In this region,
an abundance of tree-ring based reconstructions exists for streamflow (e.g., Meko et al., 2007;
Woodhouse et al., 2012, 2006), precipitation (e.g., D'Arrigo and Jacoby, 1991), and Palmer
Drought Severity Index (PDSI) (e.g., Cook et al., 2004). These tree-ring reconstructions show
that past "megadroughts" were of a duration and severity unlike any experienced in our limited
window of modern scientific record keeping (Woodhouse and Overpeck, 1998). Climate
modeling predicts intensified droughts in the semi-arid western U.S. due to an increase in
temperature and decrease in precipitation (Jones and Gutzler, 2016), although precipitation
trends are prone to higher uncertainty (Deser et al., 2014). In recent decades, warming alone has
exacerbated moisture deficits, increasing the severity of droughts and impacting streamflow on
the Upper Colorado River (Udall and Overpeck, 2017; Woodhouse et al., 2016) and the Rio
Grande (Chavarria and Gutzler, 2018; Lehner et al., 2017). With mid-range climate change
scenarios predicting a 2.7°C increase in average annual temperature by 2100 for the semi-arid
western U.S. (Gonzalez et al., 2018) the impacts on water supply from warming are likely to
continue. Revealing how temperature interacted with droughts over past centuries to millennia

using tree-ring based climate reconstructions could improve our understanding of how temperatures may influence drought severity in a warmer future.

Despite the potential influence of temperature on past droughts, there is a deficit in annual tree-ring based temperature reconstructions for the region. A recent survey of Common Era proxy records found only ten temperature-sensitive tree-ring chronologies in the states of Arizona, Colorado, New Mexico, and Utah (Emile-Geay et al., 2017). Efforts to produce a comprehensive regional temperature reconstruction in the semi-arid western U.S. have been limited due to a lack of temperature-sensitive tree-ring chronologies, and most recently, a lack of updated chronologies. Fritts and Lough (1985) produced the first tree-ring based temperature reconstruction for this region, expanding on previous work that produced a relative index of past temperature variation (Blasing and Fritts, 1976; LaMarche Jr and Stockton, 1974). Briffa et al. (1992) developed the first regional latewood density reconstruction of temperature for a gridded network that included the semi-arid western U.S. In the years since, several spatially limited temperature reconstructions have been produced for the Sierra Nevada (Graumlich, 1993), the southern Colorado Plateau (Salzer and Kipfmueller, 2005), the Great Basin (Salzer et al., 2009), and the Southern Rocky Mountains (Berkelhammer and Stott, 2012). Relative to the number of regionally developed precipitation and moisture reconstructions, temperature reconstructions are far outnumbered. With a limited set of temperature reconstructions available, a comparison between past droughts and temperature remains difficult.

Rocky Mountain bristlecone pine (*Pinus aristata* Engelm.) may provide an additional resource for this temperature reconstruction deficit. The related Great Basin bristlecone pine (*Pinus longaeva* D.K. Bailey) has been widely studied due to its 5000-year lifespan (Schulman, 1954), potential for climate reconstruction (Salzer et al., 2009), and preservation of remnant wood dating to the early Holocene (Salzer et al., 2019). While *P. longaeva* has been used for both annual precipitation (Knight et al., 2010) and temperature reconstructions (Salzer et al., 2009), research has indicated that inter-mixture of both precipitation and temperature signals is common within a *P. longaeva* sampling site due to topographic microclimates (Bunn et al., 2011) and proximity to upper tree line (Salzer et al., 2014b). Disentangling the mixed signals has involved cluster analysis (Tran et al., 2017), experimental temperature sensors (Bruening et al., 2017), and simulated tree-ring proxy growth models (Bunn et al., 2018).

Despite its extreme longevity (over 2500 years (Brunstein and Yamaguchi, 1992)) and natural habitat within major Southwest headwaters (i.e., Rio Grande and Arkansas River), *P. aristata* has not received the same level of investigation for climate sensitivity as *P. longaeva*. Limited research exists for *P. aristata* (Brunstein and Yamaguchi, 1992; Ferguson and Graybill, 1983; Krebs, 1973; LaMarche Jr and Stockton, 1974), with only two precipitation proxy records (Routson et al., 2011; Woodhouse et al., 2011) and one temperature reconstruction (Salzer and Kipfmueller, 2005). Until now, no study has systematically examined the potential for *P. aristata* as a proxy for both temperature and moisture. A better understanding of the characteristics of *P. aristata* climate signals may improve this species' potential as a multi-millennia climate record,

providing new regional temperature reconstructions and improving our understanding of past

hydroclimates.

We undertook an evaluation of *P. aristata* chronologies across the Southern Rocky Mountains of

Colorado and New Mexico (Fig. A.1) to assess the variable response to climate between and

within chronology sites. We used ten new and previously collected ring-width chronologies to

answer the following questions:

1. What do the regional set of chronologies tell us about the *P. aristata* response to climate,

   and how it varies by location and site characteristics?

2. Within each sampling site, is the climate sensitivity consistent among trees that make up

   the site chronology or is there intra-site variability as documented in previous *P.*

   longaeva studies?

3. What is the potential for developing long moisture and/or temperature reconstructions

   from this set of data?

To isolate the dominant patterns of growth variability from the ring-width datasets, we used

empirical orthogonal function (EOF, Preisendorfer and Mobley, 1988) analysis at both the

chronology and the individual tree scales. We also used a modified form of hierarchical cluster

analysis (Kipfmueller and Salzer, 2010) on a matrix of on-site correlations between the

individual samples and the local climate to isolate a third set of tree growth patterns. Following

the isolation of growth signals, we constructed time series and correlated them with a regional

gridded climate dataset to assess the relationship between *P. aristata* tree-ring growth patterns and climate. Finally, we evaluated the potential for these tree-ring growth data to be used in climate reconstructions.

A.3   MATERIAL AND METHODS

A.3.1   Study Area

This investigation is set in the Southern Rocky Mountains (Southern Rockies) of the continental United States. The Southern Rockies ecoregion is characterized by multiple ranges of high, steep mountains with peaks regularly exceeding 4000 m surrounded by valleys dropping below 2500 m (Wiken et al., 2011). This dramatic variation in topography controls all aspects of the regional climate, including temperature and precipitation. Temperature decreases with elevation, but local topography plays a role as well. Closed valleys surrounded by high peaks are susceptible to temperature inversions during the winter, with dense cold air sinking to the valley bottoms and reaching temperatures below -50°C (Doesken et al., 2003). These inversions also occur at smaller spatial scales and diurnally. Precipitation is broadly controlled by elevation with annual totals ranging from 255 mm at lower elevation sites to 1750 mm on high mountains (Wiken et al., 2011). In addition, the steep topography produces rain shadow effects throughout the Southern Rockies, resulting in sharp contrasts in precipitation due to orographic effects. The majority of annual precipitation falls as snow (Wiken et al., 2011), resulting in a snowpack reservoir that is the primary source of streamflow for the numerous rivers originating in the Southern Rockies. The depth of snowpack is controlled by elevation and aspect, with high north-facing locations maintaining the deepest snow due to lower temperatures and reduced solar

radiation. The driest season in the study area is the spring interstitial period between the end of

frontal storms in April and early May and beginning of summer thunderstorms in July. Except

for this dry period, no other distinct wet or dry seasons occur.

The natural distribution of *Pinus aristata* coincides with the southern half of the Southern

Rockies ecoregion, extending from central and southern Colorado into northern New Mexico

(Fig. A.1) (Bailey, 1970). There is an additional isolated stand of *P. aristata* on the San

Francisco Peaks in northern Arizona. *P. aristata* is primarily found on the xeric, south-facing

aspect of mountains between 2700 and 3700 m, in locations not occupied by Engelmann spruce,

subalpine fir, or aspen (Baker, 1992; Schoettle and Coop, 2017). *P. aristata* habitat coincides

with the headwaters of the Rio Grande, Arkansas, and South Platte Rivers, but is rarely found

west of the North American continental divide or north of 40°N (Gilbert et al., 2019). *P. aristata*

and *P. longaeva* have no range overlap, with the division largely demarcated by the Colorado

River (Bailey, 1970). For this investigation we focused on the Colorado and New Mexico range

of *P. aristata* (36.8°N-39.2°N, 105°W-106°W), excluding the isolated stand in Arizona.

A.3.2   Data

A.3.2.1   Tree-ring data

Ten *P. aristata* collections were used in this study — five newly sampled, four previously

developed, and one an update of a previous collection (Table A.1). The previously developed

collections were selected from our inventory of all published and unpublished *P. aristata* ring-

width data. From this inventory we selected the collections with available ring-width

measurements, low incidence of dating errors (as determined by COFECHA)(Holmes, 1983), and end dates of 2000 or later to maximize the timespan for the climate response analysis. This narrowed down the previous set of collections to four sites: Black Mountain (BLK) (Brunstein and Yamaguchi, 1992; Miller, 2014; Woodhouse et al., 2011), Summitville (SMV) (Routson et al., 2011), Sheep Mountain (SHM) (Woodhouse et al., 2011), and Windy Peak (WPK) (Woodhouse unpublished). One new collection in this study, Hermit Lake (HER), was an update of a previously collected chronology (LaMarche Jr and Stockton, 1974). Ring-width data for the five previously collected sites (including original HER time series), were obtained from the International Tree-Ring Data Bank (ITRDB) and from the unpublished collection of one of the authors. The new *P. aristata* collection sites span the length of the Sangre de Cristo Mountains from central Colorado to northern New Mexico. The five new sample collections were: Antora Peak East (APE), Little Costilla Peak - High (LCH), Little Costilla Peak - Low (LCL), North of Heart Lake (NHL), and Zapata Trail Summit (ZTS) (Fig. A.1, Table A.1). These sites were identified using location data from previous genetic sampling research (Schoettle and Coop, 2017), the Arizona - New Mexico Chapter of the SEINet botanical repository (Gilbert et al., 2019), and examination of Google Earth images. The ten sites range in elevation from 2900 m at LCL to 3680 m at HER. The majority of sites (n = 7) were located on south-aspect slopes, with SHM and LCH found on east-aspect slopes, and LCL sampled on a valley floor.

During the summers of 2018 and 2019, we collected *P. aristata* increment cores from the five new sites and one updated site (Table A.1). We selected the oldest trees for sampling based on a set of physical characteristics that indicate extreme age (strip-bark growth, reduced crown,

presence of dead pith spike) (Brunstein, 2006). At minimum, two cores were collected from each tree with an increment borer, taken at breast height (1.3m), with at least 15 trees sampled per site. At five of the six sites (APE, HER, LCH, NHL, and ZTS) trees were sampled at or near the upper tree line limit of growth, but with care to exclude trees with krumholtz morphology that could distort climate sensitivity and reduce cross-dating capacity. The cores were mounted and prepared in accordance with standard dendrochronological procedure (Stokes and Smiley, 1968), the cross-dated ring-widths were measured with a Velmex measuring stage to a precision of 0.001mm, and the measurement data was stored using the Tellervo archiving software (Brewer, 2014). The years assigned to each ring-width measurement were verified with the COFECHA software (Holmes, 1983).

Because the new samples in this study were from living trees, we made an effort to select only living trees from the previous collections. In cases where the sample type was unclear, we relied on the sample code if it indicated a remnant or a living tree. All ring-width measurements from these screened collections were then stored in the Tellervo database. Total number of ring-width samples and number of trees sampled for the sets of collections, along with mean age and chronology length, are shown in Table A.1.

A.3.2.2   Climate data

PRISM monthly gridded climate data (Daly et al., 1994) were used for correlation analysis, taking advantage of the spatial extent and long period of record of the PRISM dataset. The algorithm for the gridded PRISM data includes adjustments for orographic effects on

temperature and precipitation, taking into account elevation, slope, and aspect to simulate topographically induced variability (Daly et al., 1994). PRISM monthly total precipitation, monthly average maximum temperature, and monthly average minimum temperature from the period 1895 to 2018 were downloaded at the 0.25° resolution from the KNMI Climate Explorer (Trouet and Van Oldenborgh, 2013). The PRISM data were cropped to an area extending from 30°N to 46°N to 114°W to 98°W, centered on the study area, for use in correlation analysis (Fig. A.1, climate response region).

A.3.3 Methods

A.3.3.1 Tree-ring time series development

Our goal was to investigate the potential for multiple signals both between and within collection sites, therefore we developed two separate tree-ring datasets. The first dataset ("CHRON") was a set of chronologies from each of the 10 sites used to investigate growth patterns between sampling sites. The second dataset ("TREE") was a collection of 88 individual tree-ring series used for analysis of common tree growth patterns between trees irrespective of the sampling location. Prior to developing the two datasets, we processed the data and removed juvenile growth. If multiple core samples were collected from the same tree, we averaged together the ring-width values to produce a single time series for each tree (n = 188) (Table A.1). To remove juvenile growth, we identified the maximum common interval between all ten sites (1826-2007). We removed any ring-width series with evident juvenile growth over this period, resulting in the removal of 10 ring-width series. We used the remaining 178 ring-width series to construct the CHRON and TREE datasets.

The ten chronologies in the CHRON dataset were developed as follows: We evaluated

subsample signal strength (SSS) prior to chronology construction to identify the periods of time

with a sufficient number of tree-ring width measurements to produce a strong common signal for

each chronology (Buras, 2017). A cutoff value of 0.80 for SSS was used to determine which time

periods to select from each chronology (Wigley et al., 1984). This produced a common interval

between the ten chronologies of 1826-2007 (n = 182 years). The ring-width series for each site

were truncated to match this period and standardized using the series mean. The standardized

ring-width series were then combined into a chronology using the robust bi-weight mean in the R

package dplR (Bunn, 2008; Cook et al., 1990). Mean-value standardization was used as it

preserves potential low-frequency signals present in the measurements (Kipfmueller and Salzer,

2010). More complex detrending methods were not used for two reasons. First, almost all series

used represented the last two centuries of growth in very slow-growing, long-lived trees; the few

samples with possible juvenile growth during the period of chronology construction were

deleted, removing the need to account for the influence of age on ring-width. Second, *P. aristata*

grows in open stands in remote, undisturbed locations and has never been commercially

harvested; with little to no exogenous disturbance, any low-frequency variability is assumed to

be related to climate, and of interest to this study. The consistently slow growth, lack of

exponential growth curve and tree-level decadal variability that merit this detrending approach

are illustrated in Figure A.S1 in the supplemental materials.

The TREE dataset was developed as follows: We started with the 178 individual trees used to construct the CHRON dataset. Next, we screened for the trees with continuous data over the same time period as the CHRON dataset (1826-2007). A total of 88 time series met these criteria and were selected for use in the TREE dataset. They were truncated to the common interval of 1895-2007 and detrended by their mean-value to standardize the dataset prior to analysis. The number of trees per sampling site varied from three at HER to 16 at APE.

A.3.3.2   Determining dominant modes of tree growth variability with EOF analysis

EOF analysis was used to isolate the dominant patterns of variability in the CHRON and TREE time series datasets, and then to evaluate which sites or set of trees contributed to the primary patterns of variability. The R program "prcomp" ran EOF analysis using SVD (singular value decomposition). A covariance matrix of the tree-ring data was used in the EOF calculation because all tree-ring data were measured in equivalent units and the mean-value detrending applied to the time series reduced the potential for a single series with excess variance to dominate the EOF results (Overland and Preisendorfer, 1982). Running an EOF analysis decomposes the covariance matrix into eigenvectors and their corresponding eigenvalues. The eigenvectors (also called "loadings") are orthogonal (uncorrelated) and can be multiplied with the original dataset to produce a set of time series (Anchukaitis and Tierney, 2013). Each of the time series (or "scores") corresponds to a mode of variance, which, in this study, represents a particular pattern of tree growth over time. However, the forced orthogonality of the eigenvectors produces results that may not correspond with physical realities (Richman, 1986).

To improve the interpretability of the loadings, a rotation procedure was applied to the EOF modes.

Before applying rotation to the original EOF modes, we determined the significant number of eigenvalues to retain using a modified N-rule calculation (Anchukaitis and Tierney, 2013; Preisendorfer and Mobley, 1988). This process utilizes a Monte Carlo approach, creating 10,000 synthetic white noise (Gaussian) and red noise (lag-1 autocorrelation) datasets, applying EOF analysis to the synthetic data, then determining if the original EOF eigenvalues were greater in value than the 95th percentile of the synthetic data eigenvalues. If the original EOF eigenvalues are larger than the both the white and red noise data, they are retained. A varimax orthogonal rotation was then applied to the retained original EOF eigenvalues. This process produced the rotated EOF scores for the CHRON dataset, values we used in the climate response analysis.

We ran a modified form of EOF analysis on the TREE dataset to counter the influence of an uneven sample size between collection sites (varying from three to 16 trees). First, we applied the EOF analysis to the individual tree growth series at each site (ten runs, one per site). The modified N-rule was used to determine the number of EOF modes from each collection site to retain (Table A.3). The retained EOF modes were converted into unrotated EOF scores. EOF analysis was applied a second time to the set of unrotated EOF scores producing a final set of EOF modes. A varimax orthogonal rotation was applied to the second set of EOF modes producing rotated EOF scores. This second set of TREE EOF scores was used in our climate response analysis. The two-step process reduced the influence of sample number by converting

the ring-width data into the dominant modes of growth at each site. Whereas the CHRON EOF process highlighted a single growth signal per site (i.e., chronology), the TREE EOF process allowed sites with multiple growth signals to have both growth patterns represented in the EOF analysis.

A.3.3.3   Determining modes of variability based on tree growth response to climate

We utilized a second process to identify unique modes of tree growth variability at the tree level based on methods used in a previous study of five needle pines (Kipfmueller and Salzer, 2010). Following their approach, we first investigated the correlation between local climate and each tree growth time series, then we grouped the trees based on the types of correlations to produce clusters with similar climate responses. We then combined the tree growth series in each cluster to produce a single tree-ring time series corresponding to the climate response of each tree cluster. This time series was used to evaluate the climate response in the same manner as the EOF scores. We refer to this as the "Tree-Climate Method".

In this approach, we took the same set of 178 tree-ring time series used to produce the CHRON and TREE datasets and selected all trees with a complete period of record from 1895 to 2007 (a total of 119 trees). We chose the 1895 start date to match the period of record for PRISM data. We truncated the remaining 119 series to the 1895 to 2007 period and detrended by their mean-value as done with the CHRON and TREE datasets. Next, we extracted the PRISM monthly precipitation, minimum temperature, and maximum temperature values for the data pixel located over each chronology location. The monthly climate data were averaged into three-month

seasonal time series (previous-Fall, Winter, Spring, Summer, and Fall) in the same manner as

Kipfmueller and Salzer (2010), but with additional previous-Spring and previous-Summer

seasons. Each tree was correlated with the seasonal climate record at the sampling location and

the resulting correlations were combined into a matrix of correlations. If a tree had no significant

correlations with any climate parameter, it was dropped from the matrix, reducing the final

number of trees used for the cluster analysis. The final Tree-Climate dataset used for cluster

analysis consisted of 114 trees. We calculated the clusters from the matrix using hierarchical

cluster analysis with Euclidean distance matrices and Ward's method (Ward Jr, 1963). The

stability of the clusters was determined with bootstrapped Jaccard indices calculated by the R

function "clusterboot" (Hennig, 2007). The number of clusters to keep was determined

iteratively until the average of all the Jaccard indices was highest. Once a stable number of

clusters was determined, the tree-ring series within each cluster were combined using a biweight

robust mean to produce a single time series (Cook et al., 1990).

A.3.3.4   Tree growth/climate analysis

We assessed the relationship between the tree growth time series (from both chronology-level

and tree-level analyses) and the PRISM gridded climate data with Pearson correlation analysis

(significance assessed at $p < 0.05$). Correlations were calculated for each climate parameter

(precipitation, maximum temperature, minimum temperature) and tree growth time series, from

the April of the previous year to the end of current year growing season in September ($n = 18$

months). The correlations for months in the year prior to the growing season were evaluated

because of the high lag-1 autocorrelation present in *P. aristata* (LaMarche Jr and Stockton,

1974), which may result in a growth response to climate variation in the years after the initial climate perturbation. All correlations were calculated for the time period 1895 to 2007 as this is the common time-period between the PRISM data and all CHRON EOF, TREE EOF, and Tree-Climate time series. Because the sign of EOF eigenvectors is arbitrary, and to facilitate comparisons, we reversed the sign of one EOF time series prior to the correlation calculations. The score for this time series had a strong negative correlations with the Tree-Climate time series, which are representative of the original direction of the tree response to climate. Therefore, it was reversed to match the directionality of the Tree-Climate time series.

Because of the large number of correlations being run between tree growth time series and the climate records, a high potential for spurious false positive correlations (type I errors) between the proxy record and climate data exists (Hu et al., 2017). To adjust for the high test multiplicity and concurrent increase in type 1 errors, the False Discover Rate (FDR) procedure was applied (Benjamini and Hochberg, 1995). We ran FDR using the "p.adjust" function in R with a q-value set to 0.05, the same as our p-value threshold. In addition to the corrections for high test multiplicity, adjustments were made to account for serial correlation (i.e., autocorrelation) (Hu et al., 2017). To correct for high serial correlation an adjustment equation as defined by Dawdy and Matalas (1964) was used to calculate effective degrees of freedom v_{eff}. This adjustment increases the corresponding p-value in proportion to the increase in autocorrelation, reducing the potential for a type I errors. The FDR and v_{eff} adjustments were applied to all calculations used in the climate response correlations, while only the v_{eff} adjustment was applied to the seasonal climate relationships used in the Tree-Climate Method. FDR was unsuited for the initial Tree-

Climate Method step as the correlations were single instance (one tree-ring time series and one climate time series), therefore reducing the need to assess potential false positives.

The climate response calculations were run a second time with the low-frequency variability removed prior to correlation. We applied a 30-year Butterworth high-pass filter to both the climate time series and the tree growth time series using the pass.filt function in the R package DplR (Bunn, 2008). Removing the low-frequency variability allows for comparison of the high-frequency variances in the resulting time series. The loss in correlation strength following the application of a high-pass filter will highlight time series where the low-frequency variability was an important factor in correlation. Both the original and high-pass filtered correlation calculations were used to analyze the climate sensitivity of the tree growth time series.

From the climate response calculations, we produced a regional correlation map (Fig. A.1, climate response region) for each combination of climate parameter, month, tree growth time series, and for both the original and high-pass filtered series. These maps provide a broad overview of climate response for each time series. Next, we extracted the correlation values from a smaller region located directly over the *P. aristata* sampling sites (36°N- 40°N by 108°W- 104°W) (Fig. A.1, reduced climate response region). From this reduced region, we produced a jitter plot of all correlations for the CHRON and TREE EOF time series and the Tree-Climate time series. These plots show the correlation (for $p < 0.05$) of each tree growth time series with each monthly climate variable. They also show the variation in correlation strength whether the

data was filtered or not prior to correlation. This smaller subset was used to better represent the

local climate.

A.4   RESULTS

A.4.1   Time series produced from tree growth patterns and tree growth climate signals

The EOF analysis based on the ten chronologies resulted in two primary modes of variability

(Table A.2). The first CHRON EOF (C-1), accounting for 52% of the total variance, is composed

primarily of loadings from LCH, ZTS, NHL, APE, WPK, and HER. These six sites are all

located at the upper tree line. The second CHRON EOF (C-2), accounting for 23% of the total

variance, is characterized by the two lower elevation sites, BLK and LCL, and one upper

elevation site, WPK. Two sites, SHM, and SMV, contribute to both EOF modes, with small

positive loadings for each mode.

The first step of the TREE EOF analysis, on tree-growth series within each of the 10 sites,

yielded either one or two EOFs per site (Table A.3). Seven sites had only one dominant EOF

mode of growth, and three sites, BLK, SHM, and SMV, had two significant EOF modes within

the collection site. These EOFs, 13 in all, were then used in the second round of TREE EOF

analysis. This yielded two statistically significant TREE EOF modes (T-1 and T-2) representing

41% and 21% of the explained variance, respectively (Table A.4).

The first TREE EOF mode (T-1) was characterized by very high loadings from eight EOF time

series, including most of the higher elevation sites. The second TREE EOF mode (T-2) had high

loadings from five of the series, including the two lowest elevations sites and WPK. These loadings are similar to those in the CHRON EOF results, but the difference is found at the three sites with two EOF modes each which were split between T-1 and T-2. The weakness of the SHM and SMV CHRON loadings contrasts with the strong loadings of SHM-1 and SMV-1 into T-2 and SHM-2 and SMV-2 into T-1. This suggests that a single chronology at these sites inadvertently blends two contrasting growth signals producing a weaker overall growth signal.

The third approach for examining tree growth patterns (Tree-Climate or TC) was based on cluster analysis of 114 trees from the ten sampling sites and their responses to local climate grid points. This analysis resulted in five groupings (TC-1, TC-2, TC-3, TC-4, and TC-5) with respective Jaccard indices of 0.73, 0.86, 0.48, 0.48, and 0.77. Because Jaccard indices below 0.6 are unstable and do not indicate significant patterns (Hennig, 2007), we removed TC-3 and TC-4 (and the 37 trees associated with them). TC-1 consisted of trees from nine of the ten sampling sites, particularly NHL, ZTS, and LCH. TC-2 was dominated by trees at BLK, while TC-5 was made up of trees from six of the ten sampling sites (Table A.5). BLK was the only site in which all samples fell into one cluster.

The associations between the seven tree-growth series (two CHRON EOFs, two TREE EOFS, three Tree-Climate clusters) were examined for the common period, 1895-2007 (Fig. A.2). The EOF time series pairs (C-1/C-2 and T-1/T-2) had weak correlations with one another, a logical result as EOF modes should be orthogonal and uncorrelated. The residual correlations that do exist between EOF time series pairs are a result of the shortened period for correlation (1895-

2007) relative to the full time period for the EOF analysis (1826-2007). There are broad

similarities between the pairs of TREE EOFs and CHRON EOFs even though the TREE EOF is

an effort to optimize the common signal by identifying within-site growth signals. For example,

C-1 has a very high correlation with T-1 (0.88), while C-2 has a very high correlation with T-2

(0.96), producing two groups of time series with similar variability. The strong correlation

between the two EOF pairs increases the utility of having the Tree-Climate method as an

alternate mode of tree growth analysis. The Tree-Climate time series TC-1 and TC-5 correlate

strongly with the first group (C-1/T-1), while TC-2 correlates with the second group (C-2/T-2).

However, these correlations are not as strong as the intra-EOF correlations. The TC time series

were also all significantly correlated with one another, but TC-1 and TC-5 had the strongest

correlation of 0.78.

A.4.2   Climate Response

Climate response results indicate two main types of tree growth/climate relationships consistent

among the three sets of tree growth patterns analyses. The first relationship, found in all seven

time series, shows a negative June maximum temperature response. Six of these seven series (all

but T-1) also show a positive June precipitation response. The second, and less common, climate

response relationship was a positive correlation with minimum temperature during August and

September at three sites (C-1, T-1, and TC-1). In the following sections we will discuss the two

climate response patterns in more detail, including the influence of the high-pass filter on these

relationships and the associated spatial patterns.

A.4.2.1   June correlations

Five of the seven time series show a significant correlation with both June precipitation and temperature (C-2, T-2, TC-1, TC-2, and TC-5) (Figs. A.3 and A.4) in the original and high-pass filtered series, suggesting a robust June drought stress response to warm, dry conditions in that month. One additional series (C-1) is correlated with June precipitation, but does not show any correlation with June maximum temperature prior to high-pass filtering, and one (T-1) is not correlated June precipitation or with June maximum temperature prior to high-pass filtering. The removal of low-frequency variability in the C-1 and T-1 time series exposes an underlying high-frequency negative response to June temperature in these growth series (Figs 3 and 4).

T-2 has the strongest single negative correlation with June maximum temperature ($r = -0.62$), and the strongest single positive correlation with June precipitation ($r = 0.47$) (Fig. A.5A and Fig. A.5C, respectively), with weaker but still significant correlations after the 30-yr high-pass filtering (Fig. A.5B and Fig. A.5D, respectively). The C-2 series prior to high-pass filtering also has very strong negative June maximum temperature and positive June precipitation correlations of $r = -0.58$ and $r = 0.44$ respectively. Several of the tree growth series show positive precipitation/negative maximum temperature responses with other months; however, none of these correlations are found consistently across all seven series. Negative maximum temperature correlations during the July of the previous year are the most prevalent of these, occurring with original correlations in three of the seven time series, and with six of the seven time series after the high pass filter is applied.

The spatial patterns of the June temperature correlations are similar for these seven tree growth series, especially after application of the high-pass filter (Fig. A.6). The highest correlations are all centered directly over the study region, weakening with radial distance from this region. Tree growth associations with June precipitation are somewhat more variable. All but T-1 show correlations with the high-pass filtered tree growth series that extend in a north-south pattern coinciding with the Rocky Mountains; however, the location of strongest precipitation correlation varies between the series (Fig. A.7). The strongest June precipitation correlation is centered over the study area in the C-2, T-2, and TC-2 series, while it is centered over the northern Rocky Mountains in C-1, TC-1, and TC-5. The position of highest correlation is more stable with the June maximum temperature correlations and shifts in spatial correlation do not occur to the same degree as the precipitation climate correlations.

A.4.2.2   Minimum temperature correlations

The second main tree growth/climate pattern is an association between tree growth and minimum temperatures. Three time series (C-1, T-1, and TC-1) feature significant positive correlations with minimum temperatures during the months of August and September, prior to application of the 30-yr high pass filter (Figs 3 and 4). Two of these also have weak June moisture stress signals. The application of the high-pass filter removes any significant minimum temperature correlations in all three series. This is evident in the correlation maps for August and September shown for T-1 (Fig. A.8). The original (un-filtered) T-1 has the strongest correlation with minimum temperature in August and September, with maximum r-values of 0.49 and 0.45 respectively, but after application of the 30-year high-pass filter the correlation map shows no

significant correlations remain. The original series show a concurrent increase in both August minimum temperatures and tree-ring widths over the 20th century (Fig. A.5E). Once the high-pass filter is applied (Fig. A.5F), the trend is removed, and the correlation drops to 0.22, with a significance level of p = 0.010 after FDR and v_{eff} adjustments are applied.

A.5   DISCUSSION

The analyses described here are the first undertaken to investigate the climate information in *P. aristata* tree growth across much of its range. The tree growth/climate patterns are complex, similar to the results found by Bunn et al. (2018) for *Pinus longaeva* in the Great Basin. As with *P. longaeva*, the results from our study indicate that different growth responses occur within a single site, and in certain cases these responses indicate differing climate responses.

Our first research question asked whether common tree growth signals were found between the ten *P. aristata* chronologies, and if so, how those signals related to climate variability. The CHRON EOF analysis yielded two time series (C-1 and C-2), together accounting for 76% of the common variance among the ten chronologies. This result indicates two common tree growth signals, one for trees at higher elevations (C-1) and one for trees at lower elevations (C-2). The C-1 series primarily shows a positive association with late summer minimum temperature while C-2 displays a strong moisture stress signal (positive correlation with precipitation and negative with temperature) that is particularly strong for June. However, when stripped of low-frequency signals using the 30-yr high-pass filter, both modes share a June drought stress response. This indicates that while upper elevation trees are showing a positive low-frequency response to late

summer minimum temperatures, when examined on a more annual basis, they display a response

to June drought conditions that is similar to the lower elevation *P. aristata*. Spatial patterns of

correlations indicate some differences in the June drought stress signal, with the strongest June

precipitation correlation centered over Wyoming for C-1 and over central Colorado, and more

widespread for C-2 (Fig. A.7). The temperature patterns are more similar (Fig. A.6).

Our second question asked whether multiple climate responses may exist among trees within a

single *P. aristata* sampling site. This question addressed the issue of trees within the same

chronology having different responses to climate due to microsite conditions. Two approaches

were taken to investigate this potential problem. First, EOF analysis was performed on the

individual tree-ring width series at each of the ten collection sites, followed by an EOF analysis

on the modes produced for each site. Second, cluster analysis was performed on the pattern of

tree growth/climate correlations for each tree.

In the first case, an analysis of the two TREE EOF time series (T-1 and T-2) indicated a mix of

growth signals within several of the *P. aristata* sampling sites. The BLK, SHM, and SMV

sampling sites had two significant EOF modes after the first run of TREE EOF analysis (Table

A.3). The two modes from each site fell into either T-1 or T-2 when the second EOF analysis

was applied (Table A.4). BLK-1, SHM-1, and SMV-1 had high loadings in T-2 while BLK-2,

SHM-2, and SMV-2 had high loadings in T-1. The growth patterns of the trees within these three

sites are different enough to fall into two modes and remain separate in the subsequent EOF

analysis. If growth pattern differences are primarily related to climate, we would expect the

correlations between climate and the two TREE time series to reflect the differences. This was the case, with T-1 containing a positive, late summer correlation with minimum temperature and T-2 showing a strong June drought stress signal. These results were very similar to C-1 and C-2, respectively, with the same loss of the minimum temperature correlation for T-1 after high-pass filtering and replacement with a negative association with June (and prior summer) maximum temperature. However, the separation of different signals at BLK, SHM, and SMV sites appears to have strengthened the signal of the T-2 time series producing higher correlations with June precipitation and maximum temperature than occurs in C-2. This may indicate the mixed signals present at the BLK, SHM, and SMV sites reduced the clarity of the growth signal of their respective chronologies and subsequently of the CHRON EOF time series.

The Tree-Climate cluster analysis further suggests the potential for trees to have differing climate responses within the same sampling site. The three significant Tree-Climate clusters indicate three different tree growth responses may be present within a single sampling site. Two sites (SHM and ZTS) have trees in all three clusters, one site (BLK) has trees in a single cluster, and the remaining seven sites have trees in two of the clusters. The presence of multiple growth patterns again represents the presence of multiple climate responses. TC-1 contains a weak late summer positive minimum temperature signal similar to C-1 and T-1, while TC-2 and TC-5 exhibited a June precipitation and maximum temperature correlation similar to C-2 and T-2. Like the previous time series, the application of the 30-yr high-pass filter removed the minimum temperature signal.

An examination of the Tree-Climate clusters suggests, that in all cases (BLK being the exception), trees within a site may contain differences in climate signal that could be related to microsite conditions. These microsite differences appear to exist at both low and high elevation sampling sites. An examination of the precise location of predominantly June drought-stressed trees compared to those with low-frequency positive summer temperature response may reveal differences in microsite characteristics. The differences in climate responses among the three Tree-Climate series are subtle after the low-pass filtering, but as with the TREE EOF results, some attention to the climate signal at the tree level may help refine the climate information. These results strongly suggest that legacy *P. aristata* collections should be used with care, as they may contain trees with a mix of climate signals.

A.5.1 Physical Mechanisms for Climate Responses

The predominant June precipitation/maximum temperature correlation with tree growth we observed makes sense considering the regional climatology, the timing of tree growth, and tree physiology. First it should be noted that June is the driest or second driest month at all of sampling sites. June falls between the period of active mid-latitude winter storms and the onset of mid-summer moisture in July (Sheppard et al., 2002). June precipitation is also inversely correlated with June maximum temperature across the study region (Daly et al., 1994). While there are no published studies of cambial phenology, or the timing of wood formation, for *P. aristata*, they do exist for *P. longaeva* (Ziaco et al., 2016). *P. longaeva* is the closest genetic relative of *P. aristata* (Montes et al., 2019), therefore they likely share similar physiological traits. Analysis of cambial phenology of high altitude (3300m) *P. longaeva* indicates xylogenesis

(or onset of xylem cell formation) begins in early June and is continuous until late August at which point the annual tree-ring width is completed (Ziaco et al., 2016). The onset of xylogenesis in *P. longaeva* is driven by an interaction between soil temperature and soil moisture content. Winter snowmelt provides the moisture for *P. longaeva* xylogenesis, but the requirement of sufficient cambial warming shifts the onset of tree growth to June when the soil moisture derived from the snowpack is most depleted (Ziaco et al., 2016). As *P. aristata* is also found in areas with low June precipitation, we propose that the onset of growth for *P. aristata* is also occurring during this same period of water stress. At our study sites, low precipitation and the corresponding high maximum temperatures in June could combine to increase water stress for *P. aristata* and delay the onset of xylogenesis, resulting in a narrower tree ring. Hughes and Graumlich (1996) also found a similar relationship between *P. longaeva* growth and current spring precipitation, further supporting an indication of shared tree physiology between *P. aristata* and *P. longaeva*.

Unlike the June precipitation/maximum temperature correlation, the positive correlation with minimum temperature in C-1, T-1, and TC-1 is a low-frequency signal, not evident after the high-pass filter is applied. The correlation with minimum temperature in August and September overlaps with the period where xylogenesis is ending (Ziaco et al., 2016). Upper tree line is determined primarily by temperature controls on the process of xylogenesis, with a threshold growing season average temperature controlling the position of tree line (Körner, 2012). Trees at or near the tree line, such as our T-1 samples from APE, LCH, NHL, and ZTS, exist at the threshold for sufficient growing season temperatures, with any large deviation having potentially

out-sized effects on growth (Körner, 2012). Therefore, when the months of August and September have warmer than average minimum temperatures, this could provide the needed thermal energy for these trees to extend the period of cellular division and produce a wider tree-ring. Our results show a steady increase in T-1 and C-1 ring-widths after the mid 1800s (Fig. A.5E), corresponding with a steady Northern Hemisphere increase in temperature seen in other tree-ring proxies (Wilson et al., 2016). The trend may also correspond with increases in annual minimum temperature observed across the semi-arid western U.S. (Sambuco et al., 2020; Tang and Arnone III, 2013), and the recent rapid increase in warm nights (summer minimum temperature) seen in New Mexico (Frankson et al., 2019).

A.5.2   *Potential for climate reconstruction*

Our final question asked what the potential is for developing long moisture and/or temperature reconstructions from this set of data. The *P. aristata* June moisture stress signal (positive precipitation/negative maximum temperature correlation) has the greatest potential for long-term reconstruction. Two flavors of signal exist across the seven sites. The first is robust, found at the low elevation sites (BLK, LCP) and those sites with multiple within-site growth patterns (SHM, SMV), and maintains its correlation with June climate after high-pass filtering. The time series plot of filtered June precipitation and tree growth suggests that some decadal-scale variability exists in the precipitation data that is reflected in the tree-ring series (Fig. A.5), and this should be considered in the reconstruction process. The second flavor is weaker, found at high elevation sites, and is revealed only after the dominant minimum temperature signal is removed using high-pass filtering. Both groups could be combined to produce a single regional June moisture

reconstruction; however, if the reconstruction were to include remnant samples with unknown climate correlations, caution would warrant the creation of a climate reconstruction using only the lower elevation sites where minimum temperature is not known to have a positive effect on growth.

P. aristata also shows potential for temperature reconstruction, but further research and sampling are likely required before this can be done with confidence. One issue with these trees is the strong reduction in the positive correlation with minimum temperature for C-1 and T-1 following the application of the 30-yr high-pass filtering. This may indicate the minimum temperature correlations are mostly due to similarities in low-frequency, multi-year patterns in temperature, rather than year to year variability. A similar issue was encountered during the production of a temperature reconstruction using *P. longaeva* (Salzer et al., 2014a). In that case, a 20-year smoothing spline was used to enhance the low-frequency signals and improve the strength of the temperature correlation. A future *P. aristata* temperature reconstruction may also be improved using a similar smoothing calculation. Another issue hampering a temperature reconstruction is the question of whether remnant samples can be used with confidence to reproduce temperature. The sampling sites with temperature sensitive trees contained multiple climate response signals and the remnants at those sites may also contain a similar mix of climate signals. One prospective solution could be a demographic study of a sampling site with intensive sampling that accurately maps the distribution and cohorts of trees over multiple centuries. The shifting proximity of a remnant to upper tree line could potentially be used as a proxy for increased temperature sensitivity and allow incorporation into a temperature reconstruction. Another

approach could couple fine-scale temperature measurements across an elevational gradient at a sampling site with growth modeling to better understand the temperature thresholds that result in tree growth limited by temperature rather than moisture. Both of these approaches have been utilized with *P. longaeva* (Bruening et al., 2018, 2017; Tran et al., 2017) and could be applied to *P. aristata*.

A.6 CONCLUSIONS

Rocky Mountain bristlecone pine (*P. aristata*) has the potential to produce a skillful reconstruction of June moisture variability in the Southern Rocky Mountains, with a secondary potential to reconstruct a low-frequency component of late summer minimum temperatures contingent upon additional investigatory work. Mixed climate responses within single sampling sites necessitate the careful selection of individual trees for use in climate reconstructions when using the existing chronologies. The dominant *P. aristata* tree-ring growth signal in Colorado and New Mexico is a current year June precipitation and maximum temperature sensitivity, explained by a plausible physical mechanism. The extent of this climate response across multiple sampling sites makes it an ideal parameter for a climate reconstruction. There also exists a separate set of trees with a low-frequency long-term positive response to temperature simultaneously present in trees with a weak June drought stress response at higher frequency. These temperature sensitive trees also have a potential for climate reconstruction, albeit one requiring more intensive sampling and screening for temperature response.

There are few late-spring/early-summer tree-ring precipitation reconstructions for the western U.S. outside a *P. longaeva* reconstruction in California (Hughes and Graumlich, 1996) and a Douglas fir/Limber pine reconstruction in Wyoming (Gray et al., 2004). The majority of tree-ring precipitation reconstructions are correlated with the winter prior to the current growing season. Gridded PDSI datasets such as the North American Drought Atlas (NADA) also largely reflect a cool season moisture signal (Cook et al., 2010). Streamflow in the semi-arid western U.S. peaks in late-spring/early-summer as the winter snowpack provides water through a typically dry period. Increases in late-spring/early-summer precipitation have been shown to extend the period of snowmelt runoff in high elevation river basins (Dudley et al., 2017). A *P. aristata* reconstruction could provide a record of years with a cool, wet June versus those years with a warm, dry June, adding to our pre-instrumental understanding of this relationship between winter and early summer moisture.

The original impetus for this study was the need for more tree-ring based temperature reconstructions in the semi-arid Western U.S. While our results primarily point to a June drought signal, there does exist a weaker but still significant correlation with late summer minimum temperature. Future work is needed to overcome the limitations of this study, including the construction of chronologies with a higher number of constituent samples and a more informed approach to sampling for temperature. A next step in this work is the utilization of a process-based modeling approach (Vaganov et al., 2006; Anchukaitis et al., 2020) to better select trees for temperature sensitivity. Research on *P. aristata* cambial physiology is also needed to understand the environmental factors (including temperature) controlling ring-width growth.

This could be accomplished through intensive cambial phenology (Ziaco et al., 2016). Work on tree proxies other than ring-width, such as cellular anatomy (Ziaco et al., 2016), latewood density (Briffa et al., 2001), or blue light intensity (Campbell et al., 2007) may also produce *P. aristata* time series with stronger temperature correlations.

These results represent a first step in understanding the complexity of climate sensitivity in *P. aristata*. We assumed that a close genetic relationship between with *P. longaeva* and *P. aristata* would result in complexities that are similar to those found in *P. longaeva,* and our study confirmed this assumption. Any work utilizing existing *P. aristata* chronologies must recognize this complexity and take care in sample selection to screen for the climatic response under investigation. While our focus for this investigation was on the growth patterns of living *P. aristata* trees, we were fortunate to sample a large collection of remnant wood for future work at four sampling sites (APE, HER, NHL, and ZTS). These sites contained an abundant selection of downed trees, many over 2000 years in age. At APE and NHL, we constructed continuous chronologies dating back to 847 BCE and 778 BCE respectively. To the best of our knowledge, these represent the oldest and longest dendrochronologic collection of any tree species for both Colorado and New Mexico.

Future efforts to clarify the connection between *P. aristata* tree growth and climate variability will provide the framework to develop multi-millennial tree-ring climate reconstructions from these ancient chronologies. This work could deepen our understanding of the controls on past

hydroclimate interactions, improving our understanding of how natural variability underlies and interacts with climate change.

A.8   WORKS CITED

Anchukaitis, K.J., Evans, M.N., Hughes, M.K., Vaganov, E.A., 2020. An interpreted language implementation of the Vaganov–Shashkin tree-ring proxy system model. *Dendrochronologia* 60, 125677.

Anchukaitis, K.J., Tierney, J.E., 2013. Identifying coherent spatiotemporal modes in time-uncertain proxy paleoclimate records. *Clim. Dyn.* 41, 1291–1306.

Bailey, D.K., 1970. Phytogeography and taxonomy of Pinus subsection Balfourianae. *Ann. Mo. Bot. Gard.* 210–249.

Baker, W.L., 1992. Structure, Disturbance, and Change in the Bristlecone Pine Forests of Colorado, U.S.A. *Arct. Alp. Res.* 24, 17. https://doi.org/10.2307/1551316

Benjamini, Y., Hochberg, Y., 1995. Controlling the false discovery rate: a practical and powerful approach to multiple testing. *J. R. Stat. Soc. Ser. B Methodol.* 57, 289–300.

Berkelhammer, M., Stott, L., 2012. Secular temperature trends for the southern Rocky Mountains over the last five centuries. *Geophys.* Res. Lett. 39.

Blasing, T., Fritts, H., 1976. Reconstructing past climatic anomalies in the North Pacific and western North America from tree-ring data. *Quat. Res.* 6, 563–579.

Brewer, P.W., 2014. Data management in dendroarchaeology using Tellervo. *Radiocarbon* 56, S79–S83.

Briffa, K.R., Jones, P., Schweingruber, F., 1992. Tree-ring density reconstructions of summer temperature patterns across western North America since 1600. *J. Clim.* 5, 735–754.

Briffa, K.R., Osborn, T.J., Schweingruber, F.H., Harris, I.C., Jones, P.D., Shiyatov, S.G., Vaganov, E.A., 2001. Low-frequency temperature variations from a northern tree ring density network. *J. Geophys. Res. Atmospheres* 106, 2929–2941.

Bruening, J.M., Bunn, A.G., Salzer, M.W., 2018. A climate-driven tree line position model in the White Mountains of California over the past six millennia. *J. Biogeogr.* 45, 1067–1076.

Bruening, J.M., Tran, T.J., Bunn, A.G., Weiss, S.B., Salzer, M.W., 2017. Fine-scale modeling of bristlecone pine treeline position in the Great Basin, USA. *Environ. Res. Lett.* 12, 014008.

Brunstein, F.C., 2006. Growth-Form Characteristics of Ancient Rocky Mountain Bristlecone Pines (*Pinus aristata*), Colorado. *U.S. Geological Survey*.

Brunstein, F.C., Yamaguchi, D.K., 1992. The oldest known Rocky Mountain bristlecone pines (*Pinus aristata* Engelm.). *Arct. Alp. Res.* 24, 253–256.

Bunn, A.G., 2008. A dendrochronology program library in R (dplR). *Dendrochronologia* 26, 115–124.

Bunn, A.G., Hughes, M.K., Salzer, M.W., 2011. Topographically modified tree-ring chronologies as a potential means to improve paleoclimate inference. *Clim. Change* 105, 627–634.

Bunn, A.G., Salzer, M.W., Anchukaitis, K.J., Bruening, J.M., Hughes, M.K., 2018. Spatiotemporal variability in the climate growth response of high elevation bristlecone pine in the White Mountains of California. *Geophys. Res. Lett.* 45, 13–312.

Buras, A., 2017. A comment on the expressed population signal. *Dendrochronologia* 44, 130–132.

Campbell, R., McCarroll, D., Loader, N.J., Grudd, H., Robertson, I., Jalkanen, R., 2007. Blue intensity in Pinus sylvestris tree-rings: developing a new palaeoclimate proxy. *The Holocene* 17, 821–828.

Chavarria, S.B., Gutzler, D.S., 2018. Observed changes in climate and streamflow in the upper Rio Grande Basin. *JAWRA J. Am. Water Resour. Assoc.* 54, 644–659.

Cook, E., Briffa, K., Shiyatov, S., Mazepa, V., Jones, P., 1990. Data analysis, in: *Methods of Dendrochronology*. Springer, pp. 97–162.

Cook, E.R., Seager, R., Heim Jr, R.R., Vose, R.S., Herweijer, C., Woodhouse, C., 2010. Megadroughts in North America: Placing IPCC projections of hydroclimatic change in a long-term palaeoclimate context. *J. Quat. Sci.* 25, 48–61.

Cook, E.R., Woodhouse, C.A., Eakin, C.M., Meko, D.M., Stahle, D.W., 2004. Long-term aridity changes in the western United States. *Science* 306, 1015–1018.

Daly, C., Neilson, R.P., Phillips, D.L., 1994. A statistical-topographic model for mapping climatological precipitation over mountainous terrain. *J. Appl. Meteorol.* 33, 140–158.

D'Arrigo, R.D., Jacoby, G.C., 1991. A 1000-year record of winter precipitation from northwestern New Mexico, USA: a reconstruction from tree-rings and its relation to El Niño and the Southern Oscillation. *The Holocene* 1, 95–101.

Dawdy, D., Matalas, N., 1964. Statistical and probability analysis of hydrologic data, part III: Analysis of variance, covariance and time series, *Handbook of Applied Hydrology: A Compendium of Water-Resources Technology*. McGraw-Hill.

Deser, C., Phillips, A.S., Alexander, M.A., Smoliak, B.V., 2014. Projecting North American climate over the next 50 years: Uncertainty due to internal variability. *J. Clim.* 27, 2271–2296.

Doesken, N.J., Pielke Sr, R.A., Bliss, O.A., 2003. Climate of Colorado, *Climatography of the United States No. 60.* Colorado Climate Center, Atmospheric Science Department, Colorado State University, Fort Collins, CO.

Dudley, R.W., Hodgkins, G.A., McHale, M., Kolian, M.J., Renard, B., 2017. Trends in snowmelt-related streamflow timing in the conterminous United States. *J. Hydrol.* 547, 208–221.

Emile-Geay, J., McKay, N.P., Kaufman, D.S., Von Gunten, L., Wang, J., Anchukaitis, K.J., Abram, N.J., Addison, J.A., Curran, M.A., Evans, M.N., others, 2017. A global multiproxy database for temperature reconstructions of the Common Era. *Sci. Data* 4, 170088.

Ferguson, C.W., Graybill, Da., 1983. Dendrochronology of bristlecone pine: a progress report. *Radiocarbon* 25, 287–288.

Frankson, R., Kunkel, K.E., Stevens, L.E., Easterling, D.R., 2019. 2017: New Mexico State Climate Summary (*No. NOAA Technical Report NESDIS 149-NM*).

Fritts, H., Lough, J., 1985. An estimate of average annual temperature variations for North America, 1602 to 1961. *Clim. Change 7*, 203–224.

Gilbert, E., Gries, C., Franz, N., Landrum, L.R., Nash III, T.H., 2019. SEINet: A Centralized Specimen Resource Managed by a Distributed Network of Researchers. *Biodivers. Inf. Sci. Stand.*

Gonzalez, P., Garfin, G., Breshears, D., Brooks, K., Brown, H., Elias, E., Gunasekara, A., Huntly, N., Maldonado, J., Mantua, N., others, 2018. Southwest. Impacts Risks Adapt. U. *S. Fourth Natl. Clim. Assess.* 2, 1101–1184.

Graumlich, L.J., 1993. A 1000-year record of temperature and precipitation in the Sierra Nevada. *Quat. Res.* 39, 249–255.

Gray, S.T., Fastie, C.L., Jackson, S.T., Betancourt, J.L., 2004. Tree-ring-based reconstruction of precipitation in the Bighorn Basin, Wyoming, since 1260 AD. *J. Clim.* 17, 3855–3865.

Hennig, C., 2007. Cluster-wise assessment of cluster stability. *Comput. Stat. Data Anal.* 52, 258–271.

Holmes, R.L., 1983. Computer-assisted quality control in tree-ring dating and measurement. *Tree-Ring Bull.*

Hu, J., Emile-Geay, J., Partin, J., 2017. Correlation-based interpretations of paleoclimate data–where statistics meet past climates. *Earth Planet. Sci. Lett.* 459, 362–371.

Hughes, M.K., Graumlich, L.J., 1996. Multimillennial dendroclimatic studies from the western United States, in: *Climatic Variations and Forcing Mechanisms of the Last 2000 Years.* Springer, pp. 109–124.

Jones, S.M., Gutzler, D.S., 2016. Spatial and seasonal variations in aridification across Southwest North America. *J. Clim.* 29, 4637–4649.

Kipfmueller, K.F., Salzer, M.W., 2010. Linear trend and climate response of five-needle pines in the western United States related to treeline proximity. *Can. J. For. Res.* 40, 134–142.

Knight, T.A., Meko, D.M., Baisan, C.H., 2010. A bimillennial-length tree-ring reconstruction of precipitation for the Tavaputs Plateau, Northeastern Utah. *Quat. Res.* 73, 107–117.

Körner, C., 2012. *Alpine treelines: functional ecology of the global high elevation tree limits.* Springer Science & Business Media.

Krebs, P.V., 1973. Dendrochronology of bristlecone pine (*Pinus aristata* Engelm.) in Colorado. *Arct. Alp. Res.* 5, 149–150.

LaMarche Jr, V.C., Stockton, C.W., 1974. Chronologies from termperature-sensitive bristlecone pines at upper treeline in Western United States. *Tree-Ring Bull.*

Lehner, F., Wahl, E.R., Wood, A.W., Blatchford, D.B., Llewellyn, D., 2017. Assessing recent declines in Upper Rio Grande runoff efficiency from a paleoclimate perspective. *Geophys. Res. Lett.* 44, 4124–4133.

Meko, D.M., Woodhouse, C.A., 2011. Application of streamflow reconstruction to water resources management, in: *Dendroclimatology.* Springer, pp. 231–261.

Meko, D.M., Woodhouse, C.A., Baisan, C.A., Knight, T., Lukas, J.J., Hughes, M.K., Salzer, M.W., 2007. Medieval drought in the upper Colorado River Basin. *Geophys. Res. Lett.* 34.

Miller, K., 2014. 2,462 Years of Upper Arkansas River Basin Precipitation Reconstructed from Tree-Rings at Black Mountain (Thesis). University of Arizona, Tucson, AZ.

Montes, J.R., Peláez, P., Willyard, A., Moreno-Letelier, A., Piñero, D., Gernandt, D.S., 2019. Phylogenetics of Pinus Subsection Cembroides Engelm.(Pinaceae) Inferred from Low-Copy Nuclear Gene Sequences. *Syst. Bot.* 44, 501–518.

Overland, J.E., Preisendorfer, R., 1982. A significance test for principal components applied to a cyclone climatology. *Mon. Weather Rev.* 110, 1–4.

Preisendorfer, R.W., Mobley, C.D., 1988. Principal component analysis in meteorology and oceanography. *Dev. Atmospheric Sci.* 17.

Rehfeldt, G.E., Crookston, N.L., Warwell, M.V., Evans, J.S., 2006. Empirical analyses of plant-climate relationships for the western United States. *Int. J. Plant Sci.* 167, 1123–1150.

Richman, M.B., 1986. Rotation of principal components. *J. Climatol.* 6, 293–335.

Routson, C.C., Woodhouse, C.A., Overpeck, J.T., 2011. Second century megadrought in the Rio Grande headwaters, Colorado: How unusual was medieval drought? *Geophys. Res. Lett.* 38.

Salzer, M.W., Bunn, A.G., Graham, N.E., Hughes, M.K., 2014a. Five millennia of paleotemperature from tree-rings in the Great Basin, USA. *Clim. Dyn.* 42, 1517–1526.

Salzer, M.W., Hughes, M.K., Bunn, A.G., Kipfmueller, K.F., 2009. Recent unprecedented tree-ring growth in bristlecone pine at the highest elevations and possible causes. *Proc. Natl. Acad. Sci.* 106, 20348–20353.

Salzer, M.W., Kipfmueller, K.F., 2005. Reconstructed temperature and precipitation on a millennial timescale from tree-rings in the southern Colorado Plateau, USA. *Clim. Change* 70, 465–487.

Salzer, M.W., Larson, E.R., Bunn, A.G., Hughes, M.K., 2014b. Changing climate response in near-treeline bristlecone pine with elevation and aspect. *Environ. Res. Lett.* 9, 114007.

Salzer, M.W., Pearson, C.L., Baisan, C.H., 2019. Dating the methuselah walk bristlecone pine floating chronologies. *Tree-Ring Res.* 75, 61–66.

Sambuco, E., Mark, B.G., Patrick, N., DeGrand, J.Q., Porinchu, D.F., Reinemann, S.A., Baker, G., Box, J.E., 2020. Mountain temperature changes from embedded sensors spanning 2000m in Great Basin National Park, 2006-2018. *Front. Earth Sci.* 8, 292.

Schoettle, A.W., Coop, J.D., 2017. Range-wide conservation of *Pinus aristata*: a genetic collection with ecological context for proactive management today and resources for tomorrow. *New For.* 48, 181–199.

Schulman, E., 1954. Longevity under adversity in conifers. *Science* 119, 396–399.

Sheppard, P.R., Comrie, A.C., Packin, G.D., Angersbach, K., Hughes, M.K., 2002. The climate of the US Southwest. *Clim. Res.* 21, 219–238.

Stokes, M., Smiley, T., 1968. *Introduction to tree-ring dating.* University of Chicago. Chicago Press, IL.

Tang, G., Arnone III, J.A., 2013. Trends in surface air temperature and temperature extremes in the Great Basin during the 20th century from ground-based observations. *J. Geophys. Res. Atmospheres* 118, 3579–3589.

Tran, T.J., Bruening, J.M., Bunn, A.G., Salzer, M.W., Weiss, S.B., 2017. Cluster analysis and topoclimate modeling to examine bristlecone pine tree-ring growth signals in the Great Basin, USA. *Environ. Res. Lett.* 12, 014007.

Trouet, V., Van Oldenborgh, G.J., 2013. KNMI Climate Explorer: a web-based research tool for high-resolution paleoclimatology. *Tree-Ring Res.* 69, 3–14.

Udall, B., Overpeck, J., 2017. The twenty-first century Colorado River hot drought and implications for the future. *Water Resour. Res.* 53, 2404–2418.

Vaganov, E.A., Hughes, M.K., Shashkin, A.V., 2006. *Growth dynamics of conifer tree rings: images of past and future environments.* Springer Science & Business Media.

Ward Jr, J.H., 1963. Hierarchical grouping to optimize an objective function. *J. Am. Stat. Assoc.* 58, 236–244.

Wigley, T.M., Briffa, K.R., Jones, P.D., 1984. On the average value of correlated time series, with applications in dendroclimatology and hydrometeorology. *J. Clim. Appl. Meteorol.* 23, 201–213.

Wiken, E., Nava, F.J., Griffith, G., 2011. North American terrestrial ecoregions—level III. Comm. Environ. Coop. Montr. Can. 149.

Wilson, R., Anchukaitis, K., Briffa, K.R., Büntgen, U., Cook, E., D'arrigo, R., Davi, N., Esper, J., Frank, D., Gunnarson, B., others, 2016. Last millennium northern hemisphere summer temperatures from tree rings: Part I: The long term context. *Quat. Sci. Rev.* 134, 1–18.

Woodhouse, C.A., Gray, S.T., Meko, D.M., 2006. Updated streamflow reconstructions for the Upper Colorado River basin. *Water Resour. Res.* 42.

Woodhouse, C.A., Overpeck, J.T., 1998. 2000 years of drought variability in the central United States. *Bull. Am. Meteorol. Soc.* 79, 2693–2714.

Woodhouse, C.A., Pederson, G.T., Gray, S.T., 2011. An 1800-yr record of decadal-scale hydroclimatic variability in the upper Arkansas River basin from bristlecone pine. *Quat. Res.* 75, 483–490.

Woodhouse, C.A., Pederson, G.T., Morino, K., McAfee, S.A., McCabe, G.J., 2016. Increasing influence of air temperature on upper Colorado River streamflow. *Geophys. Res. Lett.* 43, 2174–2181.

Woodhouse, C.A., Stahle, D.W., Díaz, J.V., 2012. Rio Grande and Rio Conchos water supply variability over the past 500 years. Clim. Res. 51, 147–158.

Ziaco, E., Biondi, F., Rossi, S., Deslauriers, A., 2016. Environmental drivers of cambial phenology in Great Basin bristlecone pine. Tree Physiol. 36, 818–831.

A.9   TABLES

Table A.1. The 10 *Pinus aristata* tree-ring collections used in this study. Site names and the Site Code abbreviations used in the manuscript are listed below, along with the elevation and geographic coordinates for the sampling locations. Total samples collected (i.e., cores taken with increment corer) and the number of trees sampled at each location are also included.

Site Name	Site Code	Elev.	Longitude	Latitude	Samples Collected	# of Trees Sampled	Chronology Time Period (SSS > 0.80)	Mean Tree Age
New collections								
Antora Peak East	APE	3600m	-106.200	38.327	44	20	1513-2017	423
Little Costilla Peak High	LCH	3600m	-105.223	36.823	54	21	1700-2017	249
Little Costilla Peak Low	LCL	2900m	-105.243	36.784	40	19	1826-2017	193
North of Heart Lake	NHL	3550m	-105.450	36.792	40	16	1313-2017	553
Zapata Trail Summit	ZTS	3600m	-105.486	37.647	45	17	1726-2017	214
Update of previous collection								
Hermit Lake	HER	3680m	-105.642	38.096	59	36	1394-2017	419
Previous collections								
Black Mountain	BLK	3350m	-105.689	38.713	31	17	848-2012	901
Sheep Mountain	SHM	3475m	-106.103	39.201	37	19	1495-2007	526
Summitville	SMV	3500m	-106.632	37.438	13	12	1111-2009	718
Windy Mountain (Peak)	WPK	3650m	-106.408	37.478	18	11	1136-2007	501
				Collection Totals	381	188		

Table A.2. The CHRON EOF loadings from each sampling site for EOF's C-1 and C-2.

Site Code	C-1 EOF Loadings	C-2 EOF Loadings
APE	0.232	0.015
BLK	-0.022	0.248
HER	0.208	0.012
LCH	0.313	-0.021
LCL	-0.050	0.254
NHL	0.238	0.061
SHM	0.051	0.060
SMV	0.082	0.153
WPK	0.217	0.225
ZTS	0.280	0.041
Explained Variance	52.44%	23.41%

Table A.3. The number of trees per sampling site used in first EOF analysis and the number of significant EOF modes retained per sampling site for use in Step 2 of the TREE EOF analysis. The explained variance for each site's EOF mode is also included.

Site Code	# of Trees	# of Significant EOF Modes	Explained Variance EOF-1	Explained Variance EOF-2
APE	16	1	58.6%	-
BLK	14	2	58.14%	12.74%
HER	3	1	55.70%	-
LCH	10	1	64.51%	-
LCL	4	1	69.66%	-
NHL	12	1	57.80%	-
SHM	8	2	40.55%	23.55%
SMV	10	2	50.65%	14.59%
WPK	5	1	66.72%	-
ZTS	6	1	53.26%	-
Total	**88**	**13**		

Table A.4. The loadings for TREE EOF time series T-1 and T-2, using the EOF Scores from TREE EOF Step 1 (see Table A.3).

Step 1 TREE EOF Time Series	T-1 EOF Loadings	T-2 EOF Loadings
APE	0.902	0.004
BLK-1	0.014	0.862
BLK-2	0.827	-0.142
HER	0.384	0.220
LCH	0.928	-0.100
LCL	-0.175	0.802
NHL	0.841	0.269
SHM-1	-0.110	0.735
SHM-2	0.671	-0.094
SMV-1	0.264	0.618
SMV-2	0.689	-0.081
WPK	0.573	0.540
ZTS	0.844	0.233
Explained Variance	41.27%	21.11%

Table A.5. The number of trees used in each Tree-Climate cluster shown by sampling site. The number of total trees per side does not match the number of trees used because TC-3 and TC-4 were dropped from the analysis prior to correlation with climate.

Site Code	Total # of Trees	# of Trees Used	TC-1	TC-2	TC-5
APE	16	8	3	5	0
BLK	15	12	0	12	0
HER	5	5	3	0	2
LCH	14	11	7	0	4
LCL	9	5	2	3	0
NHL	15	12	9	0	3
SHM	8	7	3	2	2
SMV	10	3	2	1	0
WPK	7	2	1	0	1
ZTS	15	12	8	2	2
Total Trees	114	77	38	25	14

A.10   FIGURES
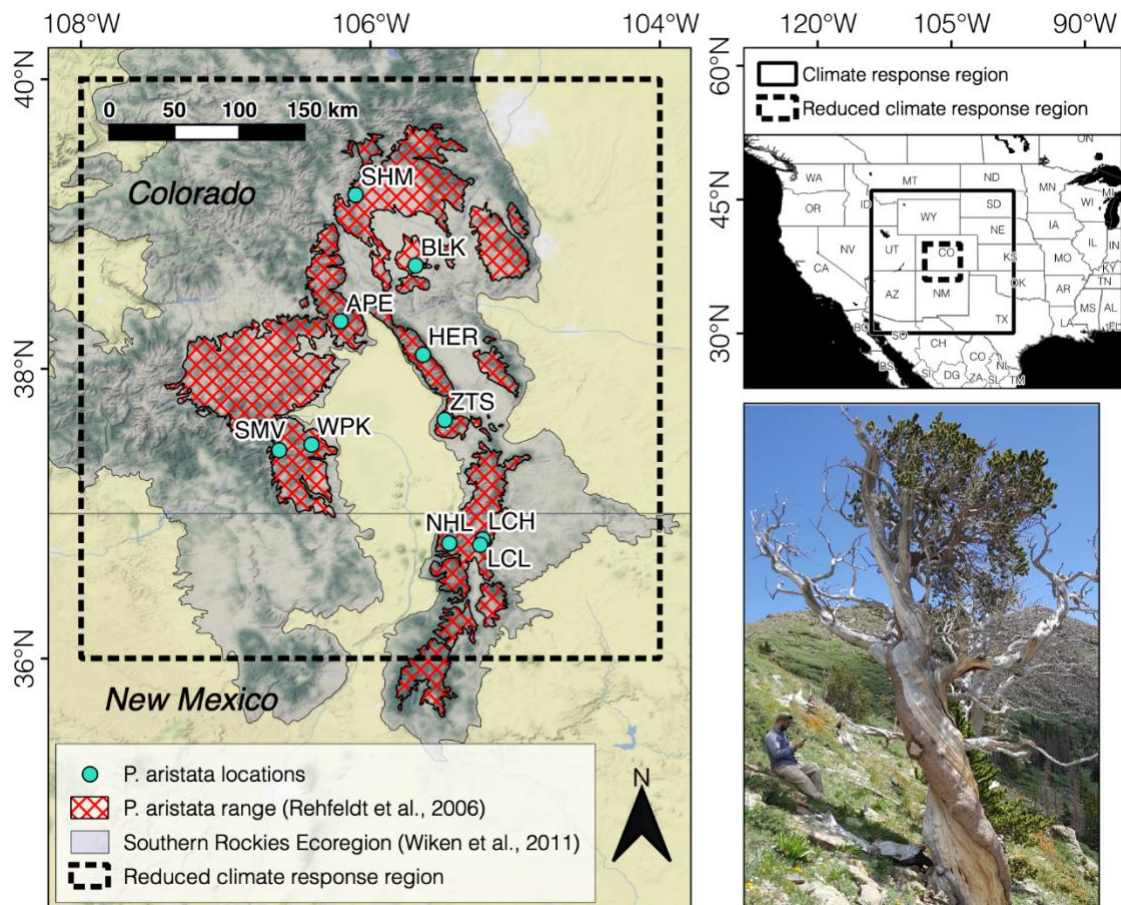
Figure A.1. Locations of *P. aristata* sampling sites used in this study (Left Panel), within the estimated range of *P. aristata* (Rehfeldt et al., 2006) and the Southern Rockies Ecoregion (Wiken et al., 2011). Location three letter codes correspond to sampling site codes in Table A.1. Upper right panel: Regions used for climate/tree growth correlations. The climate response region (solid line) shows the area used to generate correlation field maps while the dashed line box represents a reduced response region used to calculate correlations between tree growth and climate at each PRISM grid pdoint within this box. Lower right panel: >500 year-old *P. aristata* near upper tree line at the Hermit Lake collection site with narrow strip bark growth and reduced crown canopy.
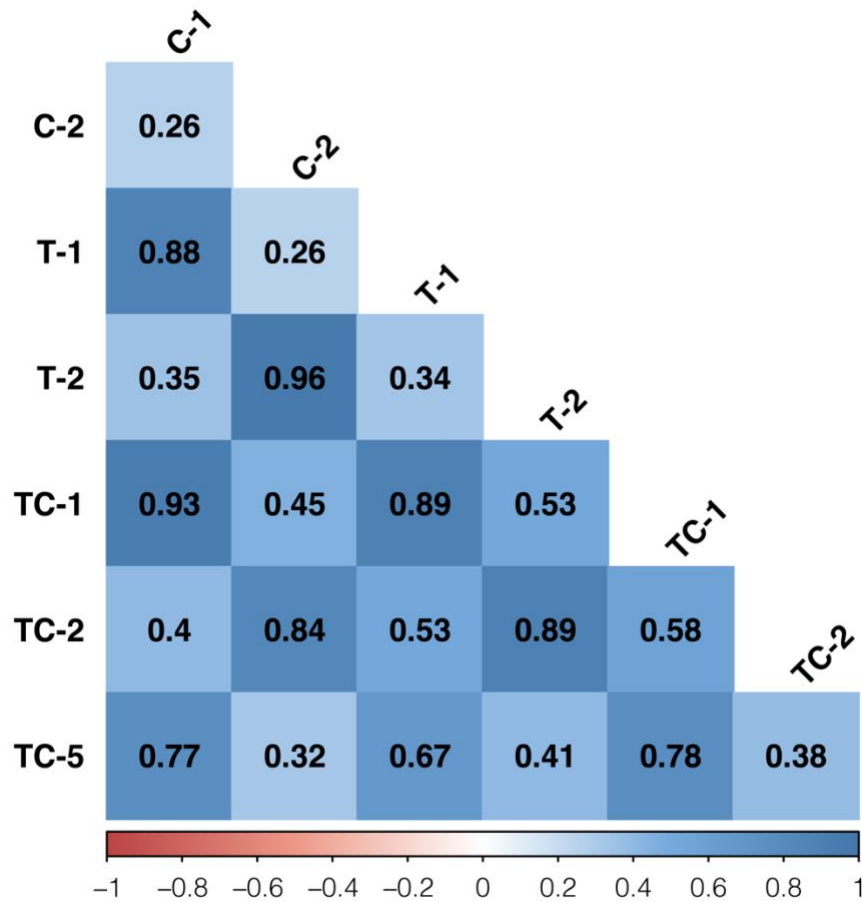
Figure A.2. Correlation Matrix between all seven time series used in analysis. Pearson correlation with a threshold value of 0.05 for analysis. Each correlation is for the common period of all seven time series (1895-2007).
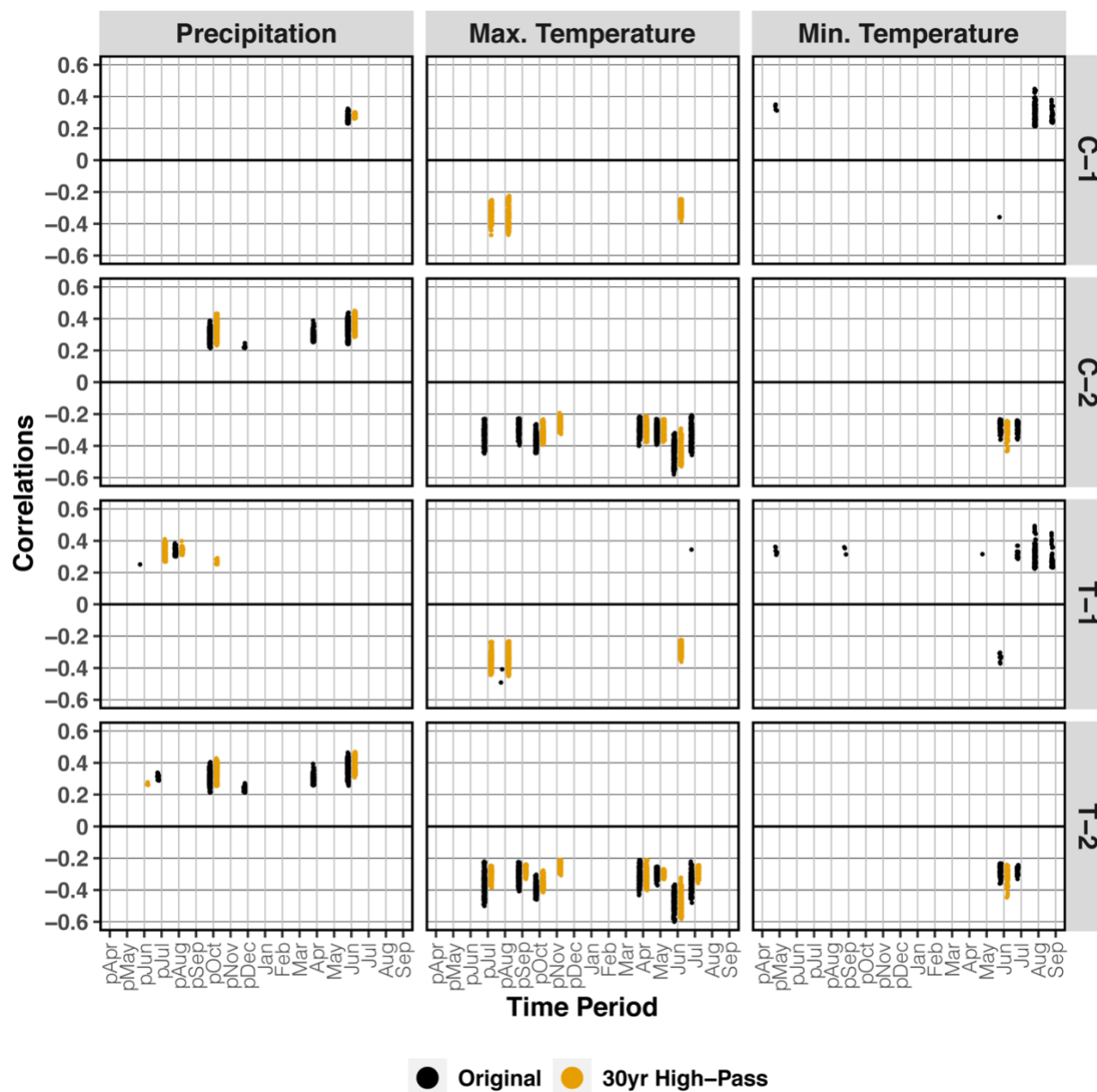
Figure A.3. Climate responses for the CHRON EOF and TREE EOF tree growth time series.
Correlation map results are compressed into jitter plots. Each cluster of points shows the range of
Pearson correlations ($p < 0.05$) for each tree growth series and monthly precipitation and
temperature, from April prior to the growth year to September of the growth year. Correlations
for the original (no filter) series are shown in black and for the 30-yr high-pass series in orange.
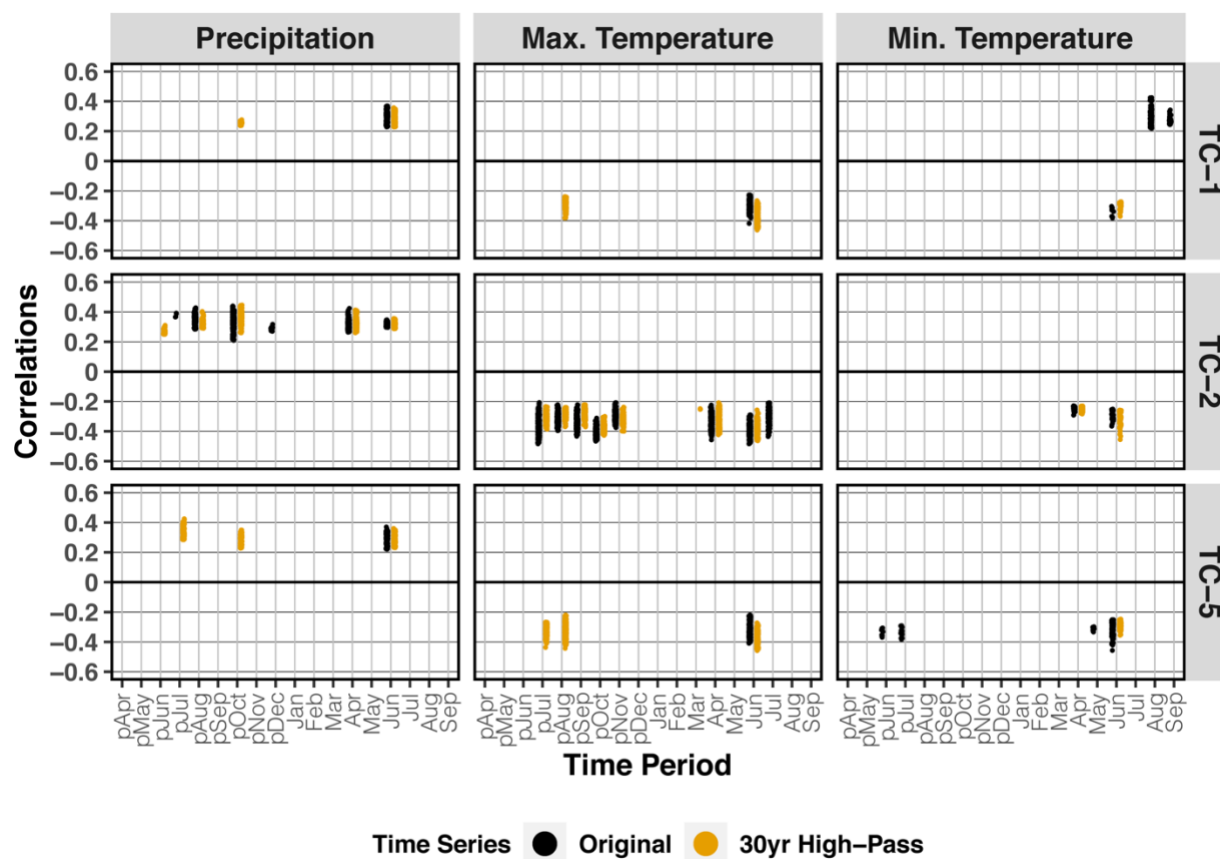
Figure A.4. Climate responses for the Tree-Climate tree growth time series. Correlation map results are compressed into jitter plots. Each cluster of points shows the range of Pearson correlations (p < 0.05) for each tree growth series and monthly precipitation and temperature, from April prior to the growth year to September of the growth year. Correlations for the original (no filter) series are shown in black and for the 30-yr high-pass series in orange.
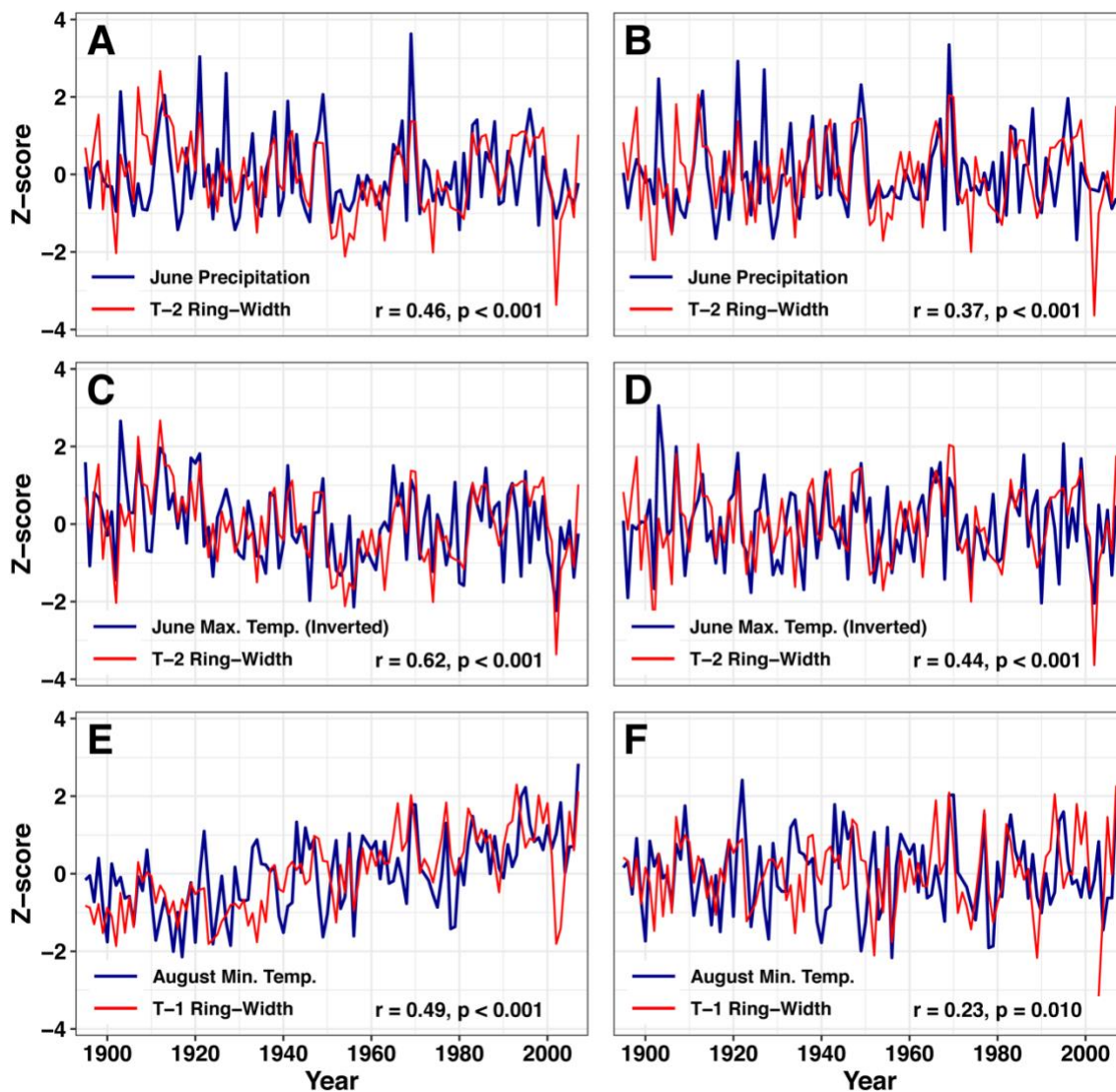
Figure A.5. Best fitting tree-growth and climate unfiltered time series (A, C, E) and the subsequent results after 30-yr high-pass filtering is applied (B, D, F) over the period 1895-2007. Climate data includes June precipitation (A, B), June maximum temperature (C, D), and August minimum temperature (E, F). Time series T-2 is used in subplots A, B, C and D, while time series T-1 is used in subplots E and F. All climate data (blue) and tree-growth data (red) is standardized to facilitate comparison. June maximum temperature data (C/D) is inverted due to the negative correlation between maximum temperature and tree growth. Correlation r-values and adjusted p-values for each subplot are included.
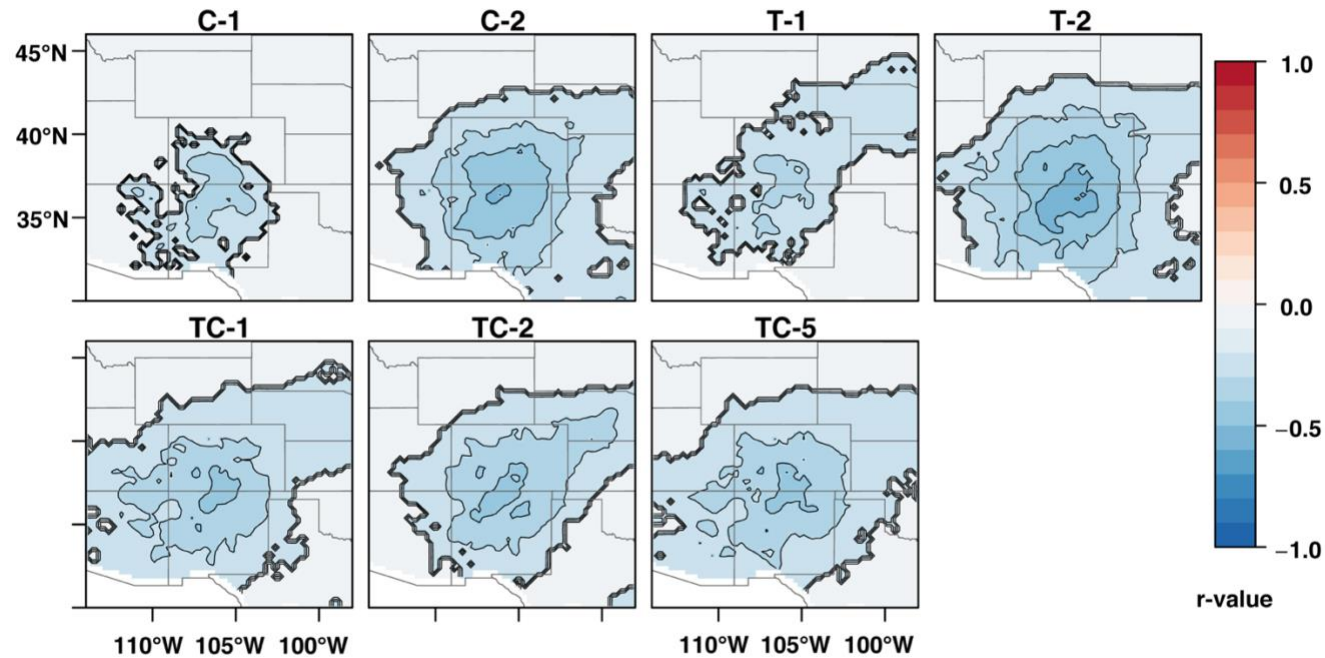
Figure A.6. June 1-month maximum temperature field correlation maps for each of the seven tree-growth series. Each colored pixel represents a significant Pearson correlation ($p < 0.05$) between the June 1-month maximum temperature at that pixel and the tree-growth series. These maps show the results when the 30-yr high-pass filter is applied to both the climate record and tree-growth time series prior to correlation. R-values are broken into intervals of 0.1 for clarity, with map contour lines delineating the boundary between each interval.
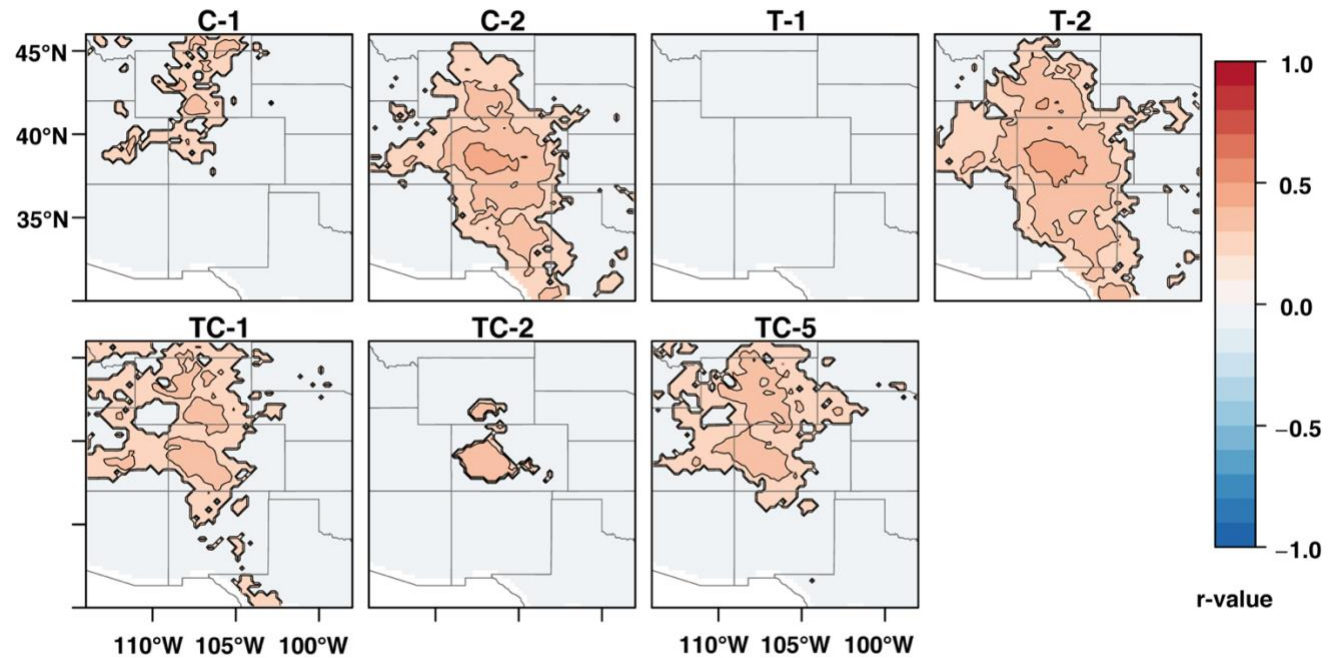
Figure A.7. June 1-month precipitation field correlation maps for each of the seven tree-growth series. Each colored pixel represents a significant Pearson correlation ($p < 0.05$) between the June 1-month precipitation at that pixel and the tree-growth series. These maps show the results when the 30-yr high-pass filter is applied to both the climate record and time series prior to correlation. R-values are broken into intervals of 0.1 for clarity, with map contour lines delineating the boundary between each interval.
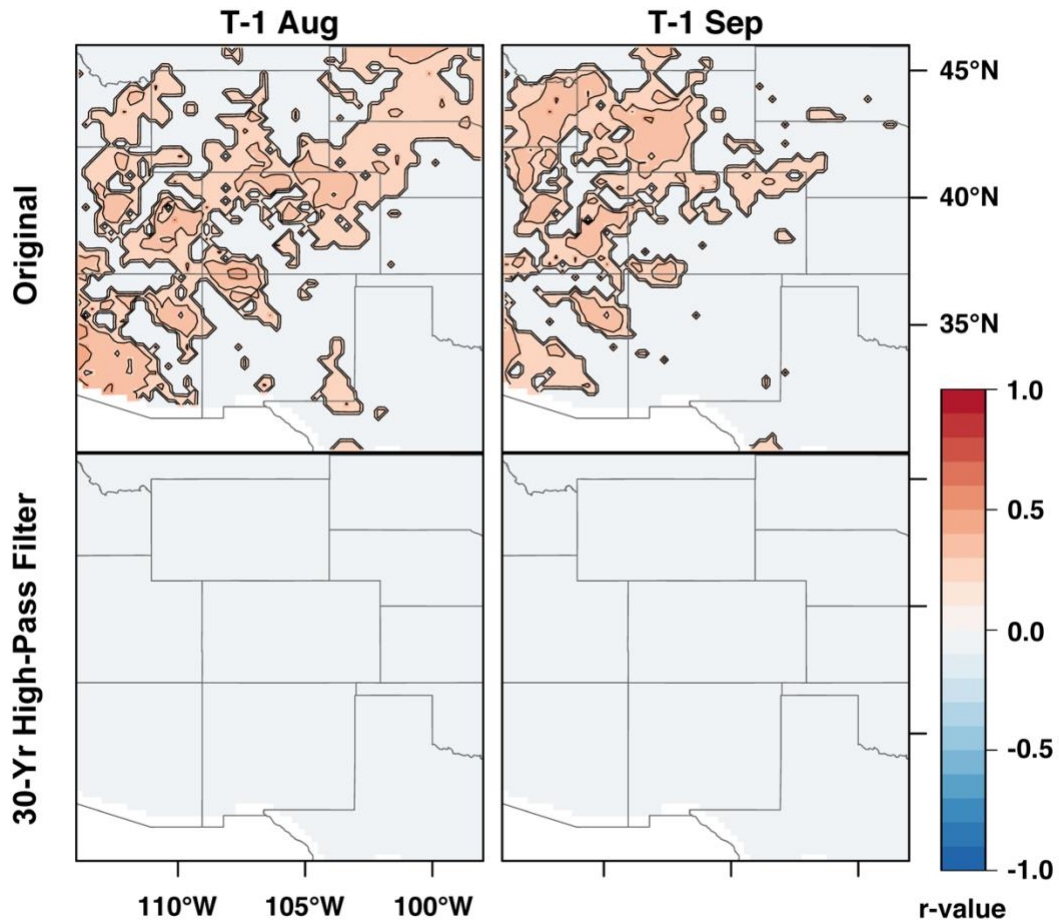
Figure A.8. August (left) and September (right) 1-month temperature field correlation maps for T-1 original (no filter) and 30-yr high-pass filtered tree-growth series. Each colored pixel represents a significant Pearson correlation ($p < 0.05$). R-values are broken into intervals of 0.1 for clarity, with map contour lines delineating the boundary between each interval.

A.11 SUPPLEMENTAL FIGURE
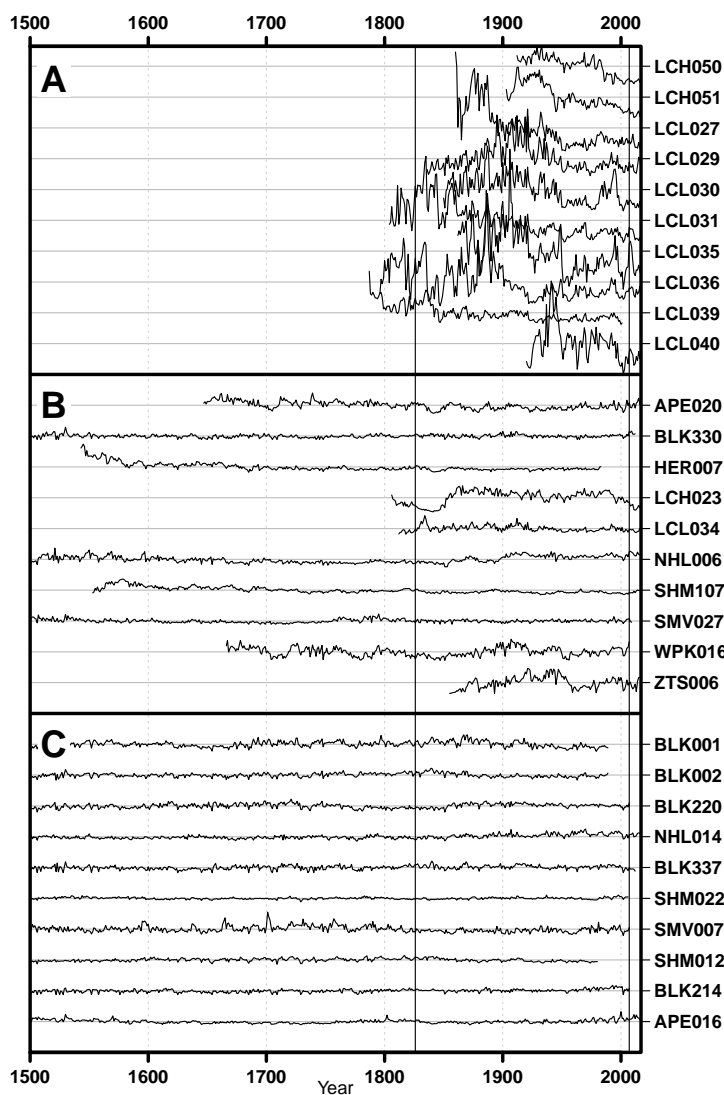
Figure A.S1. Supplemental Figure showing juvenile growth in ring width time-series. To demonstrate the outlier nature of the ten juvenile ring-width time series we removed from our analysis, we graphically compared the juvenile ring-width time series (A) with two additional sets of ring-width time series (B and C). Figure A.S1B (cont.) shows ten trees, one from each collection site, that are closest to the median length series for their respective collection site. Figure A.S1C shows the ten longest time series for the entire study (out of 188) with lengths

ranging from 1025 to 2189 years. All time series shown above are the raw ring widths which have not been detrended or modified in any way and are all presented at the same scale. The gray box represents the period of analysis (1826-2007) used in this study. Both the median length trees (B) and the oldest trees (C) clearly show the reduction in age-related influence on ring width prior to the period of our evaluation, especially compared to the juvenile trees (A). The oldest trees show a particularly stable pattern of growth over the last 500 years, with no exponential growth curve evident at all.

APPENDIX B: IN PREP - UTILIZING THE VAGANOV-SHASHKIN MODEL TO SIMULATE CLIMATE SENSITIVITY IN ROCKY MOUNTAIN BRISTLECONE PINE (*PINUS ARISTATA* ENGELM.)

William Lazar Tintor [a, b, *], Connie Woodhouse [a, b]

Paper was prepared for the journal Environmental Research Letters

[a] School of Geography, Development and Environment, University of Arizona, Tucson, AZ, 85721, USA
[b] Laboratory of Tree-Ring Research, University of Arizona, Tucson, AZ, 85721, USA

[*]Corresponding author: wtintor@email.arizona.edu (W. Tintor).

B.1   ABSTRACT

Trees at the elevational or latitudinal limits of growth play a crucial role as high resolution

proxies for past temperature variability. Rocky Mountain bristlecone pine (*Pinus aristata*

Engelm.) is a long-lived species found at upper tree line, but efforts to utilize *P. aristata* tree

rings have been hampered by mixed growth signals and weak correlations with climate. Past

work with the related Great Basin bristlecone pine utilized proxy system modeling to simulate

tree-ring growth and identify climate sensitivities. We used the Vaganov-Shashkin proxy system

model to evaluate the dynamics driving growth limitation in *P. aristata*, simulating tree-ring

development at two sites, one at the upper tree line and one near the lower elevation limit of the

species. Sensitivity tests were performed at both locations to simulate past extremes in climate.

We identified a late-spring/early summer moisture signal at the lower elevation site, which

remained stable during sensitivity tests, indicating the strong potential of bristlecone pine at this

location as a moisture-proxy in climate reconstructions. The simulated trees in the upper

elevation site were found to have moisture sensitivity which varied in timing and strength

depending on the mean temperature of the annual growing season. Sensitivity testing for the

upper site identified a robust temperature response under cooler conditions, indicating a potential

for temperature reconstruction at sites no longer limited by temperature or at locations where *P.*

aristata grows under cooler conditions. Our findings show the utility of proxy system modeling

as a tool to understand the relationship between tree-ring growth and climate variability in *P.*

aristata both in the present and under simulated past conditions.

B.2 INTRODUCTION

In the Western United States, trees at the elevational or latitudinal limits of growth have long

been recognized as the best high resolution proxies for past temperature variability (e.g.,

LaMarche Jr and Stockton 1974, Jacoby and D'Arrigo 1989). Although the tree-ring widths of

bristlecone pine (*Pinus longaeva*, Bailey 1970 and *Pinus aristata*, Engelm.) growing at upper

tree line were previously used to produce temperature reconstructions (Salzer and Kipfmueller

2005, Salzer *et al* 2014a), further reconstruction of temperature using these high elevation

bristlecone pines is difficult, due to the co-occurrence of a moisture growth signal alongside the

elevation-driven temperature sensitivity (Salzer *et al* 2014b, Bunn *et al* 2011). Recent research

also suggests that subtle topographic variability at tree line impacts the temperature sensitivity of

P. longaeva (Great Basin bristlecone pine). Only those bristlecone growing in the coldest

microclimates, with seasonal mean temperatures below a critical threshold, maintain a

temperature sensitivity evident in tree-ring growth variability (Tran *et al* 2017, Bunn *et al* 2018).

Before developing additional bristlecone-based proxies of temperature, work is needed to

disentangle the factors driving complex climate sensitivities in these species.

We build on prior research with *P. longaeva* (Bunn *et al* 2011, Tran *et al* 2017, Bruening *et al*

2017, Bunn *et al* 2018) and *P. aristata* (Salzer and Kipfmueller 2005, Routson *et al* 2011,

Woodhouse *et al* 2011) to investigative the climate sensitivity of *P. aristata* (Rocky Mountain

bristlecone pine) at a new site in New Mexico that was sampled not only at tree line, but also

near the lowest latitudinal limits of the species range (Schoettle and Coop 2017). Because of the

arid climate, we expect these *P. aristata* may be sensitive to moisture, but it may be possible that

the tree line ecotone environment is cool enough to limit growth or contain cooler microsites that limit growth. If this is the case, these trees have the potential to document temperature variability. This study seeks to determine whether these tree line *P. aristata* are limited by temperature today, and if not, whether they were limited in the past when temperatures were cooler. Our first objective was to understand the current dynamics of growth limitation related to climate in *P. aristata*, determining their utility as proxies for temperature or moisture variability. Our second objective was to evaluate changes in *P. aristata* climate sensitivity that potentially occurred during the cooler climates observed in independent paleoclimatic records, thereby determining the stability of their climate sensitivity over time.

To meet the first objective, we used two new *P. aristata* tree-ring chronologies developed for this study and a new temperature dataset recorded at each chronology site to simulate tree growth using the Vaganov-Shaskin Model (VSM) (Vaganov *et al* 2006, 2011, Anchukaitis *et al* 2020). The model outputs from the VSM were used to identify how climate limits growth and they allowed us to estimate the timing and the type of climate sensitivity experienced by trees at the two sites, one at upper tree line and one near the lower elevation limit of the species range. To address the second objective, we ran a series of sensitivity tests using modified VSM climate inputs to determine if the tree response to climate during a cooler period in the past was different from the modern period response. These sensitivity tests, in which we varied both temperature and precipitation, provided a framework to evaluate the potential for how temperature may have limited *P. aristata* growth in the past. While conducted at a single study site with only two chronologies, the results of this investigation shed light on the climate sensitivities of bristlecone

pine in the Southern Rockies, and provide insights on how best to take advantage of the multi-millennial length records from *P. aristata* to document climate variability over the Common Era (0-2000 CE).

B.3   DATA AND METHODS

B.3.1   Temperature Data Collection

The VSM requires daily climate data (precipitation and temperature) for tree growth simulation. Because site-specific seasonal mean temperature largely controls the climate sensitivity of trees (Tran *et al* 2017, Bunn *et al* 2018), the study required locally accurate temperature records. This was accomplished by placing a temperature logger on each of the 35 sampled trees for one year (Fig. B.1A and B.1B). In order to then convert the single year of logger data into multi-year temperature records for the VSM, we calibrated mean monthly data from two additional loggers placed near the closest weather station (Shuree SNOTEL Fig. B.1A). From this procedure, we derived a set of monthly temperature adjustments between the weather station and the sampling sites, converting the long-term Shuree temperature data into a synthetic multi-year (1989-2016) temperature record for each sampling site (See Supplemental B.S1 for a detailed description of this process).

B.3.2   Tree-Ring Collection and Processing

The tree-ring sampling location, Little Costilla Peak in the southern Rocky Mountains (henceforth LCP, 36.8N, 105.2W, Fig. B.1A) supports an extensive spatial distribution of *P. aristata,* allowing exploration of growth limiting conditions along an elevational gradient. The

entire southern slope of LCP is characterized by a *P. aristata*-dominant forest, with aspen and Engelmann spruce interspersed among the bristlecone overstory indicating past disturbance. We selected two sub-sites for intensive sampling: Little Costilla Peak - High (LCH), at the upper limits of growth (3600 m.a.s.l), to assess the potential of tree line *P. aristata* as a proxy for past temperatures, and Little Costilla Peak - Low (LCL), a control site near the lower limit of growth (2900 m.a.s.l.), and less likely to be temperature limited.

We used visual criteria (Brunstein 2006) to sample trees that appeared at least 100 years old, collecting two cores per tree (19 trees at LCH and 16 at LCL). The samples were prepared, cross-dated, and measured according to standard dendrochronological procedure (Stokes and Smiley 1968, Holmes 1983, Bunn 2008). Tree-ring core measurements were averaged by tree. We removed nine LCH series because the corresponding loggers were damaged or were buried by snow for over one month and we removed six LCL series due to juvenile growth. This reduced the total number of tree-ring series to 20, with ten trees per site. Because the VSM simulates tree-ring formation under ideal growing conditions, without age-related trends, we standardized each time series using a spline with a wavelength of 2/3 the series length (Cook and Peters 1981), removing low-frequency growth trends not likely to be replicated in the VSM. We used a biweight mean to develop two chronologies (LCH and LCL), each extending from 1909-2016 (n = 97 yrs.).

B.3.3   Tree-Growth Modeling

To investigate growth limitations on *P. aristata*, we began by calculating a set of seasonal

precipitation correlations and seasonal temperature partial correlations for each chronology. The

correlations and partial correlations provided an initial assessment of the *P. aristata* climate

sensitivity and a cross-reference to aid evaluation of VSM outputs. We used a seasonal

correlation analysis procedure (Seascorr, Meko *et al* 2011, Zang and Biondi 2015) at one, two,

and three month intervals from the August of the previous year to the current September,

comparing the LCH and LCL ring-width chronologies and monthly precipitation and

temperature data from (1985-2016). Because Seascorr analysis requires at least 31 years of data

for bootstrapping confidence intervals, climate data were extracted from the 4km resolution

PRISM gridded climate product (Daly *et al* 1994), at the pixel most closely corresponding with

the LCH site (36.82°N, 105.22°W) and the LCL site (36.79°N, 105.24°W).

After assessing climate correlations, we ran the Vaganov-Shashkin Model (VSM), to simulate

LCH and LCL tree-ring growth and interpret the climate relationships we found in the

correlation calculations. The VSM simulates conifer tree-ring growth using stepwise linear

functions of temperature, soil moisture, and light to estimate daily growth rates. Following the

dendrochronological principle of limiting factors (Fritts 1976), the most limiting climatic factor

controls overall growth rate, determining the number of cells produced and the width of the

annual synthetic tree ring. The accuracy of the model is assessed by comparing the synthetic

ring-width time series with the actual ring-width time series. The three VSM growth outputs

provide an estimation of timing and type of the primary climate limitation on growth, and are as

follows: the growth rate as limited by temperature, the growth rate as limited by available soil

moisture, and the overall growth rate as determined by the first two rates. Vaganov *et al* (2006, 2011) and Evans *et al* (2006) contain a complete description of the model process, and Anchukaitis *et al* (2020) describes the MATLAB version of the VSM used in this study.

The VSM simulation was run for LCL and LCH from 1989 to 2016, using the temperature time series for each chronology site and the PRISM 4km precipitation data used in the initial correlation analysis. Due to potential noise in the VSM output, caused by slight variation in the parameters used while tuning the model, we ran an ensemble of 101 VSM runs, using a preselected set of model parameters (one for each site), in a process described in Supporting Information B.S2. The simulation results (i.e., growth rates, transpiration rates, etc.) from the 101 VSM runs were averaged to produce a set of mean growth and environmental outputs for LCH and for LCL. The 28-years of simulated growth at LCL and LCH were averaged together to better facilitate comparison between two sites. Two LCH analysis years, 2007 and 2011, were selected to compare simulated instances of high and low growth rates, respectively.

B.3.4   VSM Sensitivity Testing using Reconstructed Paleoclimates

After assessment of the modern climate limitations on *P. aristata* growth, we ran a series of sensitivity tests to address our second objective concerning the VSM growth response of *P. aristata* under the past cooler conditions. The southwestern United States has experienced an annual average temperature increase of 0.9°C between 1901 and 2016 (Vose *et al* 2017) and evidence suggests the recent warming is greater than any experienced in the last millennium. The cooler conditions in previous millennium, documented through tree-ring reconstructions (Salzer

and Kipfmueller 2005, Wilson *et al* 2016), increase the possibility that presently moisture limited

trees could have been temperature limited prior to the 20th century. However, dendroclimatic

reconstructions for the western U.S. also document the occurrence of "megadroughts"

(Woodhouse and Overpeck 1998), defined as more severe than droughts experienced over the

instrumental period. While cooler conditions could result in tree growth limited by temperatures,

could severe drought outweigh this, causing growth to be limited by moisture? In order to

investigate this, the sensitivity testing targeted a period with both cooler and drier conditions.

To test the potential influence of cooler conditions on *P. aristata* climate sensitivity, we adjusted

the modern (1989-2016) VSM precipitation and temperature data to reflect past climate

conditions. We applied the adjustments to the temperature (simulating a cooler climate), to both

temperature and precipitation simultaneously (simulating a cooler climate with a megadrought),

and to precipitation alone (simulating megadrought with modern warmer temperatures). The

climate adjustments for temperature and precipitation were for the period 1573-1600 and were

derived from CCSM3 TraCE modeled data (Liu *et al* 2009) and North American Seasonal

Precipitation Atlas (NASPA, Stahle *et al* 2020) tree-ring reconstruction data, respectively (See

Supplemental B.S3 for full description of paleo-climate adjustments). This period was selected

because it was estimated by the NASPA reconstruction to be the driest period and by the TraCE

model to be the third coldest period at LCP during the last 600 years, allowing us to simulate

both colder and drier conditions using the same time period. The interval of 28 years was chosen

to match the length of the modern (1989-2016) period used in initial VSM testing. The adjusted

climate datasets were then used to run three sets of VSM sensitivity test simulations at LCH and

LCL: PTMP (past temperatures with modern precipitation), PMPP (past temperatures with past precipitation), and MTPP (modern temperatures with past precipitation). Each simulation was run 101 times for LCH and LCL, using the ensemble parameter pairs from the modern VSM runs.

B.4   RESULTS AND DISCUSSION

B.4.1   *Pinus aristata seasonal climate correlations*

Correlation analysis of ring-width chronologies at LCH and LCL produced two distinct responses to climate (Fig. B.2). The upper elevation LCH chronology had a mixed climate signal, with few monthly periods containing significant correlations. The strongest precipitation correlations (p < 0.01) were positive for late winter/early spring (Feb-Mar, Jan-Mar, and previous Nov-Apr) and the most consistent temperature partial correlation primarily reflected a strong negative correlation with prior summer temperatures (Fig. B.2A). In contrast, the lower elevation LCL ring-width chronology had a stronger precipitation signal, correlating positively with late spring/early summer precipitation, and weaker negative correlations with mid-summer temperatures (Fig. B.2B). The strongest LCL precipitation correlation was for May-June (2 month), r = 0.70. This corresponds with results from Tintor and Woodhouse (2021) which found a strong June moisture signal at LCL and at other lower elevation *P. aristata* sites across the Southern Rockies. However, the negative temperature correlation during the same spring/summer months as seen in Tintor and Woodhouse (2021) is not evident in the partial temperature correlations calculated using the Seascorr process. There is a strong negative correlation between LCL temperature and precipitation data during May (r = -0.63) and June (r =

-0.53), indicating an inverse relationship that the partial correlation calculation likely removed. The LCL and LCH correlations do not indicate any statistically significant ($p < 0.01$) positive correlation with temperature. Based on these results, a strong late spring/early summer moisture at LCL signal is evident, in agreement with previous research, while it is less clear how climate may be limiting growth at LCH.

B.4.2   *Assessing Synthetic Bristlecone Growth*

The 1989-2016 VSM simulations produced synthetic ring-width time series that closely replicate the measured ring-width chronologies at LCH and LCL (Figs. B.S1 and B.S2). The average correlations for the 101 ensemble runs are $r = 0.55$ (SD = 0.022) for LCH and $r = 0.66$ (SD = 0.024) for LCL, falling within the range of past *P. longaeva* VSM applications (Bruening *et al* 2018, Anchukaitis *et al* 2020), indicating successful simulation of *P. aristata* growth processes. The average VSM simulated growth rates (Figs. B.3A and B.3C) and environmental parameters (Figs. B.3B and B.3D) for LCH and LCL show similarities and differences. At both sites, simulated tree growth (Gr, black line) begins in April and keeps pace with the temperature limitation on growth (GrT, red line). Simultaneously, the snowpack melts and decreases to zero (SNOW, dashed black line) while replenishing soil moisture (SM, blue line). As temperatures rise through late spring, the increasing tree transpiration rate (TRANSP, black line) in the model begins to dry the simulated soil (lower SM values), and the soil moisture limitation on growth (GrW, blue line) begins to impact the growth rate. Once a drying threshold is reached (the blue line drops below the red line in Figs. B.3A and B.3C), the growth rate is now moisture limited and begins to decline. In the case of LCH, the soil moisture limitation on growth intermittently

drops below the temperature limitation threshold several times throughout the season, indicating that growth may occasionally be limited by moisture. As temperatures begin to cool in late summer, the transpiration rate is reduced and the growth may return temporarily to temperature limitation, ultimately ceasing once a temperature threshold is reached.

The LCH mean of ensemble values (Fig. B.3A, Table B.1) does not show moisture limitation until day 222 (Aug. 10th) and moisture limitation affects only 4% of the growing season days. In 21 of the 101 ensemble runs, no moisture limitation is evident, and growth remains temperature limited. The mix of moisture-limited and temperature-limited ensemble runs may explain the weaker LCH climate relationships in the correlation analysis. The LCL mean of ensemble values (Fig. B.3C, Table B.1) shows a clear moisture response beginning on day 162 (June 11th) and continuing until day 264 (Sept. 21st), with the timing of initial moisture deficit corresponding with the correlation analysis early summer precipitation relationship. Modeled environmental variables in Figure B.3B and B.3D help explain the different *P. aristata* responses at LCH and LCL. Higher average transpiration at LCH (2.91 mm/day) versus LCL (1.89 mm/day) is offset by a deeper snowpack (306 mm for LCH vs. 95 mm for LCL), keeping LCH soil moisture elevated late into the growing season thus reducing soil moisture limitations. Snowpack at LCL has also melted out by day 120 (vs. 174 at LCH). This earlier peak in soil moisture combined with less snowpack drives a faster rate of soil moisture limitation at LCL, quickly pushing the modeled trees into moisture stress in spring.

We selected two years from the LCH results to analyze annual variability within the 28-yr range of values, choosing a high-growth year (2007) and a low-growth year (2011) (Fig. B.4). There are large differences in the percentage of growing season under moisture limitation between the 2007 and 2011 (12% for 2007 vs. 50% for 2011) (Fig. B.4A and C respectively, Table B.1). There is a deeper snowpack in 2007 (346 mm vs. 221 mm in 2011) (Figs 4B and 4D), with more growing season precipitation (323 mm vs. 187 mm in 2011), and lower average growing season temperatures (9.62 C) compared to 2011 (10.82 C) (Table B.1). The higher precipitation and cooler temperatures at LCH in 2007 allow soil moisture to remain elevated later in the summer producing conditions for temperature-limited *P. aristata*. The 2011 LCH results have a similar growth pattern to the LCL VSM results, with a majority of the growing season limited by soil moisture beginning in the early summer.

This variability in climate response at LCH could explain the poor climate correlations. The trees at LCH are not insensitive to climate variability, but the response is unstable and depends on a multivariate, non-linear interaction of environmental conditions. The trees are at a threshold between climate responses, and the VSM model captures the climate sensitivity switches. Tran *et al* (2017) found the transition between type of climate sensitivity in *P. longaeva* was determined by a Seasonal Mean Temperature (SMT, Paulsen and Körner (2014)) threshold varying from 7.4 to 8.0C. Above this temperature range trees were moisture sensitive and below they were temperature sensitive. The 28-year SMT calculated from the synthetic LCH temperatures is 7.66, near the middle of this threshold range and further evidence that the current upper tree line *P. aristata* exist in a liminal space between climate sensitivities.

B.4.3   16th Century Sensitivity Testing

Using a temperature simulation (TraCE-21ka) and a precipitation reconstruction (NASPA) for a megadrought in the late 16th century (1573-1600), we adjusted the modern VSM climate parameters to run three sets of VSM sensitivity tests at the LCH and LCL sampling sites (Fig. B.5, Tables 2 and 3). The three tests evaluated 1) late 16th century temperatures with modern precipitation (PTMP), 2) late 16th century temperatures and precipitation (PTPP), and 3) modern temperatures with 16th century precipitation (MTPP). The monthly temperature adjustments using the CCSM3 TraCE simulation cooled the temperature records at LCH and LCL between 0.55°C (June) and 1.53°C (November) (Table B.S1). The precipitation adjustment from NASPA reduced the modern cool season (DJFMA) precipitation to 71.2% of the modern totals, and the summer (MJJ) to 99.6% of the modern totals (Table B.S2), clearly indicating that this was a winter drought, with similar summer precipitation to the modern 1989-2016 study period (PTMP, PTPP, MTPP)

Compared to the modern VSM runs, two of the LCH sensitivity tests with past climate parameters (Fig. B.5 PTMP-LCH and PTPP-LCH, Table B.2) produce unique results. When a late 16th century cooling adjustment is applied to the LCH model (Fig. B.5 PTMP-LCH), all moisture limitation disappears. The length of growing season drops 14 days to 101, near the 94-day limit of growth that is estimated to produce tree lines (Paulsen and Körner 2014). The addition of moisture stress from a megadrought on top of the late 16th century cooling does not change the climate response at LCH and the simulated tree growth remains entirely temperature

limited (Fig. B.5 PTPP-LCH). This suggests the LCH *P. aristata* were very likely responding to temperature during those times; we also infer that any moisture limitation inference based on the current ring-width relationship with precipitation may not hold for periods prior to the 20th century warming. Adding a megadrought to modern temperature conditions (Fig. B.5 MTPP-LCH) increases the period of moisture sensitivity to 12% of the growing season and moves the date of sensitivity up to late July. While not as dramatic as the annual variability in the 2011 LCH results (Fig. B.4C, Table B.1), this increase in moisture sensitivity would suggest that a megadrought under current conditions would further increase the moisture sensitivity of the trees at only LCH.

All three LCL sensitivity tests (Fig. B.5 PTMP-LCL, PTPP-LCL, and MTPP-LCL, and Table B.3) display a moisture limitation signature similar to that of the modern LCL run (Fig. B.3). The 16th century temperature adjustments (PTMP and PTPP, Fig. B.5 PTMP-LCL and PTPP-LCL) delay the initial onset of growth, but soil moisture limitation still begins in June (Table B.3). These sensitivity tests suggest that the LCL trees remain moisture limited even under cooler and drier conditions, increasing our confidence that a persistent, stable, and strong moisture signal occurred at LCL in the past.

B.5   CONCLUSION

This study's primary question was to determine if the tree-line *P. aristata* at LCP were limited by temperature and are therefore suitable as proxies for temperature reconstructions. The correlation analysis and VSM modeling clearly show that the upper elevation trees (LCH) are not

robustly temperature limited, while the lower elevation trees at LCL are consistently limited by moisture. The upper tree-line LCH trees switch between precipitation and temperature sensitivity depending on annual climate conditions, while the lower elevation LCL trees contain a consistent late-spring/early-summer moisture signal. VSM sensitivity testing resolved the second question of this study, whether the trees at upper tree-line were sensitive to temperature variability in the past. When the VSM simulated a cooler, 16th century climate the trees at LCH were clearly temperature limited and remained so even under extreme drought stress. Meanwhile, the same VSM sensitivity tests run at LCL indicated a stable, long-term moisture response under cooler climate regimes.

The VSM simulation and the VSM sensitivity testing highlight two points for future work: first, the LCL dataset appears highly suitable for use as a moisture-proxy in climate reconstructions, and second, trees at LCH and other tree line *P. aristata* sites should be carefully evaluated before use in climate reconstruction. Not only do the LCH trees respond to temperature thresholds from year to year, but it is possible that growth at this site was largely limited by temperature in the past. This result, however, does not broadly eliminate all tree-line *P. aristata* collections from use in future temperature reconstructions, but suggests potential opportunities. The LCH study site is located near the southernmost extent of *P. aristata* and therefore is warmer and drier than other previously sampled *P. aristata* stands. Relative to the average annual climate conditions at *P. aristata* tree line sites from Tintor and Woodhouse (2021), LCH is 3.2°C warmer (3.8°C vs. 0.6°C) and receives 243 mm less precipitation (632 mm vs. 875mm) (Daly *et al* 1994). A dendroclimatic collection sampled at a higher latitude, elevation, and/or in a cooler microclimate

may contain a temperature growth response, but researchers should take care to investigate potential mixed climate sensitivities before developing a reconstruction.

Finally, this study provided a new explanation for the apparently weaker climate sensitivity of upper elevation tree-line *P. aristata* samples seen in other research (Tintor and Woodhouse 2021). The annual VSM growth curves at LCH showed a high variability in type of climate response, switching between temperature and moisture sensitivity from year to year. These trees may not be insensitive to climate, but instead exist at a climatic threshold that results in a variable response to climate, resulting in a less clear relationship with monthly climate parameters. These results show the power of proxy system modeling to better understand the tree-ring/climate relationship, providing confirmation of the suitability of certain collections for use in climate reconstructions, while also helping researchers avoid using samples from locations where the trees may experience complex non-linear relationships with climate.

B.6   ACKNOWLEDGEMENTS

B.7   WORKS CITED

Anchukaitis K J, Evans M N, Hughes M K and Vaganov E A 2020 An interpreted language implementation of the Vaganov–Shashkin tree-ring proxy system model *Dendrochronologia* 60 125677

Bruening J M, Bunn A G and Salzer M W 2018 A climate-driven tree line position model in the White Mountains of California over the past six millennia *Journal of Biogeography* 45 1067–76

Bruening J M, Tran T J, Bunn A G, Weiss S B and Salzer M W 2017 Fine-scale modeling of bristlecone pine treeline position in the Great Basin, USA *Environmental Research Letters* 12 014008

Brunstein F C 2006 *Growth-Form Characteristics of Ancient Rocky Mountain Bristlecone Pines (Pinus aristata), Colorado* (U.S. Geological Survey)

Bunn A G 2008 A dendrochronology program library in R (dplR) *Dendrochronologia* 26 115–24

Bunn A G, Hughes M K and Salzer M W 2011 Topographically modified tree-ring chronologies as a potential means to improve paleoclimate inference *Climatic Change* 105 627–34

Bunn A G, Salzer M W, Anchukaitis K J, Bruening J M and Hughes M K 2018 Spatiotemporal variability in the climate growth response of high elevation bristlecone pine in the White Mountains of California *Geophysical Research Letters* 45 13–312

Cook E R and Peters K 1981 The smoothing spline: a new approach to standardizing forest interior tree-ring width series for dendroclimatic studies

Daly C, Neilson R P and Phillips D L 1994 A statistical-topographic model for mapping climatological precipitation over mountainous terrain *Journal of applied meteorology* 33 140–58

Evans M, Reichert B K, Kaplan A, Anchukaitis K J, Vaganov E, Hughes M and Cane M 2006 A forward modeling approach to paleoclimatic interpretation of tree-ring data *Journal of Geophysical Research: Biogeosciences* 111

Fritts H 1976 *Tree rings and climate* (Elsevier)

Holden Z A, Klene A E, Keefe R F and Moisen G G 2013 Design and evaluation of an inexpensive radiation shield for monitoring surface air temperatures *Agricultural and forest meteorology* 180 281–6

Holmes R L 1983 Computer-assisted quality control in tree-ring dating and measurement *Tree-Ring Bulletin*

Jacoby G C and D'Arrigo R 1989 Reconstructed Northern Hemisphere annual temperature since 1671 based on high-latitude tree-ring data from North America *Climatic Change* 14 39–59

LaMarche Jr V C and Stockton C W 1974 Chronologies from temperature-sensitive bristlecone pines at upper treeline in Western United States *Tree-Ring Bulletin*

Liu Z, Otto-Bliesner B L, He F, Brady E C, Tomas R, Clark P U, Carlson A E, Lynch-Stieglitz J, Curry W, Brook E, Erickson D, Jacob R, Kutzbach J and Cheng J 2009 Transient Simulation of Last Deglaciation with a New Mechanism for Bolling-Allerod Warming *Science* 325 310–4

Meko D M, Touchan R and Anchukaitis K J 2011 Seascorr: A MATLAB program for identifying the seasonal climate signal in an annual tree-ring time series *Computers & Geosciences* 37 1234–41

Paulsen J and Körner C 2014 A climate-based model to predict potential treeline position around the globe *Alpine Botany* 124 1–12

Routson C C, Woodhouse C A and Overpeck J T 2011 Second century megadrought in the Rio Grande headwaters, Colorado: How unusual was medieval drought? *Geophysical Research Letters* 38

Salzer M W, Bunn A G, Graham N E and Hughes M K 2014a Five millennia of paleotemperature from tree-rings in the Great Basin, USA *Climate Dynamics* 42 1517–26

Salzer M W and Kipfmueller K F 2005 Reconstructed temperature and precipitation on a millennial timescale from tree-rings in the southern Colorado Plateau, USA *Climatic Change* 70 465–87

Salzer M W, Larson E R, Bunn A G and Hughes M K 2014b Changing climate response in near-treeline bristlecone pine with elevation and aspect *Environmental Research Letters* 9 114007

Schoettle A W and Coop J D 2017 Range-wide conservation of *Pinus aristata*: a genetic collection with ecological context for proactive management today and resources for tomorrow *New forests* 48 181–99

Stahle D W, Cook E R, Burnette D J, Torbenson M C, Howard I M, Griffin D, Diaz J V, Cook B I, Williams A P, Watson E, and others 2020 Dynamics, variability, and change in seasonal precipitation reconstructions for North America *Journal of Climate* 33 3173–95

Stokes M and Smiley T 1968 *Introduction to tree-ring dating. University of Chicago* (Chicago Press, IL)

Tintor W L and Woodhouse C A 2021 The variable climate response of Rocky Mountain bristlecone pine (*Pinus aristata* Engelm.) *Dendrochronologia* 68 125846

Tran T J, Bruening J M, Bunn A G, Salzer M W and Weiss S B 2017 Cluster analysis and topoclimate modeling to examine bristlecone pine tree-ring growth signals in the Great Basin, USA *Environmental Research Letters* 12 014007

Vaganov E A, Anchukaitis K J and Evans M N 2011 How well understood are the processes that create dendroclimatic records? A mechanistic model of the climatic control on conifer tree-ring growth dynamics *Dendroclimatology* (Springer) pp 37–75

Vaganov E A, Hughes M K and Shashkin A V 2006 *Growth dynamics of conifer tree rings: images of past and future environments* vol 183 (Springer Science & Business Media)

Vose R S, Easterling D R, Kunkel K E, LeGrande A N and Wehner M F 2017 *Ch. 6: Temperature Changes in the United States. Climate Science Special Report: Fourth National Climate Assessment, Volume I* (U.S. Global Change Research Program) Online: https://science2017.globalchange.gov/chapter/6/

Wilson R, Anchukaitis K, Briffa K R, Büntgen U, Cook E, D'arrigo R, Davi N, Esper J, Frank D, Gunnarson B, and others 2016 Last millennium northern hemisphere summer temperatures from tree rings: Part I: The long term context *Quaternary Science Reviews* 134 1–18

Woodhouse C A and Overpeck J T 1998 2000 years of drought variability in the central United States *Bulletin of the American Meteorological Society* 79 2693–714

Woodhouse C A, Pederson G T and Gray S T 2011 An 1800-yr record of decadal-scale hydroclimatic variability in the upper Arkansas River basin from bristlecone pine *Quaternary Research* 75 483–90

Zang C and Biondi F 2015 treeclim: an R package for the numerical calibration of proxy-climate relationships *Ecography* 38 431–6

B.8   TABLES

Table B.1. Summary output data for 1989-2016 VSM simulations at LCL and LCH. First and second columns display results for 28-yr average of LCL and LCH mean ensemble runs. Third and fourth columns display the same output data for the individual LCH years, 2007 and 2011, representing a high growth and a low growth year, respectively.

	LCL - Average	LCH - Average	LCH - 2007	LCH - 2011
Date Growth Starts	116 (25-Apr)	157 (5-Jun)	152 (1-Jun)	168 (16-Jun)
Date Growth Stops	288 (15-Oct)	271 (27-Sep)	277 (4-Oct)	276 (3-Oct)
Growing Season Length	173	114	125	108
Date Moisture becomes Growth Limiting	162 (11-Jun)	222 (10-Aug)	226 (14-Aug)	182 (1-Jul)
Growing Season % Days Moisture Limited	60%	4%	12%	50%
Growing Season Average Temp. (C)	11.60	9.75	9.62	10.82
Growing Season Total Precip. (mm)	300	246	323	187
Avg. Transpiration Rate (mm)	1.89	2.91	3.18	2.88
Max. Snowpack (mm)	95	306	346	221
Date of Max Snowpack	61 (2-Mar)	111 (21-Apr)	117 (27-Apr)	105 (15-Apr)

Table B.2. Comparison of LCH Modern VSM run to VSM sensitivity tests using TraCE temperature and NASPA precipitation data from the late 1500s megadrought. The first and second rows show which temperature and precipitation dataset were used for each run.

LCH	Modern	PTMP (Past Temp. w/ Modern Precip.)	PTPP (Past Temp. w/ Past Precip.)	MTPP (Modern Temp. w/ Past Precip.)
Temperature Data	Synth. LCH	TraCE adj. Synth. LCH	TraCE adj. Synth. LCH	Synth. LCH
Precipitation Data	PRISM	PRISM	NASPA adj. PRISM	NASPA adj. PRISM
Date Growth Starts	157 (5-Jun)	165 (13-Jun)	165 (13-Jun)	157 (5-Jun)
Date Growth Stops	271 (27-Sep)	266 (22-Sep)	266 (22-Sep)	271 (27-Sep)
Growing Season Length	114	101	101	114
Date Moisture becomes Growth Limiting	224 (12-Aug)	NA	NA	201 (20-Jul)
Growing Season % Days Moisture Limited	4%	NA	NA	12%
Avg. Transpiration Rate (mm)	2.91	2.71	2.59	2.74
Max. Snowpack (mm)	306	352	267	230
Date of Max Snowpack	111 (21-Apr)	124 (4-May)	124 (4-May)	105 (15-Apr)

Table B.3. Comparison of LCL Modern VSM run to VSM sensitivity tests using TraCE temperature and NASPA precipitation data from the late 1500s megadrought. The first and second rows show which temperature and precipitation dataset were used for each run.

LCL	Modern	PTMP (Past Temp. w/ Modern Precip.)	PTPP (Past Temp. w/ Past Precip.)	MTPP (Modern Temp. w/ Past Precip.)
Temperature Data	Synth. LCL	TraCE adj. Synth. LCL	TraCE adj. Synth. LCL	Synth. LCL
Precipitation Data	PRISM	PRISM	NASPA adj. PRISM	NASPA adj. PRISM
Date Growth Starts	116 (25-Apr)	128 (8-May)	128 (8-May)	116 (26-Apr)
Date Growth Stops	288 (15-Oct)	283 (10-Oct)	283 (10-Oct)	289 (15-Oct)
Growing Season Length	173	155	155	172
Date Moisture becomes Growth Limiting	162 (11-Jun)	170 (19-Jun)	168 (17-Jun)	161 (10-Jun)
Growing Season % Days Moisture Limited	60%	58%	59%	60%
Avg. Transpiration Rate (mm)	1.89	1.92	1.82	1.80
Max. Snowpack (mm)	95	135	98	66
Date of Max Snowpack	61 (2-Mar)	72 (13-Mar)	72 (13-Mar)	68 (9-Mar)
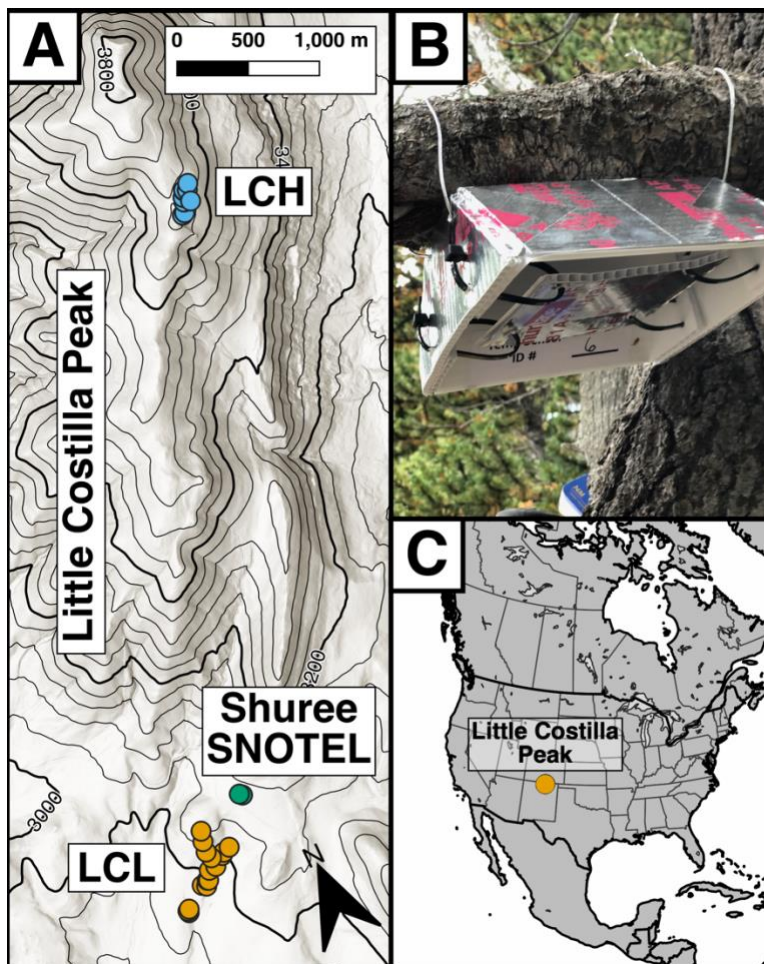
Figure B.1. Map of study area for this investigation.

A) A detailed map of the Little Costilla Peak ridgeline with the locations of the LCH (blue) and LCH (orange) sampling sites and iButton sensor placements highlighted. Shown in green are the iButton sensor sites located on trees adjacent to the Shuree SNOTEL (USDA Natural Resources Conservation Service SNOTEL S1169). Elevation contours in meters. B) A closeup of the temperature shield based on a modified design from Holden *et al* (2013) used to house the iButton sensors during our analysis. C) Overview map of the Little Costilla Peak location within the Continental United States.
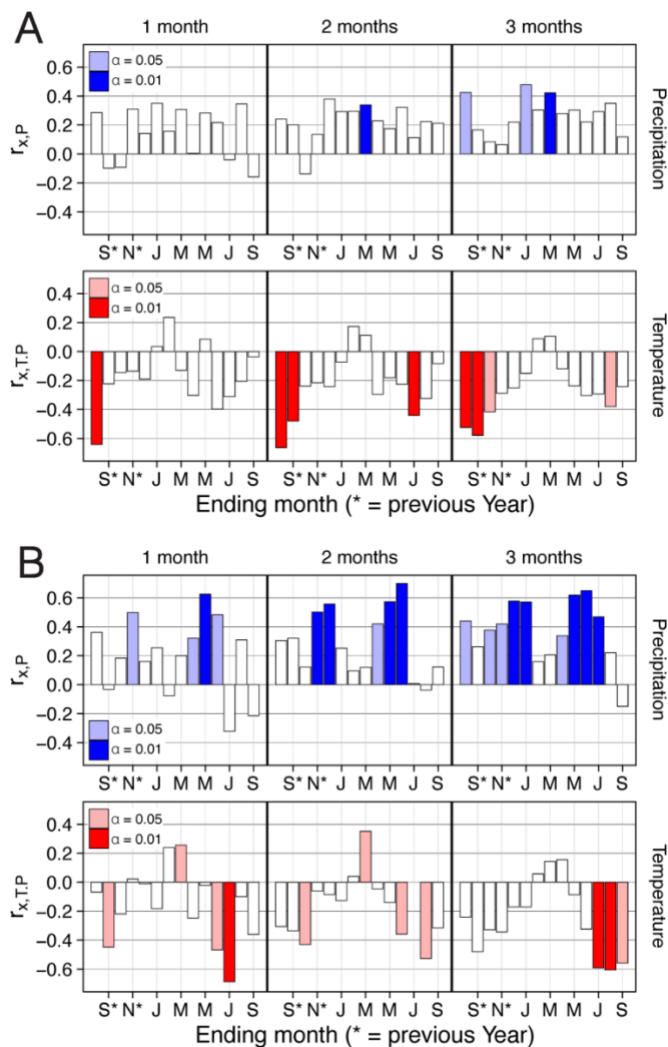
Figure B.2. Seascorr seasonal correlations and partial correlations for A) LCH and B) LCL chronologies with PRISM gridded precipitation and temperature data at the chronology locations. The upper row of each graph (blue bars) shows the correlation between the chronology and monthly precipitation. The lower row of each graph (red bars) shows the partial correlations between the chronologies and monthly temperature, with the precipitation correlation removed. Climate correlations are shown for 1, 2, and 3 month long seasonal averages, with the month on the graphic indicating the last month of the particular season. Light blue and red bars in A and B indicate correlations with significance values (p) below 0.05, while dark blue and red bars indicated correlations with significance values (p) below 0.01.
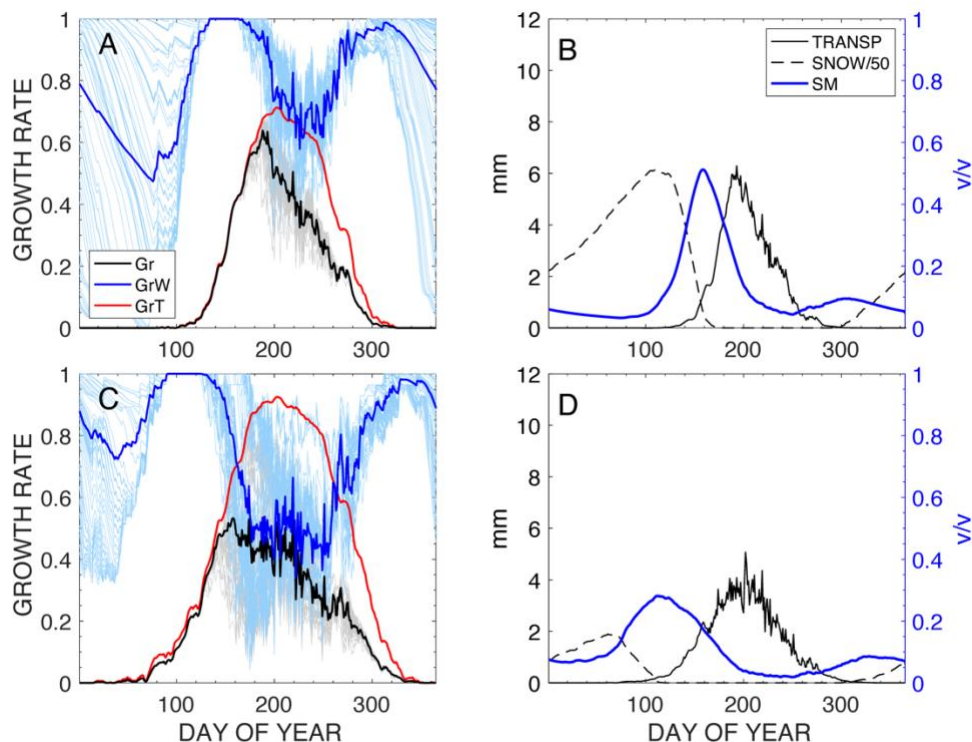
Figure B.3. LCH (A & B) and LCL (C & D) average ensemble growth rates and average environmental variables for 1989-2016 VSM runs. A and C: Light gray lines represent the 28-year average overall *P. aristata* VSM growth rate for each of the 101 ensemble members and dark gray lines indicate the ensemble mean of growth (Gr). Light blue lines represent the growth rate as limited by soil moisture averaged over 28-years for each ensemble member, and the dark blue line is the ensemble mean of soil-moisture limited growth (GrW). The red line is the same across all ensemble members and represents the temperature limitations on growth (GrT). It is unaffected by the selection of ensemble input parameters. When the dark blue line dips below the red line in A and C, the model has shifted from temperature limitations on growth to soil-moisture limitations on growth. 28-year environmental parameter averages are shown in B and D. They are responsible for controlling the growth rate in A and C. The dark blue line in B and D represents average soil moisture (SM) as a unitless ratio of total soil moisture capacity. The solid black line is the average of ensemble plant transpiration rates by day of year (TRANSP), and is measured in mm. The dashed black line is the depth of snowpack (SNOW) by day of year and has been adjusted by dividing the value (in mm) by 50 to improve legibility of the graphic.
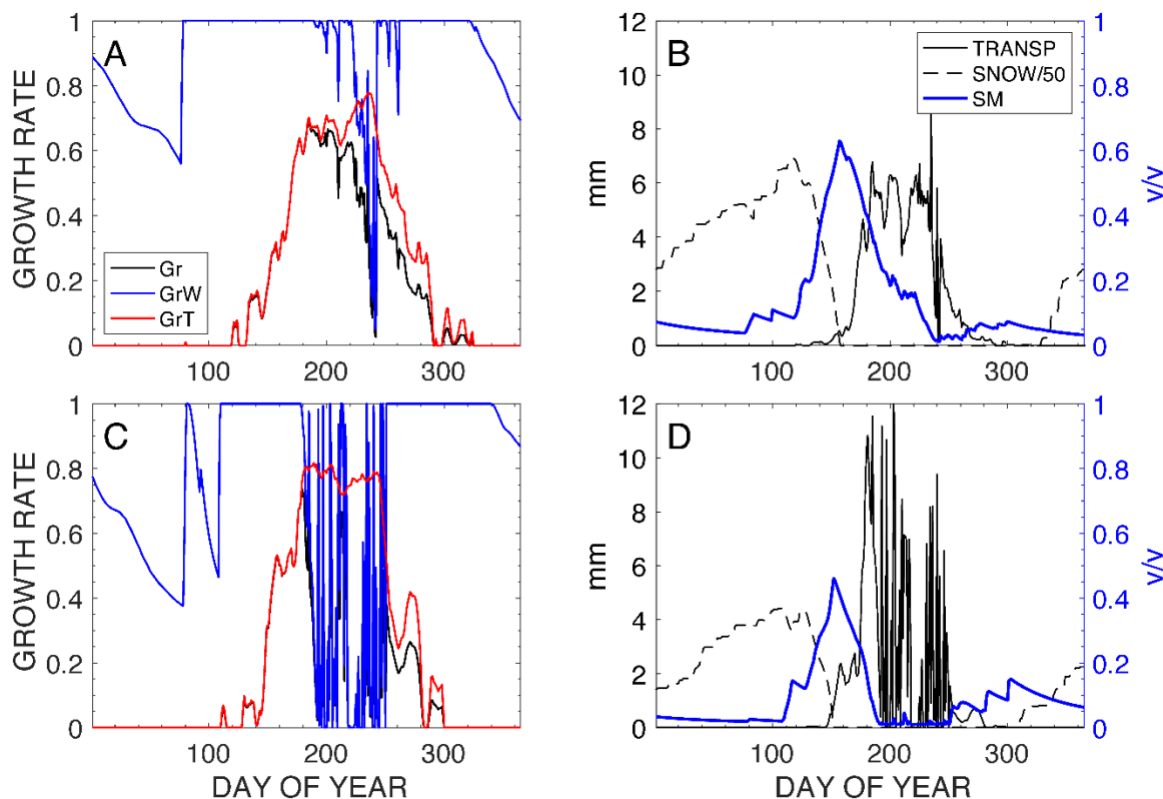
Figure B.4. VSM ensemble average values for LCH in 2007 (A & B), a high-growth year, and LCH in 2011 (C & D), a low-growth year. A and C: The black line represents the mean *P. aristata* VSM growth rate (Gr) for the 101 ensemble members in 2007 (A) and 2011 (C). The blue line represents the mean soil-moisture limited growth rate (GrW) for the 101 ensemble members. The red line represents the temperature limitations on growth (GrT) and is the same across all ensemble members. The intermittent nature of the Gr (black line) and GrW (blue line) in 2011 (C) is due to an abrupt stop-start of growth in the VSM. Environmental parameter values for 2007 and 2011 are shown in B and D, respectively. They are responsible for controlling the growth rate in A and C. The dark blue line in B and D represents average soil moisture (SM) as a unitless ratio of total soil moisture capacity. The solid black line is the average of ensemble plant transpiration rates by day of year (TRANSP), and is measured in mm. The dashed black line is the depth of snowpack (SNOW) by day of year and has been adjusted by dividing the value (in mm) by 50 to improve legibility of the graphic. The transpiration rate in 2011 is intermittent due to the abrupt stop-start growth in the VSM that also impacts the growth parameters.
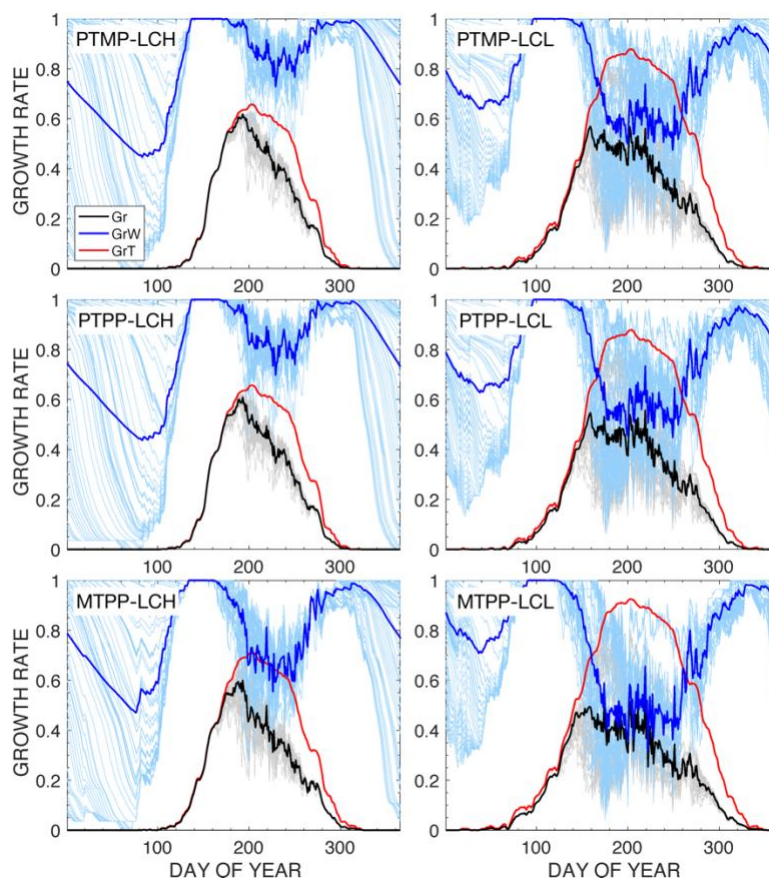
Figure B.5. Ensemble growth rate graphs for PTMP, PTPP, and MTPP sensitivity tests at LCH (A, C, and E) and LCL (B, D, and F). Each row represents a sensitivity test: **PTMP** (A & B) (past temperatures with modern precipitation, simulating cooling alone), **PTPP** (C & D) (past temperatures with past precipitation, simulating megadrought and cooling together), and **MTPP** (E & F) (modern temperatures with past precipitation, simulating megadrought. As in Figure B.3, light gray lines represent the 28-year average overall *P. aristata* VSM growth rate for each of the 101 ensemble members and dark gray lines indicate the ensemble mean of growth (Gr). Light blue lines represent the growth rate as limited by soil moisture averaged over 28-years for each ensemble member, and the dark blue line is the ensemble mean of soil-moisture limited growth (GrW). The red line is the same across all ensemble members and represents the temperature limitations on growth (GrT). It is unaffected by the selection of ensemble input parameters. When the dark blue line dips below the red line the model has shifted from temperature limitations on growth to soil-moisture limitations on growth.

B.10   SUPPLEMENTAL INFORMATION

B.10.S1   iButton Data Procedure

The iButtons (Maxim Integrated, San Jose CA model DS1922L-F5) collected bi-hourly temperature data for a full year, from October 2018 through October 2019 (n = 4380 observations). They were placed at 37 locations (19 at LCH, 16 at LCL, 2 at Shuree SNOTEL). Sensors were housed in hand-made radiation shielding based on a modified Holden et al (2013) design (Fig. 1B). During this interval, two LCH radiation shields were destroyed and seven LCH sensors were buried under snow at for at least one month during the growing season, reducing the total number of usable sensors to 26. We used a snow burial procedure developed in Sambuco *et al* (2020) to remove temperature data if the daily temperatures remain below 0°C and the diurnal temperature range is less than 5°C.

Prior to producing the synthetic temperature datasets for LCH and LCL, we first addressed the known issue of ad-hoc temperature shielding producing biased temperature measurements (Terando *et al* 2017) by comparing bi-hourly data at the Shuree SNOTEL USDA NRCS S1169 (SHU) to the bi-hourly data collected at the two iButtons (Sensor J and Sensor L, or J/L) we placed in trees nearby. Because of a lapse in SHU data over a period of the comparison time, we utilized homogenized temperature records from two nearby SNOTEL sites (North Costilla (NCO) and Red River Pass #2 (RRP)) (Oyler *et al* 2015) to fill missing data at SHU. We constructed a linear regression with NCO and RRP data to fill the missing SHU SNOTEL data, and the resulting synthetic SHU data had a spearman correlation with the original SHU data of r = 0.9864. We also ran a Wilcoxon paired rank sum test between the synthetic SHU and the

original SHU data, and the result passed, indicating the datasets do not have significant differences.

There was also an additional 4 month lapse in data at the J/L sensors located next to the SHU, and this data was filled using an hourly linear regression (one regression for each bi-hour period, 12 total) constructed from another nearby iButton sensor (Sensor 17). The correlation between J/L and 17 was very high (r = 0.9926) and passed the Wilcoxon paired rank sum test. We then compared the daily average temperature of the synthetic J/L data with the daily average temperature of the synthetic SHU data. We ran our comparison by month and the differences between the two datasets resulted in a set of monthly adjustments for the J/L data. These adjustments remove the bias caused by the temperature shielding. We applied these adjustments to the 26 LCH and LCL iButton sensors.

Next, we compared each of the 26 daily averages from the additional iButtons to the daily averages from J/L. We used the monthly differences between the J/L sensors and all of the other sensors later when constructing long-term temperature records. Because the synthetic J/L data after temperature shield correction is essentially the same value as the synthetic SHU data, we could assume that the 28 year record we produced for SHU (1989-2016) would match a 28-year record produced at the J/L trees. If we applied the monthly differences between the J/L sensors and the remaining 26 iButton sensors, then we could convert the 28-year record of temperature at SHU into a 28-year record at each of the sampled trees. After we applied this conversion, we were left with 26 28-year temperature records at each tree. We removed 6 sensors from the LCL

calculation due to the juvenile growth detected in the ring-width time series, reducing the total number of LCL series to 10. We then averaged together the 10 LCL and 10 LCH 28-year records to produce a single temperature time series for each site. These synthetic LCL and LCH daily average temperature time series were the datasets we then used in the VSM model.

B.10.S2   VSM Tuning Procedure

Tuning the VSM model parameters to produce an accurate synthetic ring-width time series was accomplished by iteratively running sensitivity tests on 24 parameters and determined that jointly varying the soil drainage rate (rated) and a transpiration coefficient (k3) best replicated real *P. aristata* ring-width variability. To select the best pairing of these parameters for the LCH and LCL simulations, we used a modified form of the Latin Hypercube sampling design (Stein 1987) to generate 10050 parameter pairs of 'rated' and 'k3' values drawn respectively from fixed intervals of 0.001 to 0.005 and 0.15 to 0.35, respectively. Using every parameter pair from the Latin Hypercube, we ran 10050 28-year simulations (1989-2016, or modern run) for both LCH and LCL. Because of the potential for noise in the VSM due to slight variances in parameters producing non-linear edge effects, we chose not to select a single best simulation (i.e., highest correlation between actual and synthetic ring-width time series), but instead opted to select the top 1% of simulations (n = 101 runs) and produce an ensemble of those values. The simulation results (i.e., growth rates, transpiration rates, etc.) from these top 1% of parameter pairs were averaged to produce a single mean of outputs for LCH and for LCL, allowing simplified internal analysis and intercomparison between sites.

B.10.S3   Paleo-climate Adjustment Procedure

To determine the temperature adjustment for the sensitivity testing we used the CCSM3 TraCE

paleotemperature simulations for the pixel located over LCP (Liu *et al* 2009) smoothed with a

30-yr spline. The TraCE simulation produced monthly output, but only until 1990, thus

preventing us from calculating a temperature anomaly relative to the modern VSM baseline.

Recognizing this limitation, we used the last 40 years of the simulation (1950-1990) as a baseline

and converted absolute temperatures to anomalies. The resulting anomaly record at LCP for the

last millennium showed all periods prior to the instrumental record were at least 0.47°C cooler

than the modern baseline. Given consistent cooler temperatures, we chose to select temperature

data from the same period as the precipitation adjustment (1573-1600, see below) as it allowed a

complete simulation of the late 16th century megadrought. Coincidently, the late 16th century was

the third coldest period over the last millennium at LCP in the TraCE simulation. We extracted

the monthly anomalies for 1587 (the midpoint of 1573-1600) (Table B.S1). The resulting 1587

anomalies were used to adjust the modern synthetic LCH and LCL temperatures by month,

allowing the VSM to simulate the 16th century temperatures. We chose not to utilize the TraCE

precipitation reconstructions because of model difficulty replicating the North American

monsoon (He 2011), representing 25% of annual precipitation at LCP (Daly *et al* 1994).

For the precipitation adjustment to simulate a megadrought we utilized the North American

Seasonal Precipitation Atlas (NASPA, Stahle *et al* 2020), a 600-year gridded reconstruction of

cool-season (December to April, DJFMA) and warm-season (May to July, MJJ) precipitation.

We extracted reconstructed precipitation data from the nine 0.5° pixels located closest to LCP

(36°N-37.5°N,104.5°W-106°W), averaged the nine time series by year, and applied a running

28-year average to the annual data (matching the 28-yr 1989-2016 modern run). We found 1573-

1600 to be the driest 28-year period between 1400 and 2016, matching previous research

identifying this period as most severe Western U.S. megadrought of the last millennium (Stahle

et al 2000, Williams *et al* 2020). We also extracted the NASPA 28-yr precipitation average from

the same time as the modern 1989-2016 VSM run. Comparing the modern period with the late

16th century megadrought, we evaluated the difference in the 28-yr means of DFJMA and MJJ

precipitation and applied these monthly proportional reductions to the 1989-2016 PRISM

precipitation data from the modern VSM run (Table B.S2). No August to November

precipitation reconstruction exists over the same period, so we conservatively kept those PRISM

precipitation months unadjusted.

B.10.S4   Supplemental Tables

Table B.S1. TraCE-21ka 30-yr spline difference in temperature between 1950-1990 average and 1587. These numbers are used to shift LCH and LCL temperatures by month replicating temperatures at time of late 1500s megadrought.

Month	1587 Temperature Shift
Jan	-1.004
Feb	-1.492
Mar	-1.425
Apr	-1.003
May	-1.342
Jun	-0.558
Jul	-0.804
Aug	-0.803
Sep	-0.676
Oct	-1.082
Nov	-1.530
Dec	-0.652
Annual Average	-1.031

Table B.S2. North American Seasonal Precipitation Average differences between 1573-1600 and 1989-2016 DJFMA and MJJ 28-yr averages. The proportional reduction applied to data prior to VSM model runs is included.

	DJFMA	MJJ
1573-1600 NASPA Precip. Avg.	77.60 mm	134.22 mm
1989-2016 NASPA Precip. Avg.	108.97 mm	134.82 mm
Difference	-31.37 mm	-0.59 mm
Proportion Reduction	0.712	0.996
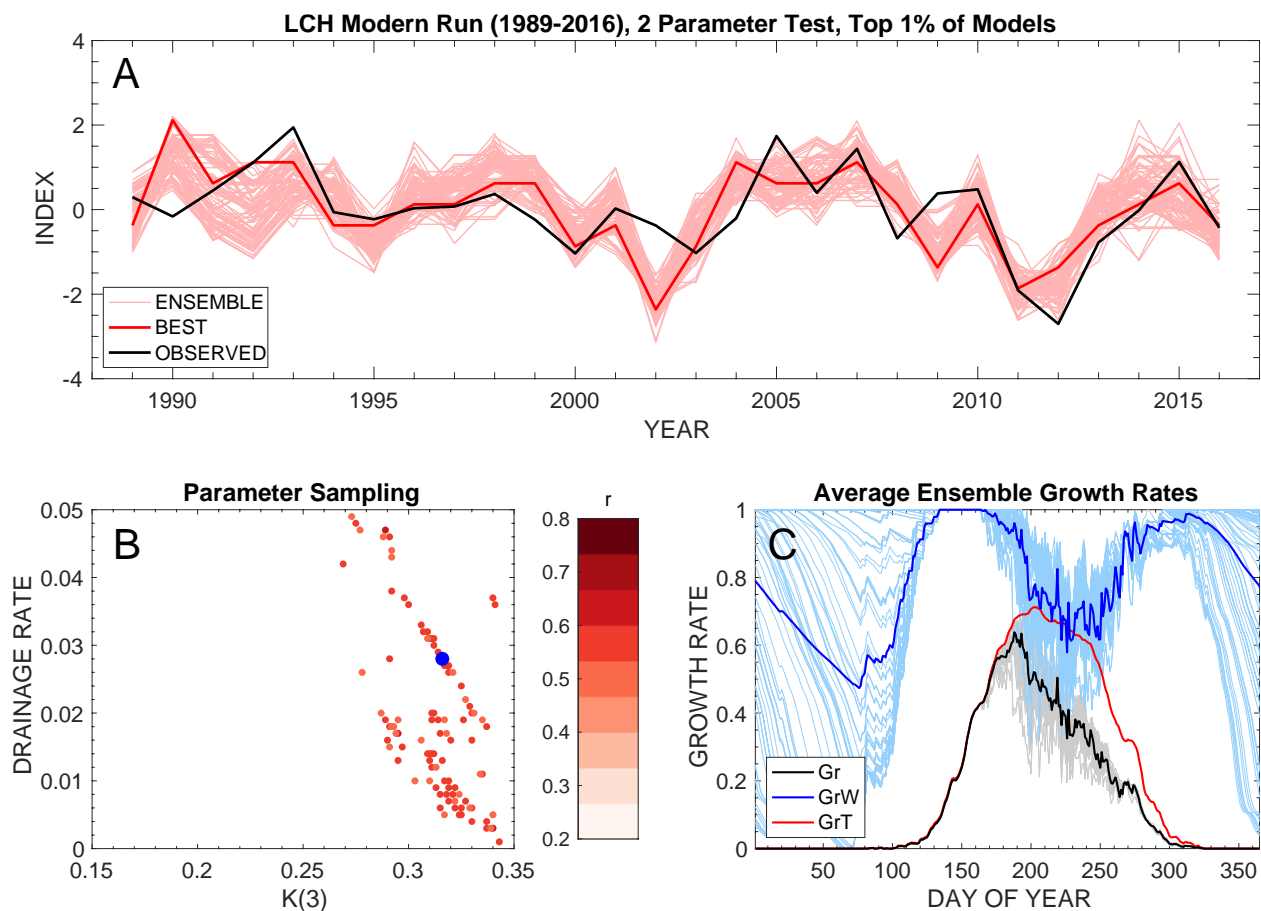
Figure B.S1. Full results for top 1% of LCH ensemble runs. Upper graph shows synthetic time series of each ensemble member with the highest correlating member highlighted. Lower left graph shows the parameter values for the top 1% ensemble (101 parameter pairs). Blue dot highlights parameter pair producing the highest correlation between synthetic time series and measured time series. Lower right graph shows average ensemble growth rates averaged over 28 years.
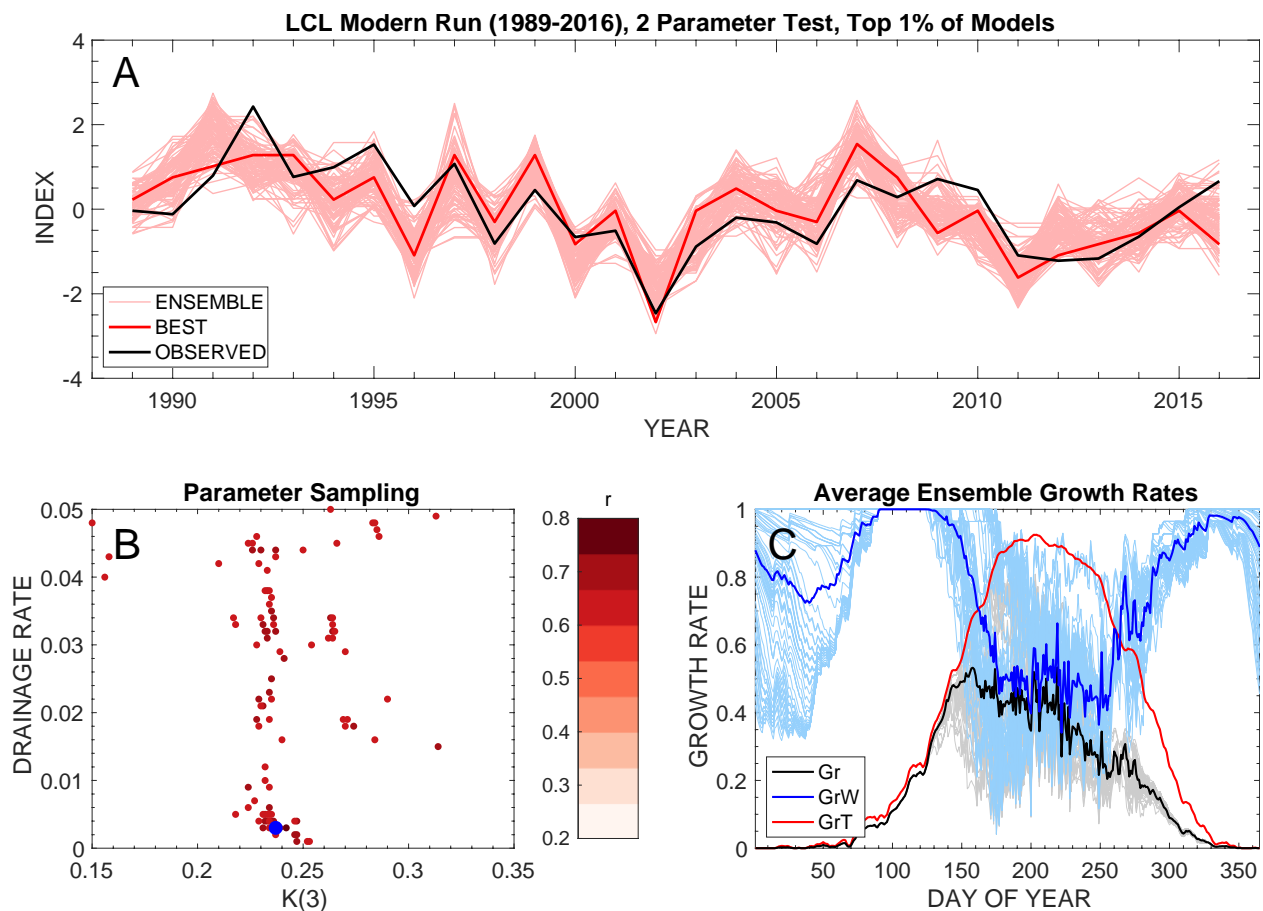
Figure B.S2. Full results of top 1% of LCL ensemble runs. Upper graph shows synthetic time series of each ensemble member with the highest correlating member highlighted. Lower left graph shows the parameter values for the top 1% ensemble (101 parameter pairs). Blue dot highlights parameter pair producing the highest correlation between synthetic time series and measured time series. Lower right graph shows average ensemble growth rates averaged over 28 years.

B.10.S6   Supplemental Works Cited

Daly C, Neilson R P and Phillips D L 1994 A statistical-topographic model for mapping climatological precipitation over mountainous terrain *Journal of applied meteorology* 33 140–58

He F 2011 *Simulating transient climate evolution of the last deglaciation with CCSM 3* vol 72

Liu Z, Otto-Bliesner B L, He F, Brady E C, Tomas R, Clark P U, Carlson A E, Lynch-Stieglitz J, Curry W, Brook E, Erickson D, Jacob R, Kutzbach J and Cheng J 2009 Transient Simulation of Last Deglaciation with a New Mechanism for Bolling-Allerod Warming *Science* 325 310–4

Oyler J W, Ballantyne A, Jencso K, Sweet M and Running S W 2015 Creating a topoclimatic daily air temperature dataset for the conterminous United States using homogenized station data and remotely sensed land skin temperature *International Journal of Climatology* 35 2258–79

Sambuco E, Mark B G, Patrick N, DeGrand J Q, Porinchu D F, Reinemann S A, Baker G and Box J E 2020 Mountain temperature changes from embedded sensors spanning 2000m in Great Basin National Park, 2006-2018 *Frontiers in Earth Science* 8 292

Stahle D W, Cook E R, Burnette D J, Torbenson M C, Howard I M, Griffin D, Diaz J V, Cook B I, Williams A P, Watson E, and others 2020 Dynamics, variability, and change in seasonal precipitation reconstructions for North America *Journal of Climate* 33 3173–95

Stahle D W, Cook E R, Cleaveland M K, Therrell M D, Meko D M, Grissino-Mayer H D, Watson E and Luckman B H 2000 Tree-ring data document 16th century megadrought over North America *Eos, Transactions American Geophysical Union* 81 121–5

Stein M 1987 Large sample properties of simulations using Latin hypercube sampling *Technometrics* 29 143–51

Terando A J, Youngsteadt E, Meineke E K and Prado S G 2017 Ad hoc instrumentation methods in ecological studies produce highly biased temperature measurements *Ecology and evolution* 7 9890–904

Williams A P, Cook E R, Smerdon J E, Cook B I, Abatzoglou J T, Bolles K, Baek S H, Badger A M and Livneh B 2020 Large contribution from anthropogenic warming to an emerging North American megadrought *Science* 368 314–8

APPENDIX C: IN PREP - THE INFLUENCE OF RECENT AND RECONSTRUCTED SPRING HYDROCLIMATE CONDITIONS ON THE RIO GRANDE HEADWATERS

William Lazar Tintor [a, b, *], Connie Woodhouse [a, b]

Paper was prepared for the journal Water Resources Research

[a] School of Geography, Development and Environment, University of Arizona, Tucson, AZ, 85721, USA
[b] Laboratory of Tree-Ring Research, University of Arizona, Tucson, AZ, 85721, USA

[*] Corresponding author: wtintor@email.arizona.edu (W. Tintor).

C.1 ABSTRACT

The majority of upper Rio Grande spring and summer streamflow originates as snow, allowing the prediction of streamflow volumes using systematized snowpack measurements. Recent declines in snowpack prediction power suggests other factors, including spring hydroclimate (temperature and precipitation), may increasingly determining streamflow volumes. In a stressed, over-apportioned Rio Grande, understanding the past impact of spring hydroclimate conditions on streamflow is necessary to prepare for future changes. We evaluated the observed relationship between snowpack, spring hydroclimate conditions, and streamflow volumes in the Rio Grande headwaters, identifying years when extreme spring conditions coincide with streamflow volumes outside those predicted by the winter snowpack. We also produced a new 1560-year April-June spring hydroclimate tree-ring reconstruction for the Rio Grande headwaters, which we compared with a previously produced snowpack reconstruction (Pederson et al., 2011) to assess the pre-instrumental snowpack-spring hydroclimate relationship. We found it was rare (16% of years) in the observed data for extreme spring hydroclimate conditions to alter streamflow volumes (both positively and negatively). The reconstructed snowpack-spring hydroclimate annual relationship was similar to the observed annual relationship, suggesting a similarly low probability of extreme spring conditions altering streamflow in the past. Comparison of multidecadal fluctuations in the reconstructed snowpack and spring hydroclimate datasets indicated a weak, unstable relationship, interrupted by intervals of coherent, simultaneous shifts, often during extreme droughts or pluvials. With increasing temperatures expected to decrease snowpack contribution to Rio Grande streamflow, the occurrence of cool, wet springs to supplement deficits will become increasingly important. Unfortunately, both the observed and reconstructed

datasets suggest that the occurrence of such cool, wet springs is rare and should not be expected to regularly supplement Rio Grande streamflow.

C.2   INTRODUCTION

The Rio Grande (Río Bravo del Norte, in Spanish) is the fifth-longest river in North America, running 3,060 km and draining 517,000 km^2. It originates as snowpack in the mountains of Colorado, passing through or draining three U.S. states and five Mexican states before emptying into the Gulf of Mexico (USGS, 2021b). It is a major source for municipal and agricultural water supply while also acting as a natural boundary between the Mexico and the United States (Blythe & Schmidt, 2018; Udall, 2020). As a result of extensive development and overuse, portions of the Rio Grande between New Mexico and Texas now cease flowing for several months a year (Blythe & Schmidt, 2018; Udall, 2020). Management of the limited, remaining water resources in the upper Rio Grande region (Colorado, New Mexico, and Texas) operates within the rules of the Rio Grande Compact, an inter-state agreement to apportion streamflow between the three states. The compact rules are driven by streamflow measurements at several locations along the Rio Grande and its tributaries (Paddock, 2001). One of these locations, the Del Norte gage along the Rio Grande, measures the single greatest source of water for the upper Rio Grande and is therefore a key metric used in the administration of the Rio Grande Compact (Paddock, 2001). For this reason, when the USDA-NRCS (U.S. Department of Agriculture Natural Resources Conservation Service) publishes the water supply forecast (WSF) on April 1st of each year, water managers throughout the upper Rio Grande incorporate this forecast into their annual planning (Vandiver, 1999).

The Rio Grande WSFs issued by the NRCS are based both on measurements of SWE (snow water equivalent, or the amount of water stored in the snowpack), and antecedent precipitation measured in the watershed above the Del Norte measurement gage. The high correlation between SWE measurements on April 1st and the ensuing streamflow volumes has historically allowed for statistically significant prediction skill (Garen, 1992; Pagano et al., 2009) although declines in prediction skill for WSFs have been observed since the 1980s (Pagano et al., 2004). Efforts to incorporate temperature forecasts into WSFs (Lehner et al., 2017) or utilize ensembles of machine-learning based WSFs (Fleming et al., 2021) have improved the skill of WSF, but snowpack measurements remain a central feature of the streamflow prediction process. On April 7, 2021, the NRCS WSF for the Del Norte gage estimated that streamflow would only reach 71% of average (NRCS-NWCC, 2021).With the prediction of below-average runoff, combined with ongoing inter-state compact deficits, severe shortages for users on the Rio Grande were expected (Davis, 2021a). In response, water managers delayed the start of irrigation throughout central New Mexico (Davis, 2021a) and warned the public that the Rio Grande through Albuquerque, New Mexico could go dry for the first time in 30 years (Davis, 2021b). Despite predictions of severe deficits, by the end of June 2021 total streamflow through the Del Norte gage was above the forecasted volume (Colorado DWR, 2021), while well-timed precipitation, combined with creative water management (Davis, 2021c), prevented the Rio Grande through Albuquerque from completely drying. Anecdotally, the 2021 reprieve on the Rio Grande was explained by a strong North American Monsoon (NAM, Adams & Comrie, 1997) supplying sufficient precipitation to keep streamflow elevated and the river continuous (Davis, 2021d; Fleck, 2021).

While significant summer precipitation events from the NAM can increase streamflow on the Rio Grande, the streamflow on the Rio Grande was higher than predicted in June of 2021, before the onset of the NAM. A comparison between the spring hydroclimate conditions in 2021 and those during the same period in 2020 may provide a better explanation for the reprieve seen on the Rio Grande.

In 2020, the NRCS April 1st WSF predicted the Rio Grande at Del Norte gage would see 69% of average streamflow volume, similar to the 2021 prediction (NRCS-NWCC, 2020, 2021). However, the 2021 April to June streamflow volume at Del Norte was 18% greater than the same period in 2020 (378 M m^3 vs. 319 M m^3)(Colorado DWR, 2021). What drove the difference between streamflow volumes when the flow predictions for both years were so similar? One potential explanation may lie with the difference in spring hydroclimate (i.e., precipitation plus the effects of temperature) in the two years. April to June precipitation totals for the headwaters of the Rio Grande showed a 264% increase in spring precipitation from 2020 to 2021 (37 mm and 97 mm, respectively) (Menne et al., 2018). All three months saw more precipitation in 2021 than 2020, with the largest increase occurring in May 2021, with precipitation over four times greater than May 2020 (50 mm vs. 12 mm, respectively). Spring temperatures were similarly divergent, with April and May cooler in 2021 than in 2020, and the three month temperature average dropping from 9.9 °C in 2020 to 9.4 °C in 2021. Again, May 2021 stands out, with daily average temperatures more than a full degree C cooler than May 2020 (10.6 °C and 9 °C, respectively)(Menne et al., 2018). The combination of cooler and wetter conditions in 2021

(relative to 2020), is likely to explain the disparate spring streamflow volumes in spite of similar April 1 WSFs.

The period following the April 1st WSF, but prior to the July start of the NAM, represents a gradient in the headwaters of the Rio Grande, with the cool season moisture in April transitioning to warm and dry pre-monsoon conditions in June. The October to March period, during which snowpack accumulates, contributes 45% of total annual precipitation, while the NAM period from July to August contributes another 34% of total annual precipitation. From April to June, the region experiences relatively dry conditions, with total precipitation only contributing to 21% of the annual total. The likelihood of precipitation also decreases over this period, with monthly totals dropping from 38 mm in April to 20 mm in June, gradually reducing the potential for additional precipitation to contribute to streamflow. Hypothetically, an unusually cool, wet spring could make a perceptible contribution to Rio Grande streamflow. With climate change predicted to impact the Rio Grande through decreased snowpack volumes and a corresponding reduction in streamflow (Elias et al., 2015; Hurd & Coonrod, 2012; Llewellyn & Vaddey, 2013), climate conditions from April to June (between peak snowpack and the start of the NAM) may increasingly impact Rio Grande streamflow volumes (Chavarria & Gutzler, 2018). A better understanding of the relationship between winter snowpack and spring hydroclimate conditions, and the associated impact on streamflow is needed. How often in the observed record has a warm, dry winter followed by a cool, wet spring occurred at the same time streamflow was higher than expected given the winter snowpack? Does the inverse of this occur, with a wet winter and a warm, dry spring coinciding with lower than anticipated streamflow?

Could an analysis of paleoclimate reconstructions of snowpack and spring hydroclimate, based on tree-ring measurements, provide a more complete context to evaluate this relationship and how it has evolved over time?

To answer these questions, this study focuses on the Rio Grande Headwaters (RGHW), the northernmost sub-basin of the Rio Grande, the location of the Del Norte gage, and a region responsible for more than 50% of the total streamflow in the upper Rio Grande. The primary objectives of this study are as follows: (1) Evaluate the relationship between snowpack, spring hydroclimate conditions, and streamflow volumes of the Rio Grande using instrumental data, identifying years when spring hydroclimate conditions coincide with spring streamflow volumes that are outside anticipated streamflows based on preceding winter snowpack. (2) Assess the pre-instrumental period relationship between snowpack and spring conditions over the past 15 centuries in order to situate the observed relationship between snowpack and spring hydroclimate conditions within a broader historic context. The pre-instrumental relationship was examined using a previously produced, tree-ring reconstruction of SWE (Pederson et al., 2011), and a newly developed tree-ring reconstruction of spring hydroclimate conditions in the RGHW. The new spring hydroclimate reconstruction utilized the tree-ring widths of Rocky Mountain bristlecone pine (*Pinus aristata*, Englem.), recently identified as a species sensitive to moisture and temperature variability during the period from late-spring to early-summer (Tintor & Woodhouse, 2021).

C.3   BACKGROUND AND DATA

C.3.1   The Rio Grande Headwaters

This study centers on the RGHW (USGS HUC 130100), the northern-most sub-basin of the upper Rio Grande (Fig. C.1, inset). The RGHW covers 19,715 km^2 in southern Colorado and Northern New Mexico. It contributes 50% of annual streamflow for the upper Rio Grande, despite comprising only 17% of the total upper Rio Grande watershed (Blythe & Schmidt, 2018; USGS, 2021b). It is a high elevation watershed ranging from 4,374 m at Blanca Peak to 2,255 m along the Rio Grande at the Colorado/New Mexico border. The RGHW is bounded by the San Juan Mountains to the west and the Sangre de Cristo Mountains to the east, with the arid San Luis Valley between the two ranges (Fig. C.1). The average annual precipitation for the RGHW (as approximated by Colorado Climate Division 5, Fig. C.1) is 430 mm/yr. (1991-2020), Menne et al., 2018). June is the driest month with 20 mm/mo., while August is the wettest with 56 mm/mo. (Fig. C.2A). The average temperatures for the RGHW range from -6.5 °C in January to 16.0 °C in July (Fig. C.2A). The climate division average values of precipitation and temperature mask wide variability within the RGHW that results from elevation and topography. For example, the lower elevation town of Alamosa (2,300 m) in the San Luis Valley receives 185 mm/yr. of precipitation, while the higher elevation Wolf Creek Summit (3,350 m) in the San Juan Mountains receives 1,270 mm/yr. (Menne et al., 2018). During the summer, average July temperatures are 18.1 °C for Alamosa and 11.8 °C for Wolf Creek Summit, with temperature generally decreasing as elevation increases. In the winter, cold-air inversions in the San Luis Valley result in average January temperatures of -8.7 °C in Alamosa, below the -8.2 °C average at Wolf Creek Summit (Menne et al., 2018).

C.3.2   Snowpack, Spring Hydroclimate, and Spring Streamflow Observed Data

Observed SWE, spring hydroclimate, and spring streamflow datasets for the RGHW were used

to address the first objective of this study (Table C.1), using the common interval of 1937-2004.

In addition to the three primary datasets, Colorado Climate Division 5 monthly total precipitation

and average temperatures (covering 1902-2004) were also used for further analysis of the results

(Menne et al., 2018).

The SWE dataset used in this study was the standardized index of April 1 SWE developed by

Pederson et al. (2011) and originally produced as part of a multi-century evaluation of SWE

variability throughout the Rocky Mountains (Table C.1A). Although individual April 1 SWE

measurements exist back to 1937 for the RGHW, the number and location of the snow course

sites has varied over time, making the construction of a single long-term observed record

difficult. Pederson et al. (2011) solved this by converting each available SWE record in the basin

to a standard score, then averaging the available standard scores by year to develop a single

annual SWE value for the RGHW (along with many other watersheds).

The SPEI (Standardized Precipitation-Evapotranspiration Index, Vicente-Serrano et al., 2010)

was selected to represent spring hydroclimate conditions in the RGHW as it incorporated both

precipitation and temperature into the index calculation (Table C.1A). As demonstrated in the

opening example, both spring precipitation and temperature likely play a role in influencing

streamflow volumes outside those predicted by prior winter snowpack. The SPEI drought index

incorporates both climatic conditions in its formulation, starting with the total precipitation and subtracting the influence of temperature on available moisture through a calculation of potential evapotranspiration (FAO-56 Penman–Monteith equation (Allen et al., 1998)). The SPEI value can be calculated for periods of variable length (1-month to 48-months) and for this study the SPEI 3-month dataset was used. April to June 3-month SPEI values were extracted from eight $0.5°$ x $0.5°$ pixels corresponding with the area of the RGHW (Fig. C.1, Trouet & Van Oldenborgh, 2013; Vicente-Serrano et al., 2010). The eight time-series were averaged together for the years 1937-2004 to produce a single spring SPEI dataset for the RGHW (Table C.1A).

The Del Norte gage (USGS gage 8220000) was chosen to represent April to June Rio Grande streamflow totals in this study (Table C.1B). The Del Norte gage was chosen due to its long period of record, relative lack of upstream modification, and sizeable representation of total streamflow in the RGHW. Established along the Rio Grande in 1890 and relocated to the current location in 1908, the Del Norte gage has a continuous monthly record over the common interval (1937-2004). Four reservoirs (totaling 156 M m^3 of storage) and six minor trans-basin diversions lie upstream from the Del Norte gage (USGS, 2021a). Monthly naturalized Del Norte streamflows from 1957 to 2020 account for the upstream reservoir storage and diversions (USGS, 2021a) and have a high correlation with the original, unadjusted monthly Del Norte streamflow volumes during the same period (r = 0.99), in agreement with previous assessments of the minimal impact of human management on Del Norte streamflows (Chavarria & Gutzler, 2018). From 1937-2004 the Del Norte gage averaged 750 M m^3 of streamflow a year with 453 M m^3 of streamflow during the April-June period (60% of annual streamflow). May and June were

the months with the highest runoff (Fig. C.2B), reflecting the contribution from snowpack melting. The Del Norte gage represented 83% of total annual streamflows in the RGHW, therefore this record is a good representation of total RGHW headwaters streamflow (Blythe and Schmidt 2018).

Because the SWE and spring SPEI datasets were standardized indices and the RGHW spring streamflow measurement was in absolute, the indices of SWE and spring SPEI and the streamflow measurements were converted to percentile values in order to facilitate the comparison between these different hydroclimatic metrics. The percentile ranks ranged from 1st to 99th percentile, with the 50th percentile indicating the median value for each time series.

C.3.3   Reconstructed Snowpack and Spring Hydroclimate Conditions

To answer the second objective and assess the pre-instrumental relationship between snowpack and spring hydroclimate conditions in the RGHW, tree-ring based reconstructions of SWE and spring SPEI were used. For SWE, the Pederson et al. (2011) 1600-year reconstruction of April 1 SWE variability in the RGHW was used. The SWE reconstruction (Table C.1B) was composed of four nested reconstructions developed from eight tree-ring chronologies. The four regression models used to develop the SWE index were shown to skillfully reproduce SWE variability during the instrumental period (1937-2004) with R^2_{adj} values dropping from 0.58 to 0.29 as reconstruction length increased (Pederson et al., 2011). The SWE reconstruction was shortened to 445-2004 CE to match the coverage period of the spring SPEI reconstruction developed for this study.

Previous research by Tintor & Woodhouse (2021) indicated a late spring/early-summer moisture signal was reflected in the annual ring-width measurements of *P. aristata*. The moisture signal was represented by the co-occurrence of a strong positive correlation with precipitation and an even stronger negative correlation with maximum temperatures. Because the SPEI drought index incorporates both precipitation and temperature, it corresponds with the spring hydroclimate stress signal contained tree-ring widths of *P. aristata*. Initial Pearson correlations between the observed 3-month April-June SPEI values and *P. aristata* chronologies confirm this (r = 0.62), showing a higher correlation than that seen between *P. aristata* and RGHW spring precipitation (r = 0.55) or *P. aristata* and spring temperature (r = -0.54). This relationship between *P. aristata* and observed spring SPEI was utilized to produce a multi-century reconstruction of spring SPEI.

The reconstruction of the spring SPEI is discussed in full detail in the Supplemental information (Text C.S1, Tables C.S1 and C.S2, Figures C.S1 and C.S2). What follows is a brief overview of the key reconstruction steps. *P. aristata* chronologies identified by Tintor & Woodhouse (2021) as having a significant correlation (p < 0.05) with the observed spring SPEI were selected (five in total, Fig. C.1). The *P. aristata* chronologies were pre-whitened to remove autocorrelation because they contained significant first-order autocorrelation which the observed spring SPEI time series lacked (AR1= 0.36, p < 0.05 and AR1 = -0.17, p = 0.96, respectively). Since the *P. aristata* pre-whitened (or residual) chronologies varied by length, successively longer, but increasingly less skillful multiple linear regression models were developed. These models were then nested backwards to produce a single spring SPEI reconstruction. The individual models

were cross-validated using Leave-One-Out and k-folds methodology (Wong, 2015). The skill (R^2_{adj}) of the reconstruction models ranged from 0.45 to 0.39, with decreasing skill as reconstruction length increased (Table C.S1). The nested reconstruction covered the period of 445-2004 and was used for the comparison with the SWE reconstruction developed by Pederson et al. (2011).

A reconstruction of spring SPEI using the original chronologies (with autocorrelation retained) was also produced for this study. By retaining low-frequency information in the tree-ring data, this reconstruction (here, called the standard chronology reconstruction) was more suitable for assessment of low-frequency shifts in spring SPEI. This reconstruction was developed using the same nested model methodology and covered the same time period as the reconstruction produced using the residual chronologies (445-2004), but the lower model skill (R^2_{adj} ranging from 0.33 to 0.32) reduced suitability for comparison with the annual reconstructed SWE values (Table C.S1).

Similar to the observed data, the SWE reconstruction and spring SPEI reconstruction were converted to percentile rank values to facilitate comparison. Percentile values were calculated for the reconstructions for both the full reconstruction period (445-2004) and the instrumental period (1937-2004).

C.4   OBSERVED INFLUENCE OF SNOWPACK AND SPRING HYDROCLIMATE ON STREAMFLOW

        VOLUMES

The first objective of this study was to assess the relationship between observed SWE, spring

SPEI, and spring streamflow for the RGHW. The three observed records were cross-correlated

using Pearson correlation coefficients assessed at $p < 0.05$ (Table C.2A). Spring streamflow and

SWE were strongly and positively correlated ($r = 0.79$), while spring streamflow and spring SPEI

had a lower but still significant positive correlation ($r = 0.49$, Table C.2A). Spring SPEI and

SWE also showed a weak, but still significant, positive correlation ($r = 0.37$, Table C.2A).

Because both SWE and spring SPEI are assumed to influence spring streamflow, partial

correlations were run, removing the influence of SWE (or spring SPEI) prior to the respective

correlations between spring SPEI (or SWE) and spring streamflow. This produces a SWE/spring

streamflow partial correlation of $r = 0.75$, and a spring SPEI/spring streamflow partial correlation

of $r = 0.35$.

Given the strong, significant relationship between SWE and spring streamflow shown in both

full and partial correlations, snowpack is clearly an important control on Rio Grande streamflow

volumes from April to June, much more so than spring hydroclimate conditions (as represented

by SPEI). This finding corresponds with the NRCS streamflow predictions process which

implicitly assumes SWE is the largest (among several) drivers of spring streamflow (Pagano et

al., 2009). However, correlation analysis may not capture the full picture of the relationship

between SWE, spring streamflow, and spring hydroclimate. For example, a year with extremely

low SWE may be followed by a very cool, wet spring (i.e., high SPEI). These conditions may

result in an increase in spring streamflows to volumes higher than anticipated based on the April 1 SWE measurement. The increase may be enough to ameliorate the lowest flows, but it will not completely replace streamflow lost due to a low snowpack. A correlation analysis would indicate a below average SWE led to a below average spring streamflow, but it would miss the nuance that the below average streamflow was higher than expected due to the influence of the cool, wet spring (high SPEI).

To capture the finer distinctions in the relationships between spring SPEI, SWE, and spring streamflow (FLOW, from here on), the percentile rank values for each dataset were compared to identify outlier years when the difference between the percentile ranks were relatively large. The first step in this process compared the annual percentile ranks of spring SPEI and SWE, categorizing a year as an outlier when the percentile ranks between the two indices differed by at least one quintile (20 percentile ranks). This analysis identified 37 outlier years (out of 68 total) where SPEI and SWE differed by at least one quintile. Within the 37 outlier years, SPEI was greater than SWE (SPEI>SWE) for 17 years, while SPEI was less than SWE (SPEI<SWE) during the remaining 20 years (Table C.S3). The second step in the analysis assessed the relationship between FLOW and SWE during the 37 SWE/SPEI outlier years. Because of the strong relationship between FLOW and SWE (as identified in correlation analysis), this process was intended to identify years when the FLOW was more (or less) than expected based on the SWE for that year. Similar to the first step, the FLOW and SWE percentile rank values were compared, with outlier years identified as those with at least a one quintile difference. Of the 17 years where SPEI>SWE, five years had percentile ranks of FLOW one quintile greater than

SWE (FLOW>SWE), while the remaining 12 years had FLOW and SWE percentiles within one quintile (Table C.3). Assessing the FLOW/SWE relationship for the 20 years when SPEI<SWE, only six years were outliers and all six had FLOW less than SWE (FLOW<SWE) by at least one quintile (Table C.3).

For further examination, each of the 37 SPEI/SWE outlier years was categorized into a specific grouping based on the groupings described above, first on the SPEI/SWE relationship (SPEI>SWE, SPEI<SWE) and second on the FLOW/SWE relationship (FLOW>SWE, FLOW<SWE, or FLOW is not different from SWE). The percentile values of SWE, spring SPEI, and FLOW for the years within each of the four categories were averaged together (Table C.3). Additional seasonal temperature and seasonal precipitation percentile values for the years within each category were also averaged. The seasons included: previous October to previous December, January to March, and April to June.

During the five years when SPEI>SWE and FLOW>SWE, spring SPEI is moderately high (66th percentile), while the winter snowpack is very low (19th percentile), and spring streamflow is just above the median (55th percentile). The average seasonal climate conditions for these year help explain these conditions. Precipitation in the fall to early winter period is near the median, but January to March is dry and very warm (80th percentile), leading to lower SWE. In contrast, the spring is wet (71st percentile), with temperatures slightly below median (46th percentile). Compared with the 12 years where SPEI>SWE but FLOW was within one quintile of SWE, the five years with both SPEI>SWE and FLOW>SWE have a wetter early winter, a warmer

October-March, and spring FLOW that was slightly above median. The SPEI>SWE and

FLOW>SWE years also had a much lower SWE, suggesting that when snowpack is extremely

low, spring conditions may have a greater relative contribution. Additionally, the increase in

previous October to previous December precipitation seen in FLOW>SWE years may lessen the

impact of the January to March dry period on the RGHW hydrologic system, resulting in a less

extreme drop in soil moisture or shallow groundwater levels. When the January to March dry

period is then followed by an increased amount of spring precipitation, less moisture may be lost

to dry soil or to shallow groundwater, resulting in a larger increase to streamflow and creating

the FLOW>SWE conditions. The reverse of this mechanism may play a role in determining why

six of the twenty years with SPEI<SWE resulted in FLOW<SWE. All 20 SPEI<SWE years had

similar January to March precipitation and April to June temperatures, but a difference in the

previous October to previous December climate conditions once again may have played a role.

During this early winter period, the six FLOW<SWE years were warmer and drier than the other

14 years. This likely resulted in a drier RGHW hydrologic system going into the spring runoff,

one that a large snowpack produced by a cool and wet January to March could not overcome,

and thus leading to a lower FLOW than expected from the SWE measurements.

C.5   UNDERSTANDING THE PAST RELATIONSHIP BETWEEN SNOWPACK AND SPRING
       HYDROCLIMATE

The second objective of this study centered on understanding the pre-instrumental relationship

between snowpack and spring hydroclimate conditions in order to situate the observed

relationship between SWE and spring SPEI within a broader historic context. To assess this pre-

instrumental relationship, the reconstruction of SWE from Pederson et al. (2011) and the two

new reconstructions of spring SPEI were used (Table C.1B). Because the spring SPEI

reconstruction composed of residual chronologies (here called "spring SPEI reconstruction")

better simulated the year-to-year variability during the instrumental period and matched the lack

of autocorrelation seen in the calibration data, it was used in the annual comparison with

reconstructed SWE. The spring SPEI standard chronology reconstruction was reserved for

comparisons between reconstructions requiring the retention of low-frequency variability. The

first step in addressing the second objective was to examine the ability of the of spring SPEI and

SWE reconstructions to capture the relationships in the observed data. Once that was established,

the multi-century relationships between spring SPEI and SWE relationship were assessed, with a

focus on extreme events (i.e., megadroughts or extended pluvials).

Both spring SPEI reconstructions were correlated with the SWE reconstruction over the

instrumental period (1937-2004). Both reconstructions had moderate and significant correlations

with SWE (respectively, r = 0.533 and r = 0.504, Table C.2B), slightly stronger than the

correlation calculated between observed SPEI and SWE index data (r = 0.365, Table C.2B). This

indicates the reconstructions may slightly overestimate the connection between SPEI and SWE,

although the SPEI and SWE reconstructions were developed using independent sets of

chronologies, reducing the likelihood of covariance between tree-ring data.

The comparisons between the reconstructions of SWE and spring SPEI based on percentile

values for the instrumental period producing results similar to the comparison between the

observed SWE and spring SPEI percentiles, especially in the years where SPEI>SWE (Fig. C.3, last two columns). Although the proportion of years compared are similar, the percent of years with SPEI<SWE was slightly overestimated, while the percent years where SPEI and SWE were within one quintile was correspondingly underestimated. The underestimation of years with SPEI/SWE percentile ranks within one quintile may counter the impact of a slightly stronger correlation between the reconstructed SPEI and SWE (relative to observed data) and the potential for an increase in non-outlier SPEI/SWE years due to the increased correlation. To further assess the similarity between the observed and reconstructed series, the annual percentile difference between SWE and spring SPEI percentiles was calculated for the observed data and reconstructed data by subtracting the SWE percentile rank from the spring SPEI percentile rank for each year in the observation period (1937-2004). This process allowed for a visual assessment of reconstruction skill capturing the annual variability of the difference between the indices (Figure C.S3). The annual percentile difference values for the reconstructed and observed data were moderately and significantly correlated ($r = 0.606$, $p < 0.05$) indicating skill in capturing annual percentile differences between SWE and SPEI.

C.5.1 Reconstructed Percentile Rank Comparison

The reconstructed spring SPEI and SWE percentiles were compared for the full reconstruction period (445-2004), and the years were categorized as either SPEI>SWE, SPEI<SWE, or SPEI within one quintile of SWE (Fig. C.3, far left column). During the full reconstruction period, 47% of years had SPEI within one quintile of SWE, while both SPEI<SWE and SPEI>SWE each constituted 26% of the years (rounding may result in total percentages not equal to 100%).

The same analysis was carried out by century to examine the frequency of the three types of years, from the 6th through the 20th century (Fig. C.3). This revealed a variability in the percentages from century to century, with slightly less variability in the percent of years when spring was drier relative to winter snowpack (SPEI<SWE). Two centuries, the 7th and the 13th, both had fewer than 40% of years when SPEI was within one quintile of SWE. The 7th century also stands out as having the highest percent of years when spring was wet relative to the winter snowpack. Although relatively large increases in spring precipitation do not necessarily result in higher streamflows (as shown in the observed comparisons), poor snowpack years in the 7th century were more likely to be followed by a cooler, wetter spring that may have, in turn, boosted spring streamflow. Conversely, the 14th century had the highest percent of years when spring was relatively drier than winter, increasing the chance that a warm, dry spring during this century may have been more likely to negatively impact streamflow volumes.

Because the comparison analysis between SPEI and SWE reconstructions used percentile rank values, the years when SPEI<SWE and SPEI>SWE were determined by the relative difference between the two indices not the actual values of SPEI and SWE. To investigate the actual values of SWE and SPEI in these years, the average values of SPEI and SWE were calculated for the years when SPEI>SWE and years when SPEI<SWE (Figures 4A and 4B, respectively), both for the full reconstruction and by century. In years when SPEI<SWE, average SPEI is always below the median and average SWE is always greater than the median, that is, winters tend to have a higher snowpack, and springs are warm and dry (Fig. C.4A). The reverse is true for years when SPEI>SWE, with average SPEI always greater than the median and average SWE always less

than the median (Fig. C.4B). However, there is considerable variability from century to century.

For example, SPEI>SWE years in the 17th century were characterized by extremely wet and cool

springs (average SPEI = 0.99) and close to average snowpacks (average SWE = -0.21), while

SPEI>SWE years in the 6th century were characterized more by extremely low snowpacks

(average SWE = -0.91) followed by moderately wetter springs (average SPEI = 0.45). Years

when spring was drier relative to the preceding winter had similar variability in average SPEI

and SWE values. For example, the 6th century again stands out, in this case, with very high

snowpack (average SWE = 0.93), and only moderately warm/dry spring (average SPEI = -0.41).

In the percentile comparisons (Fig. C.3), this does not stand out as a notable century. These

results highlight how, within the constraints of the SPEI<SWE and SPEI>SWE categorization,

the relative value of the climate indices can be quite variable from century to century.

C.5.2   Climate Relationships during Megadroughts and Extended Pluvials

The relationships between SWE and spring SPEI in the reconstructions were also evaluated

during periods of persistent drought or pluvials. The most extreme droughts and pluvials were

identified using a regional time series of June-August PDSI (Palmer Drought Severity Index)

data from the NADA (North American Drought Atlas, Cook et al., 2004), averaging grid point

reconstructions from eight NADA pixels corresponding to the RGHW (and matching the 0.5° x

0.5° SPEI data coverage (Fig. C.1)). The regional PDSI reconstruction was smoothed with a 20-

year spline (Bunn, 2008) to highlight decadal variability. The five highest and five lowest PDSI

values were selected from the smoothed data as representations of the wettest and driest non-

overlapping periods. Because the smoothing process integrated data from before and after each

PDSI value, the period that represented this value included the 10 years prior and after the year of the value, resulting in a 21-year interval used in the analysis. PDSI was chosen to identify the extremes conditions because of the length of the index and because June-August PDSI reflects antecedent conditions that include both winter and spring moisture (St. George et al., 2010).

The percent of years when SPEI>SWE or SPEI<SWE exhibits more variability during the drought and pluvial events compared to the century specific analysis (Fig. C.5). During the five strongest pluvial events, spring conditions were relatively drier than the preceding winter 43% of the time, while only 11% of pluvial years had a spring that was wetter than the preceding winter. This disparity may be explained by the carryover of soil moisture from preceding months that are included in the PDSI calculation. While the NADA was intended to reconstruct June-August drought conditions, St. George et al. (2010) identified the potential in the Southwestern United States for strong moisture anomalies in the winter to be carried over into the calculation of summer PDSI. If that is the case, the SWE reconstruction and the PDSI reconstruction may represent the same winter hydrologic conditions. This is supported by the strong correlation ($r = 0.627$, $p < 0.05$) between the annual SWE reconstruction and the NADA PDSI over the full reconstruction period. Therefore, major pluvial events identified using PDSI are more likely to be characterized by extremely high snowpack years, making years when spring conditions are wetter than winter conditions less likely to occur.

The same bias in the identification of extreme droughts could be assumed, with PDSI values largely driven by reduced winter snowpacks, and spring conditions generally wetter than the

preceding winter. While this holds for the late 13th and late 16th century megadroughts (with 0%

and 5% of years where SPEI<SWE, respectively), the remaining three megadroughts each have

at least 19% of years where springs are drier than the preceding winters. This has potential

implications for spring streamflow during the megadrought events. The observational

comparisons indicated that a dry spring following an above average snowpack has the potential

to reduce spring streamflow, therefore a dry spring following a below average snowpack may

further decrease spring streamflow, resulting in extremely reduced streamflows. Overall, the

analysis of extreme events from the PDSI record indicates that megadroughts may be a product

of both winter and spring conditions, while extreme pluvials are more likely to be driven by

winter snowpack alone.

C.5.3   Multi-Decadal Variability in Snowpack and Spring Hydroclimatic Reconstructions

As a final analysis, the spring SPEI standard chronology reconstruction was compared with the

SWE reconstruction to evaluate long-term, low-frequency variability and identify the way these

climate parameters may have interacted during the persistent extreme events identified from the

PDSI reconstruction. Both reconstructions were smoothed with a 20-year spline (Bunn, 2008) to

highlight decadal variability (Fig. C.6). A consistent relationship is not evident between

reconstructed SWE and spring SPEI, and this is further corroborated by the weak, but still

significant Pearson correlation coefficient ($r = 0.313$, $p < 0.05$, p-value calculated using

autocorrelation adjusted effective degrees of freedom (Hu et al., 2017)). Periods of coherence

between the reconstructions in the 10th and 11th centuries are followed by periods with little

similarity between the two indices the 12th to the 15th century, such as the large difference

between SWE and spring SPEI conditions after 1200. The reconstructions again have more temporal coherence starting in the 16th century and this pattern continues until the present (Fig. C.6).

The periods of megadrought and extreme pluvials indicated in Figure C.6 help highlight the dynamics between spring SPEI and SWE reconstructions. During the five pluvials, SWE and SPEI are consistently positive, with SWE values greater than spring SPEI values in all but one period (the early 19th century pluvial). This pattern is largely in agreement with the previous comparison between the SPEI and SWE percentile ranks during extreme pluvials, which indicated the pluvials were driven primarily by winter, not spring, conditions. Periods when spring SPEI is elevated, such as the mid 7th and late 14th centuries, do not correspond with pluvial events identified in the PDSI, likely because the concurrent winter snowpack was not similarly elevated. In certain instances when snowpack is elevated but spring SPEI is severely depressed (such as the late 11th century), it does appear that the reduced spring SPEI prevented the conditions for a pluvial in the PDSI record.

During the five megadroughts, the SWE and SPEI values were all negative with the exception of spring SPEI during the 6th century megadrought. The megadroughts in the late 13th and 16th centuries are notable because of the simultaneous drops in both SWE and SPEI that occurred. Both the 13th century "Great Drought" and the 16th century megadrought have been identified in other tree-ring based reconstructions due to their duration and severity (Douglass, 1929; Stahle et al., 2000, 2007). A recent reconstruction found that the late 16th century drought was the most

severe period of summer soil moisture deficits in the southwestern portion of North America between 800 and 2019 (Williams et al., 2020). However, both reconstructions were based on the reproduction of winter or summer variability, or both in conjunction. The reconstruction of spring SPEI produced for this study indicates that a third season, spring, may have additionally contribution to the severity of these droughts due to the conjoined effects of winter and spring moisture deficits.

C.6   CONCLUSION

The introduction to this study proposed that a cool, wet spring after a warm, dry winter in the RGHW could potentially increase spring streamflow on the Rio Grande relative to those streamflows expected given the preceding winter snowpack. The first objective of this study was to identify the relationship between observed snowpack, spring hydroclimate, and spring streamflow data in the RGHW, first identifying years when large differences between snowpack and spring hydroclimate may have occurred and second determining whether those years coincided with increases in streamflow relative to snowpack-based expectations. After conversion to percentile rank values, we identified a majority of years in the observed record (37 out of 68 years) as having a significant difference between snowpack and spring hydroclimate conditions. Additionally, 11 of those 37 years had a significant difference between snowpack and spring streamflow, with five of the 11 years having streamflows greater than expected based on snowpack and the remaining six years having streamflows less than expected based on snowpack. Therefore, while rare, there was evidence that during five years (out of 68) the cooler

and wetter spring hydroclimate conditions coincided with spring streamflows on the Rio Grande that were higher than the streamflow volumes expected based on the previous snowpack.

The preceding late-fall to early-winter climate conditions may have been the key factor determining why the 11 years with differences between streamflow and snowpack occurred. A cool, wet early winter (previous October to previous December) followed by a warm, dry late winter (January to March) and a cool, wet spring (April to June) are associated with an increase streamflow relative to snowpack. One explanation is the early season moisture may increase the relative moisture content of the RGHW hydrologic system (soil moisture, shallow groundwater, etc.); thus, despite a warmer and drier late-winter, when spring moisture returns, it is not absorbed by the hydrologic system but quickly results in streamflow. The reverse of these climatic conditions (dry early winter, wet January-March, then warm, dry spring) corresponds with a reduction in streamflow relative to snowpack. The preceding warm, dry conditions in the early winter may reduce total moisture in the hydrologic system and lead to reductions in streamflow that can't be compensated by a greater snowfall in late-winter.

With climate change expected to increase winter temperatures in the RGHW, snowpack is projected to decrease (Llewellyn & Vaddey, 2013). A warmer winter will lead to both an earlier start and a longer period of snowmelt that will reduce the yield from the snowpack due to increased rates of sublimation and evapotranspiration (Barnhart et al., 2016; Harpold & Brooks, 2018). If reductions in snowpack and reductions in spring streamflow relative to snowpack totals were to become common, a cool, wet spring may have an even larger impact on streamflow

volumes. This is similar to findings from Chavarria and Gutzler (2018), where it was argued that continued warming will result in spring precipitation playing a large role in Rio Grande streamflows. All five years where cool, wet springs increased streamflow relative to snowpacks occurred during the latter half of instrumental period, as temperatures in the RGHW were already increasing, indicating that this shift may have already begun.

The second objective of this study evaluated the relationship between winter snowpack and spring hydroclimate conditions over the past 16 centuries in order to provide a broader context for the observed comparison of snowpack and spring hydroclimate conditions. The April to June SPEI reconstruction developed in this study to address this objective is the first reconstruction of a late-spring/early summer drought index specifically produced for the RGHW or the wider southwestern United States. The reconstruction successfully captures variability in April-June SPEI and provides a new, more than 1500 year record of paleoclimate conditions for a unique time of year. Although moisture reconstructions in the RGHW typically have higher skill (e.g., Woodhouse et al., 2012), by utilizing *P. aristata* as a paleo-climate proxy we traded reconstruction skill for a longer period of record. The tests for reconstruction stability in the supplemental material confirm the SPEI reconstruction is statistically robust. The comparison of this new reconstruction of spring SPEI with the previously produced reconstruction of SWE (Pederson et al., 2011) gives insight into the relationship between these seasonal hydroclimatic variables.

Comparing the relationship between reconstructed spring SPEI and SWE for the instrumental

period (1937-2004) with reconstructed relationship for the full reconstruction period (445-2004),

there is a similarity in the percentage of years falling into the categories of SPEI>SWE,

SPEI<SWE, or SPEI and SWE within one quintile. However, when the full reconstruction is

analyzed by century, there is more variability evident in the century-specific percentages,

particularly so with years when spring SPEI is greater than winter snowpack. Although this

larger variability might suggest certain centuries had an increased likelihood for a cool, wet

spring which could result in an increase in streamflow relative to snowpack, it is important to

recall from the observational data that only 29% of years when SPEI>SWE saw a concomitant

increase in streamflow relative to snowpack. Applying this ratio (29%) to the reconstructed data

can produce an estimated percentage of years where a wet spring may have resulted in increased

streamflow volumes. The 6th century had the highest percent of SPEI>SWE years at 37% (or 37

out of 100 years), but the application of the observational ratio results in an estimation of only 10

years where wet spring conditions may have resulted in a larger streamflow relative to

snowpack. This once in a decade occurrence (10%) is very similar to the 7% of years seen in the

observed record. Therefore, while the comparison process does show century to century

variability in the relationship between reconstructed spring SPEI and SWE, this variability does

not necessarily mean the likelihood of extreme spring hydroclimate conditions altering

streamflow volumes is markedly different than that observed during the instrumental period.

Examination of SWE and spring SPEI during periods of megadroughts and extreme pluvials

provides further insight into the interaction between the winter snow and spring hydroclimate

conditions. The pluvial events, as defined by the PDSI reconstruction for the RGHW (Cook et al., 2004), were largely driven by increases in snowpack relative to spring hydroclimatic conditions, and it was very rare for spring SPEI to be larger than winter SWE. Therefore, the chance that a cool, wet spring could increase streamflow relative to snowpack during a pluvial was also reduced. The plot of 20-yr smoothed SPEI and SWE reconstructions reinforce this conclusion, with all but one of the pluvials coinciding with periods where SWE values were greater than SPEI values. All of these findings point to the dominance of winter precipitation during pluvial events in the RGHW and the weak additive effect of spring hydroclimatic conditions on the pluvials.

Conversely, the megadroughts in the RGHW saw a relatively large percentage of years (compared to the pluvials) where spring conditions may have added to the severity of the event. The megadrought periods were more likely to see values of spring SPEI lower than winter SWE, increasing the chance that a dry spring may have further exacerbated low streamflow on the Rio Grande. While spring conditions do appear to have a larger influence on the RGHW megadroughts, they alone do not drive lower PDSI values, as several periods with extremely low SPEI values and moderate to high SWE values do not coincide with megadroughts. Finally, the late 16th century megadrought stands out for the coinciding severity of the declines in spring SPEI and SWE. Previous reconstructions identified this period as one of the most severe droughts in the western United States, however the reconstructions were developed for either winter or summer conditions (Stahle et al., 2000, 2007; Williams et al., 2020). This novel reconstruction of spring SPEI also shows that a steep decline in spring precipitation during the

late 16th century may have provided an additional factor which contributed to the severity of the megadrought.

The results presented here indicate it is possible for spring hydroclimatic conditions to have a significant influence on Rio Grande spring streamflow, producing changes in runoff volume different than that expected from snowpack alone. With increasing temperatures expected in the RGHW, the importance of a cool, wet spring which partially ameliorates the effects of a poor snowpack will continue to increase. However, both instrumental and reconstruction-based comparisons between snowpack and spring hydroclimate indicate that the potential for an extremely wet spring to increase streamflow is rare. Water managers therefore should both recognize the increasing importance of these events, while simultaneously tempering expectations that they will alleviate the increasingly likelihood of climate-induced drought stress on the Rio Grande.

C.7   ACKNOWLEDGEMENTS

C.8   WORKS CITED

Adams, D. K., & Comrie, A. C. (1997). The North American Monsoon. *Bulletin of the American Meteorological Society*, *78*(10), 2197–2213. https://doi.org/10.1175/1520-0477(1997)078<2197:TNAM>2.0.CO;2

Allen, R. G., Pereira, L. S., Raes, D., & Smith, M. (1998). Crop evapotranspiration-Guidelines for computing crop water requirements-FAO Irrigation and drainage paper 56. *FAO, Rome*, *300*(9), D05109.

Barnhart, T. B., Molotch, N. P., Livneh, B., Harpold, A. A., Knowles, J. F., & Schneider, D. (2016). Snowmelt rate dictates streamflow. *Geophysical Research Letters*, 43(15), 8006–8016. https://doi.org/10.1002/2016GL069690

Blythe, T. L., & Schmidt, J. C. (2018). Estimating the Natural Flow Regime of Rivers With Long-Standing Development: The Northern Branch of the Rio Grande. *Water Resources Research*, 54(2), 1212–1236. https://doi.org/10.1002/2017WR021919

Bunn, A. G. (2008). A dendrochronology program library in R (dplR). *Dendrochronologia*, *26*(2), 115–124. https://doi.org/10.1016/j.dendro.2008.01.002

Chavarria, S. B., & Gutzler, D. S. (2018). Observed Changes in Climate and Streamflow in the Upper Rio Grande Basin. *JAWRA Journal of the American Water Resources Association*, *54*(3), 644–659. https://doi.org/10.1111/1752-1688.12640

Colorado DWR. (2021). Rio Grande Near Del Norte, CO (RIODELCO). Colorado Division of Water Resources Department of Natural Resources. Retrieved from https://dwr.state.co.us/Tools/Stations/RIODELCO?params=DISCHRG

Cook, E. R., Woodhouse, C. A., Eakin, C. M., Meko, D. M., & Stahle, D. W. (2004). Long-Term Aridity Changes in the Western United States. *Science*, *306*(5698), 1015–1018. https://doi.org/10.1126/science.1102586

Davis, T. (2021a, January 31). NM water managers warn communities to prepare for low Rio Grande. *Albuquerque Journal*. Retrieved from https://www.abqjournal.com/2354734/nm-water-managers-warn-communities-to-prepare-for-low-rio-grande.html

Davis, T. (2021b, April 16). Dismal outlook for Rio Grande. *Albuquerque Journal*. Retrieved from https://www.abqjournal.com/2381114/dismal-outlook-for-rio-grande.html

Davis, T. (2021c, June 25). From Rio Grande to 'Rio Sand'? *Albuquerque Journal*. Retrieved from https://www.abqjournal.com/2403720/from-rio-grande-to-rio-sand-ex-iconic-river-may-go-dry-through-abq-this-summer.html

Davis, T. (2021d, July 30). Rains ease New Mexico's short-term drought. *Albuquerque Journal.* Retrieved from https://www.abqjournal.com/2415050/rains-ease-new-mexicos-shortterm-drought.html

Douglass, A. E. (1929). The secret of the Southwest solved by talkative tree rings. *National Geographic*, 56(6), 737–770.

Elias, E. H., Rango, A., Steele, C. M., Mejia, J. F., & Smith, R. (2015). Assessing climate change impacts on water availability of snowmelt-dominated basins of the Upper Rio Grande basin. *Journal of Hydrology: Regional Studies*, 3, 525–546. https://doi.org/10.1016/j.ejrh.2015.04.004

Fleck, J. (2021, July 28). New Mexico's Rio Grande, bailed out by an impressive monsoon [Blog]. Retrieved from http://www.inkstain.net/fleck/2021/07/new-mexicos-rio-grande-bailed-out-by-an-impressive-monsoon/

Fleming, S. W., Garen, D. C., Goodbody, A. G., McCarthy, C. S., & Landers, L. C. (2021). Assessing the new Natural Resources Conservation Service water supply forecast model for the American West: A challenging test of explainable, automated, ensemble artificial intelligence. *Journal of Hydrology*, 602, 126782. https://doi.org/10.1016/j.jhydrol.2021.126782

Garen, D. C. (1992). Improved Techniques in Regression-Based Streamflow Volume Forecasting. *Journal of Water Resources Planning and Management*, 118(6), 654–670. https://doi.org/10.1061/(ASCE)0733-9496(1992)118:6(654)

Harpold, A. A., & Brooks, P. D. (2018). Humidity determines snowpack ablation under a warming climate. *Proceedings of the National Academy of Sciences*, 115(6), 1215–1220. https://doi.org/10.1073/pnas.1716789115

Hu, J., Emile-Geay, J., & Partin, J. (2017). Correlation-based interpretations of paleoclimate data – where statistics meet past climates. *Earth and Planetary Science Letters*, *459*, 362–371. https://doi.org/10.1016/j.epsl.2016.11.048

Hurd, B., & Coonrod, J. (2012). Hydro-economic consequences of climate change in the upper Rio Grande. *Climate Research*, 53(2), 103–118. https://doi.org/10.3354/cr01092

Lehner, F., Wood, A. W., Llewellyn, D., Blatchford, D. B., Goodbody, A. G., & Pappenberger, F. (2017). Mitigating the Impacts of Climate Nonstationarity on Seasonal Streamflow Predictability in the U.S. Southwest. *Geophysical Research Letters*, 44(24). https://doi.org/10.1002/2017GL076043

Llewellyn, D., & Vaddey, S. (2013). *West-Wide Climate Risk Assessment: Upper Rio Grande Impact Assessment: Report*. US Department of the Interior, Bureau of Reclamation, Upper Colorado Region

Menne, M. J., Williams, C. N., Gleason, B. E., Rennie, J. J., & Lawrimore, J. H. (2018). The Global Historical Climatology Network Monthly Temperature Dataset, Version 4. *Journal of Climate*, 31(24), 9835–9854. https://doi.org/10.1175/JCLI-D-18-0094.1

NRCS-NWCC. (2020). *Colorado Streamflow Forecast Summary: April 1, 2020*. Portland, OR: Natural Resouces Conservation Service - National Water and Climate Center. Retrieved from https://www.wcc.nrcs.usda.gov/ftpref/support/water/SummaryReports/CO/BFcst_4_2020 .pdf?

NRCS-NWCC. (2021). *Colorado Streamflow Forecast Summary: April 1, 2021*. Portland, OR: Natural Resouces Conservation Service - National Water and Climate Center. Retrieved from https://www.wcc.nrcs.usda.gov/ftpref/support/water/SummaryReports/CO/BFcst_4_2021 .pdf?

Paddock, W. A. (2001). The Rio Grande Compact of 1938. *U. Denv. Water L. Rev.*, 5, 1.

Pagano, T., Garen, D., & Sorooshian, S. (2004). Evaluation of Official Western U.S. Seasonal Water Supply Outlooks, 1922–2002. *Journal of Hydrometeorology*, 5(5), 896–909. https://doi.org/10.1175/1525-7541(2004)005<0896:EOOWUS>2.0.CO;2

Pagano, T. C., Garen, D. C., Perkins, T. R., & Pasteris, P. A. (2009). Daily Updating of Operational Statistical Seasonal Water Supply Forecasts for the western U.S. *JAWRA Journal of the American Water Resources Association*, 45(3), 767–778. https://doi.org/10.1111/j.1752-1688.2009.00321.x

Pederson, G. T., Gray, S. T., Woodhouse, C. A., Betancourt, J. L., Fagre, D. B., Littell, J. S., et al. (2011). The Unusual Nature of Recent Snowpack Declines in the North American Cordillera. *Science*, 333(6040), 332–335. https://doi.org/10.1126/science.1201570

St. George, S., Meko, D. M., & Cook, E. R. (2010). The seasonality of precipitation signals embedded within the North American Drought Atlas. *The Holocene*, 20(6), 983–988. https://doi.org/10.1177/0959683610365937

Stahle, D. W., Cook, E. R., Cleaveland, M. K., Therrell, M. D., Meko, D. M., Grissino-Mayer, H. D., et al. (2000). Tree-ring data document 16th century megadrought over North America. *Eos, Transactions American Geophysical Union*, *81*(12), 121. https://doi.org/10.1029/00EO00076

Stahle, D. W., Fye, F. K., Cook, E. R., & Griffin, R. D. (2007). Tree-ring reconstructed megadroughts over North America since a.d. 1300. *Climatic Change*, 83(1–2), 133–149. https://doi.org/10.1007/s10584-006-9171-x

Tintor, W. L., & Woodhouse, C. A. (2021). The variable climate response of Rocky Mountain bristlecone pine (*Pinus aristata* Engelm.). *Dendrochronologia*, 68, 125846. https://doi.org/10.1016/j.dendro.2021.125846

Trouet, V., & Van Oldenborgh, G. J. (2013). KNMI Climate Explorer: A Web-Based Research Tool for High-Resolution Paleoclimatology. *Tree-Ring Research*, *69*(1), 3–13. https://doi.org/10.3959/1536-1098-69.1.3

Udall, B. H. (2020). 7 Running on Empty: Southwestern Water Supplies and Climate Change. In *Standing between Life and Extinction* (pp. 109–123). University of Chicago Press.

USGS. (2021a). USGS Water Data for the Nation: US Geological Survey National Water Information System database. https://doi.org/10.5066/F7P55KJN

USGS. (2021b). Watershed Boundary Dataset Data Model (v2.3): U.S. Geological Survey database.

Vandiver, S. (1999, December). How Colorado Meets Its Obligation Under the Rio Grande Compact. Presentation presented at the 44th Annual New Mexico Water Conference: The Rio Grande Compact: It's the Law!, Santa Fe, New Mexico.

Vicente-Serrano, S. M., Beguería, S., & López-Moreno, J. I. (2010). A Multiscalar Drought Index Sensitive to Global Warming: The Standardized Precipitation Evapotranspiration Index. *Journal of Climate*, 23(7), 1696–1718. https://doi.org/10.1175/2009JCLI2909.1

Williams, A. P., Cook, E. R., Smerdon, J. E., Cook, B. I., Abatzoglou, J. T., Bolles, K., et al. (2020). Large contribution from anthropogenic warming to an emerging North American megadrought. *Science*, 368(6488), 314–318. https://doi.org/10.1126/science.aaz9600

Wong, T.-T. (2015). Performance evaluation of classification algorithms by k-fold and leave-one-out cross validation. *Pattern Recognition*, *48*(9), 2839–2846. https://doi.org/10.1016/j.patcog.2015.03.009

Woodhouse, C., Stahle, D., & Villanueva Díaz, J. (2012). Rio Grande and Rio Conchos water supply variability over the past 500 years. *Climate Research*, *51*(2), 147–158. https://doi.org/10.3354/cr01059

C.9   TABLES

Table C.1. Observed (A) and reconstructed (B) time series used in this study.

A)

Time Series Abbreviation	Time Series Full Name	Years	Source
SWE	Rio Grande Headwaters April 1 Snow Water Equivalent	1937-2004	Pederson et al., 2011
Spring SPEI	Rio Grande Headwaters April-June Standardized Precipitation-Evapotranspiration Index	1902-2018	Vicente-Serrano et al., 2010
Spring streamflow	Del Norte gage along the Rio Grande April-June Streamflow	1908-2021	USGS, 2021a

B)

Time Series Abbreviation	Time Series Full Name	Years	Source
SWE	Reconstructed Rio Grande Headwaters April 1 Snow Water Equivalent	369-2005	Pederson et al., 2011
Spring SPEI	Reconstruction of Rio Grande Headwaters April-June Standardized Precipitation-Evapotranspiration Index using residual chronologies	445-2004	This study
Spring SPEI (Std. Chron.)	Reconstruction of Rio Grande Headwaters April-June Standardized Precipitation-Evapotranspiration Index using standard chronologies	445-2004	This study

Table C.2. Correlations between all observational datasets (A) and correlations between reconstruction datasets of SWE and spring SPEI based on residual chronologies (B). The correlations are calculated for the instrumental period 1937-2004 and the reconstruction based on standard chronologies is in parentheses.

A)

	SWE	Spring SPEI	Spring Streamflow
SWE	1.000	~	~
Spring SPEI	0.365	1.000	~
Spring Streamflow	0.785	0.486	1.000

B)

	SWE	Spring SPEI
SWE	1.000	~
Spring SPEI (Std. Chron.)	0.553 (0.504)	1.000

Table C.3. Number of years and average percentile values for SWE, spring SPEI, spring streamflow, seasonal precipitation, and seasonal temperature for years classified by the relationships between SPEI/SWE and FLOW/SWE. Colors codes correspond with average percentile values: greens/blues = wet/cool; oranges/red= dry/warm; white=near median.

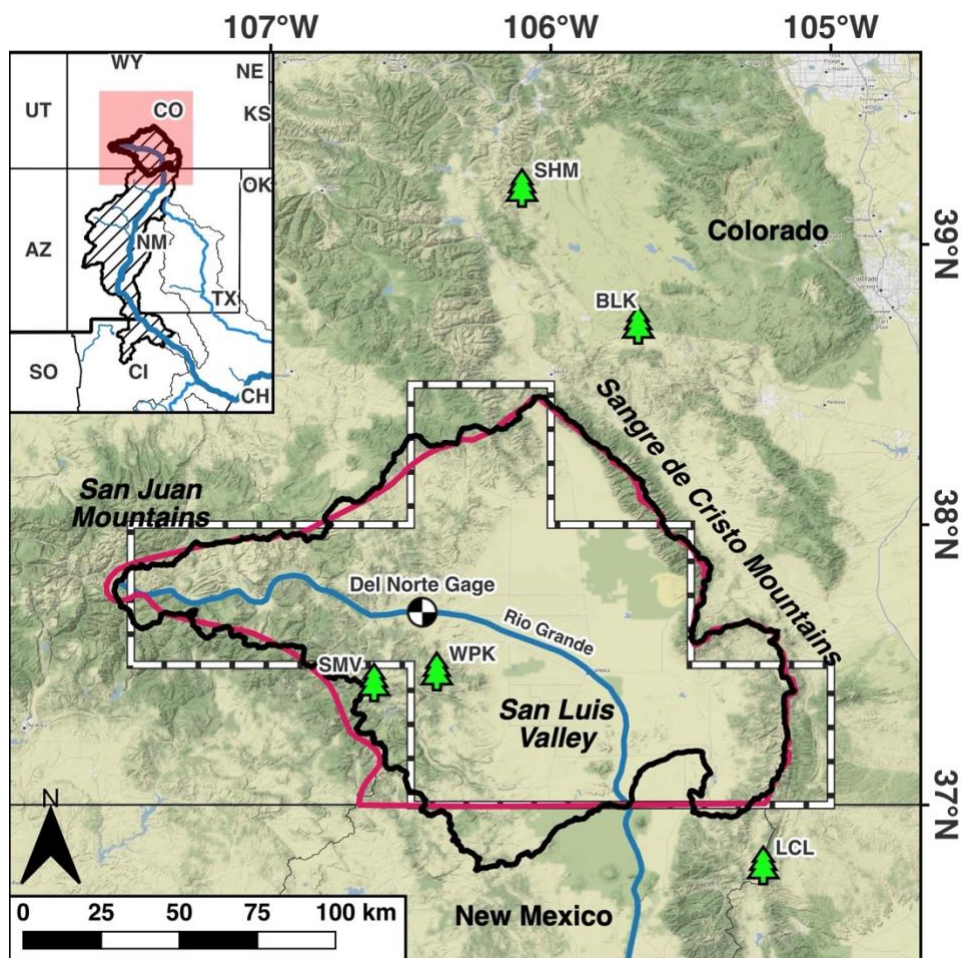| | | # Yrs. | SWE | Spring SPEI | Spring Flow | Precipitation | | | Temperature | | |
						pOct-pDec	Jan-Mar	Apr-Jun	pOct-pDec	Jan-Mar	Apr-Jun
SPEI > SWE	**FLOW > SWE**	5	**19**	**66**	**55**	**52**	**30**	**71**	**67**	**80**	**46**
	FLOW ≯ SWE	12	32	73	33	38	32	70	59	64	41
SPEI < SWE	**FLOW < SWE**	6	**65**	**33**	**37**	**33**	**64**	**40**	**59**	**48**	**58**
	FLOW ≮ SWE	14	65	30	65	69	61	32	39	38	59

C.10 FIGURES

Figure C.1. Study area map showing the Rio Grande Headwaters Basin (RGHW, thick black line), the GHCN Colorado Climate Division 5 (thick red line), and the outline of the gridded product pixels used to select SPEI and PDSI data (dashed black and white line). The Del Norte Gage (black and white circle) and the *P. aristata* chronologies (green trees) used in this study are also indicated. The inset shows the study area in the context of the upper Rio Grande Basin (hashed black lines).
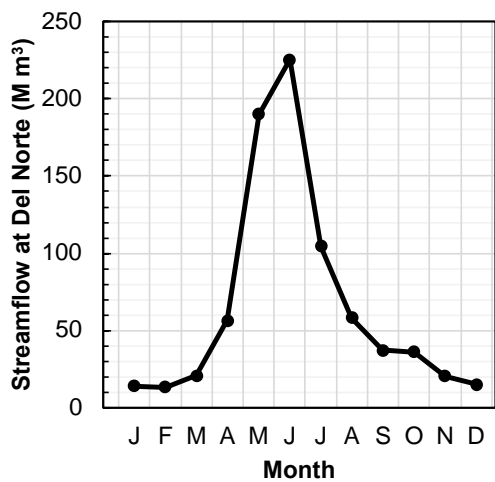
A)
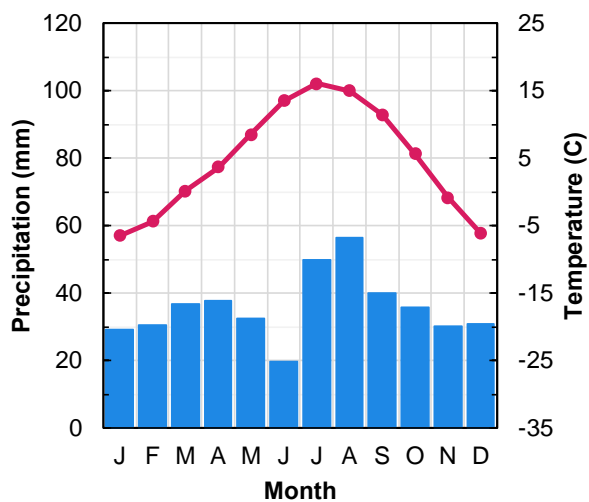
B)

Figure C.2. Climograph (A) of the average monthly temperatures (red) and monthly precipitation totals (blue) for the Colorado Climate Division 5 from 1991-2020 (Menne et al., 2018). Hydrograph (B) with average monthly total streamflow from 1908-2020 for the Del Norte gage along the Rio Grande (U.S. Geological Survey Gage 8220000).
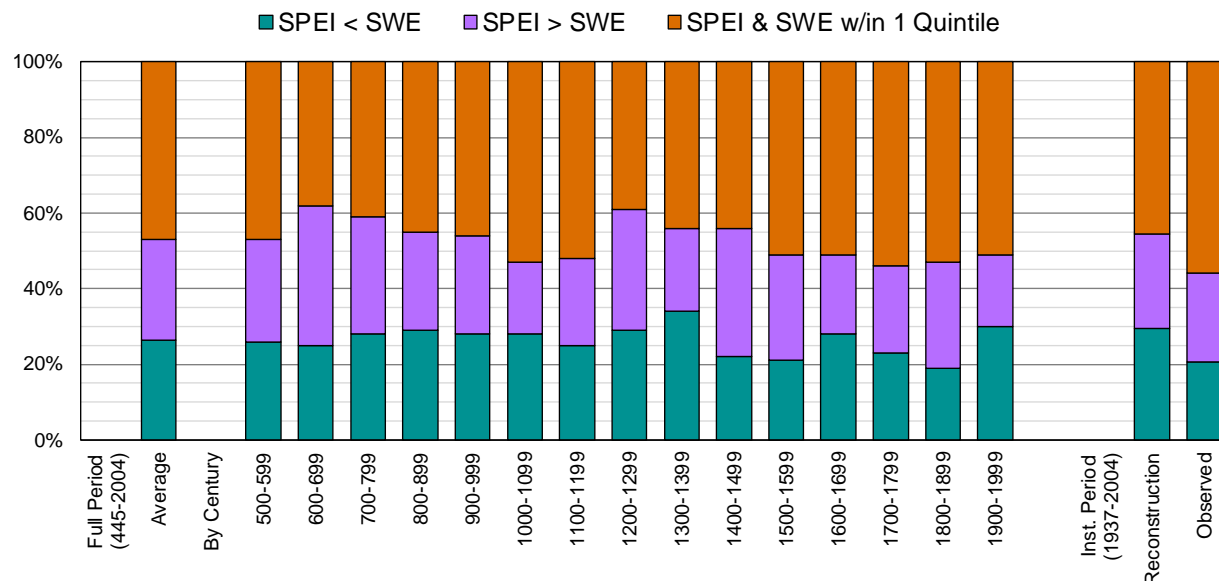
Figure C.3. Percentile rank comparison between the spring SPEI reconstruction and the SWE reconstruction(Pederson et al. 2011). Each column shows the percent of years with a specific SPEI and SWE percentile relationship (SPEI<SWE, SPEI>SWE, SPEI within one quintile of SWE). Years with SPEI<SWE had spring conditions that were warmer and drier than the preceding winters, while SPEI>SWE years had spring conditions that were cooler and wetter than the preceding winters. The first column shows the percentages for the full period of the reconstruction (445-2004) followed by the percentages by century (6th to 20th centuries). The last two columns show the percentile relationship percentages during the instrumental period (1937-2004) for the reconstructed and observed data.
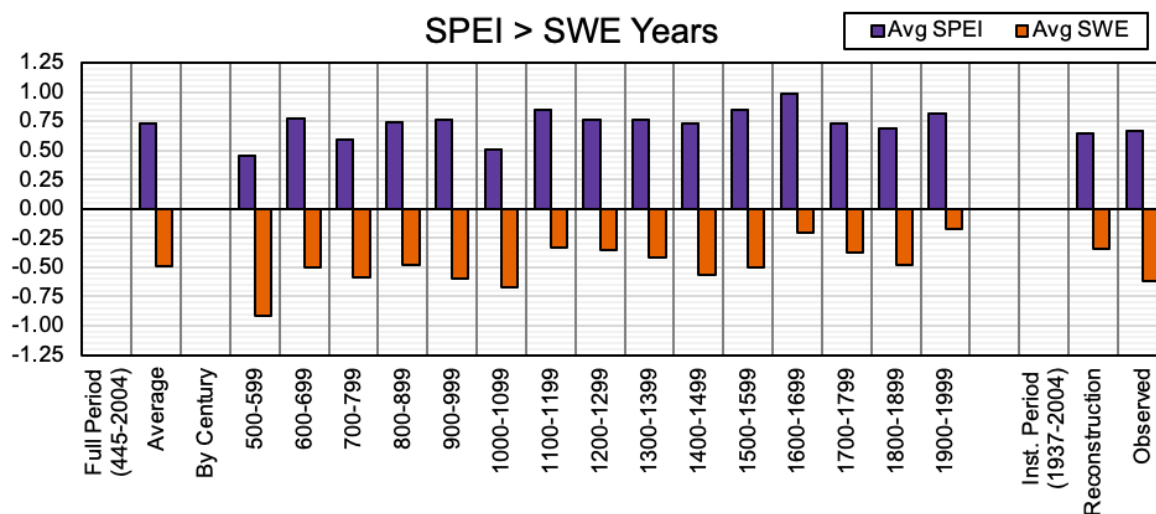
A)
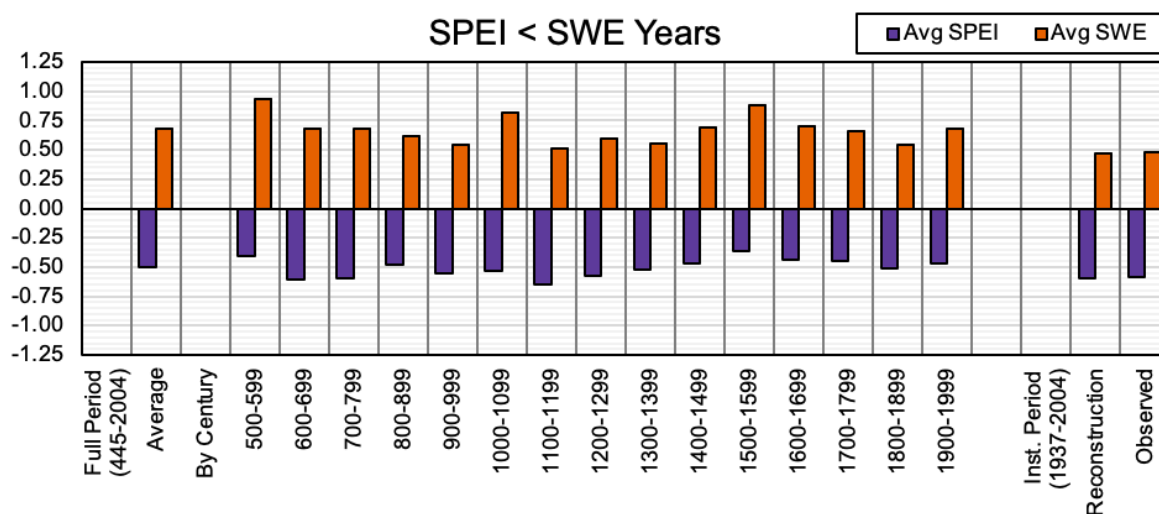
B)

Figure C.4. The average SPEI and SWE values during years when (A) spring conditions were warmer and drier than the preceding winter (SPEI<SWE) and (B) spring conditions were cooler and wetter than the preceding winter (SPEI>SWE). Values are shown for the full reconstruction period (445-2004, left hand column), by century (middle 15 columns), and the instrumental period (1937-2004, 2 right hand columns). The instrumental period average values are for the reconstructed and the observed data.
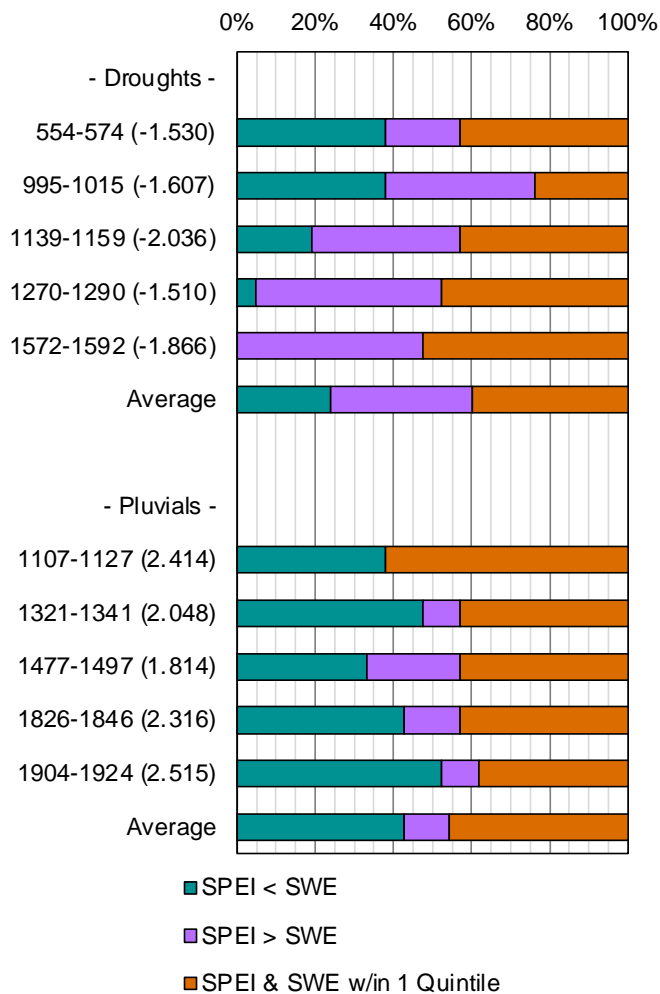
Figure C.5. Percentile rank comparison between the RGHW spring SPEI and SWE reconstructions during the top five megadroughts (top) and top five pluvials (bottom) as determined from the RGHW PDSI reconstruction (PDSI values of middle year in parenthesis). Each bar shows the percent of years with a specific SPEI and SWE percentile relationship (SPEI<SWE, SPEI>SWE, SPEI within one quintile of SWE). Years with SPEI<SWE had spring conditions that were warmer and drier than the preceding winters, while SPEI>SWE years had spring conditions that were cooler and wetter than the preceding winters. In addition, average percentile rank comparison percentages for the five megadroughts and for the five pluvials were calculated.
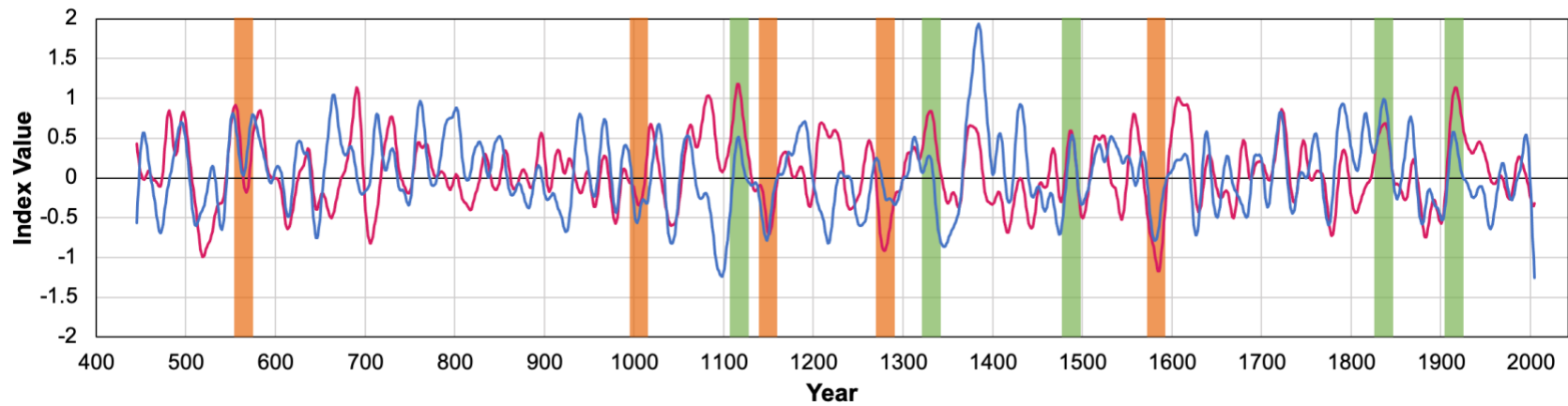
Figure C.6. Standard chronology reconstruction of spring SPEI (blue) and reconstruction of SWE (red) over the full period of reconstruction (445-2004), smoothed with a 20-yr smoothed spline. The top five 21-year megadroughts (orange) and pluvial events (green), identified using RGHW PDSI, are highlighted.

C.11   SUPPLEMENTAL INFORMATION

C.11.S1   Chronology Preparation and Screening

The chronologies included in the predictor pool for the reconstruction model included all Rocky

Mountain bristlecone pine (*Pinus aristata* Engelm.) chronologies used by Tintor & Woodhouse

(2021) for their broad based evaluation of *P. aristata* climate sensitivity. Standardization and

chronology development followed the approach from Woodhouse & Pederson (2018) with tree-

ring widths conservatively detrended using a negative exponential/straight line fit using the

"dplR" package (Bunn, 2008). Individual series were variance stabilized using a power

transformation to account for changing numbers of samples over time (Cook & Peters, 1997)

then combined into a single site specific chronology using a robust bi-weight mean (Cook &

Kairiukstis, 2013). Both standard (retaining autocorrelation) and residual (removing

autocorrelation) versions of the site-specific chronologies were produced. Chronologies were

then screened for significant correlations with the Rio Grande Headwaters April-June

Standardized Precipitation-Evapotranspiration Index (RGHW AMJ SPEI) data over the 1900-

2006 common interval. Five of the 11 chronologies from Tintor and Woodhouse (2021) passed

the screening test: Black Mountain (BLK), Little Costilla Peak Low (LCL), Sheep Mountain

(SHM), Summitville (SMV), Windy Peak (WPK). The locations of the five chronologies are

shown in Figure C.1.

C.11.S2   Reconstruction Development

The reconstruction process used a truncated version of the SSR (single-site reconstruction)

process from Meko (1997), with two reconstructions produced (one using residual chronologies

and one using standard chronologies). The process began with all five of the chronologies, and

includes the chronologies lagged forward and backward 1 and 2 years. This resulted in a total 25

potential predictors (5 original, 5 lag1, 5 lag2, 5 lead1, 5 lead2). This was done to capture

potential multi-year biologic responses to climate still present in the time series after detrending.

The 25 time series were then correlated with instrumental spring SPEI data from 1902-2004 (2

years taken off the beginning and the end due to the lag). A forward stepwise regression was then

run on the time series, with new additions halted when the predictor produced a decrease in the

Reduction of Error (RE) statistic (Cook & Kairiukstis, 2013). This process was repeated after

removing the shortest chronology (in this case LCL), running the preceding steps on the

remaining 20 time series. This process was repeated a third, and final, time, removing the second

shortest chronology (SHM), again using the preceding process, this time on 15 time series. The

process was stopped when the number of chronologies dropped below 3. This methodology was

run twice, once for standard chronologies and once for residual chronologies.

The final suite of models was selected using adjusted coefficient of determination (R^2_{adj}) values,

Durbin Watson test, and cross-validation statistics (Tables C.S1 and C.S2). The Durbin Watson

test identified whether excessive autocorrelation in the residual values of the reconstruction

models was present. High autocorrelation in the residual values may lead to an underestimation

of true standard errors and a suggestion of significance where there is none. The "cvTools"

package was used to calculate cross-validation using the Leave-One-Out and the K-folds

methods (Table C.S1, Alfons, 2012). The K-folds method withheld a random set of 10 sequential

observations from the model fitting then tested the prediction accuracy, repeating the process 100

times. Split sample statistics were calculated for each model as an additional check (Table C.S2).

The periods used in the split sample statistics were 1902-1952 and 1953-2004.

The descriptive statistics for both the residual and standard chronology based spring SPEI reconstruction models are shown in Supplemental Table C.S1. The skill (R^2_{adj}) of the models based on residual chronologies ranged from 0.45 to 0.39 as the length of the reconstruction increased. The skill of the models based on standard chronologies was slightly less (0.33 to 0.32), but in both cases the RE (Standard Error) and RMSE (Root Mean Square of Error) statistics indicate good validation for all of the models. The residuals of all reconstruction models meet the assumption of a lack of significant low order autocorrelation (as determined by Durbin-Watson test). The split sample RE (Reduction of Error) and RMSEv statistics are similar to those for the full period and further suggest the stability of the reconstruction models over time (Table C.S2). In the residual chronology models BLK is the leading predictor in all three models, while in the standard chronology models SMV is the leading predictor in the longer model and BLK is the leading predictor in the shortest model. All but one of the reconstruction models incorporate at least one predictor which is lagged forward one year.

All three models developed using residual chronologies were chosen for the reconstruction, while only two were chosen for the reconstruction using standard chronologies as two of the models had identical inputs and therefore identical statistical properties (Table C.S1). To develop the final full nested reconstructions, the mean and variance for each reconstruction were scaled to match the mean and variance for the instrumental spring SPEI data. Although this is a common practice, it should be acknowledged that scaling the mean and variance can result in an increase in reconstruction error in some years. The mean and variance stabilized reconstructions using residual chronologies and reconstructions using standard chronologies were then nested

backward in time to generate, respectively, a single reconstruction for the residual chronologies and single reconstruction for standard chronologies, both spanning the period 445-2004 CE. A comparison of the observed and reconstructed spring SPEI time series for the residual and standard reconstructions are shown in Figures C.S1 and C.S2 respectively.

C.11.S3   Supplemental Tables

Table C.S1. Descriptive statistics for spring SPEI reconstructions developed using residual (A) and standard (B) chronologies. In the equations section, P1 (and N1) indicates a chronology lagged forward (or backward) by 1 year.

A) Spring SPEI Reconstruction using Residual Chronologies

Model	Reconstruction Years	Predictors	Calibration Period	R^2_{adj}	Standard Error (SE)	Leave-One-Out Cross Validation (RMSE$_v$)	K-folds Mean Value (RMSE$_v$)	AR1	D-W Test	D-W P-value
1R	445-1609	3	1902-2004	0.392	0.726	0.743	0.744	-0.284	2.277	0.156
2R	1610-1805	7	1902-2004	0.443	0.694	0.720	0.722	-0.269	2.160	0.388
3R	1806-2004	6	1902-2004	0.447	0.692	0.710	0.711	-0.078	2.054	0.746

Model	Equation
1R	AMJ SPEI = -1.766 + 0.633*WPK + 0.8198*SMV + 0.992*BLK - 0.628*P1_SMV
2R	AMJ SPEI = -1.902 + 0.806*WPK + 0.645*SMV + 1.516*BLK - 1.253*SHM - 0.894*P1_SMV + 1.484*P1_SHM - 0.357*N1_WPK
3R	AMJ SPEI = -2.642 + 0.948*WPK + 1.232*BLK + 1.025*LCL - 1.029*SHM - 0.995*P1_SMV + 1.467*P1_SHM

B) Spring SPEI Reconstruction using Standard Chronologies

Model	Reconstruction Years	Predictors	Calibration Period	R^2_{adj}	Standard Error (SE)	Leave-One-Out Cross Validation (RMSE$_v$)	K-folds Mean Value (RMSE$_v$)	AR1	D-W Test	D-W P-value
1S	445-1610	2	1902-2004	0.318	0.768	0.778	0.778	0.309	2.271	0.194
2S	1611-2004	5	1902-2004	0.334	0.760	0.781	0.782	0.358	2.187	0.448

Model	Equation
1S	AMJ SPEI = -2.043 + 1.140*SMV + 0.988*BLK
2S	AMJ SPEI = -2.143 + 1.253*SMV + 1.332*BLK - 1.024*SHM + 1.217*P1_SHM - 0.474*P1_WPK

Table C.S2. Split-sample calibration and validation for the spring SPEI reconstruction models using residual chronologies (A) and standard chronologies (B).

A) Split Period Calibration of Spring SPEI Reconstruction using Residual Chronologies

Model	Model Time Span	Calibration Period	n	Early Calibration		Late Validation	
				R^2_{adj}	SE	RE	$RMSE_v$
1R	445-1609	1902-1952	51	0.404	0.719	0.347	0.762
2R	1610-1805	1902-1952	51	0.398	0.723	0.438	0.707
3R	1806-2004	1902-1952	51	0.350	0.751	0.482	0.679
Model	Model Time Span	Calibration Period	n	Late Calibration		Early Validation	
				R^2_{adj}	SE	RE	$RMSE_v$
1R	445-1609	1953-2004	52	0.388	0.731	0.228	0.809
2R	1610-1805	1953-2004	52	0.469	0.682	0.332	0.753
3R	1806-2004	1953-2004	52	0.510	0.654	0.351	0.742

B) Split Period Calibration of Spring SPEI Reconstruction using Standard Chronologies

Model	Model Time Span	Calibration Period	n	Early Calibration		Late Validation	
				R^2_{adj}	SE	RE	$RMSE_v$
1S	443-1607	1902-1952	51	0.386	0.730	0.241	0.822
2S	1608-2004	1902-1952	51	0.363	0.743	0.256	0.813
Model	Model Time Span	Calibration Period	n	Late Calibration		Early Validation	
				R^2_{adj}	SE	RE	$RMSE_v$
1S	443-1607	1953-2004	52	0.236	0.817	0.390	0.720
2S	1608-2004	1953-2004	52	0.287	0.789	0.266	0.790

Table C.S3. Years in each SPEI/SWE and FLOW/SWE categorization based on the percentile value relationships of the instrumental dataset from 1937-2004.Less than and greater than symbols represent *at least* one quintile difference in the ranking.

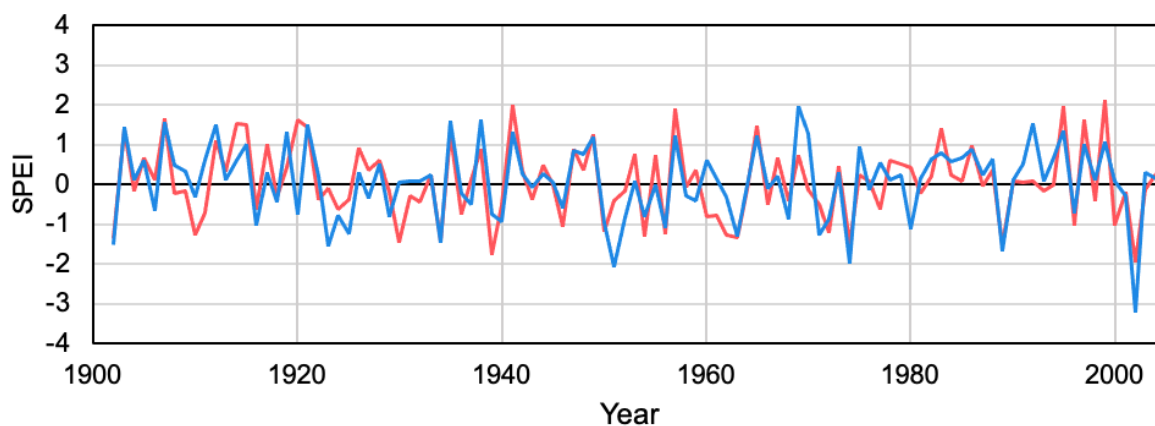| SPEI > SWE		SPEI < SWE	
FLOW > SWE	FLOW ≯ SWE	FLOW < SWE	FLOW ≮ SWE
1971	1947	1937	1939
1986	1953	1943	1950
1990	1955	1945	1952
1999	1959	1956	1954
2004	1967	1974	1960
	1977	1993	1961
	1978		1962
	1981		1968
	1983		1975
	1988		1979
	1995		1985
	1997		1987
			1989
			2001

C.11.S4   Supplemental Figures

Figure C.S1. Comparison between the observed spring SPEI (red) and the spring SPEI reconstruction constructed with residual chronologies (blue) over the common interval of 1902-2004.
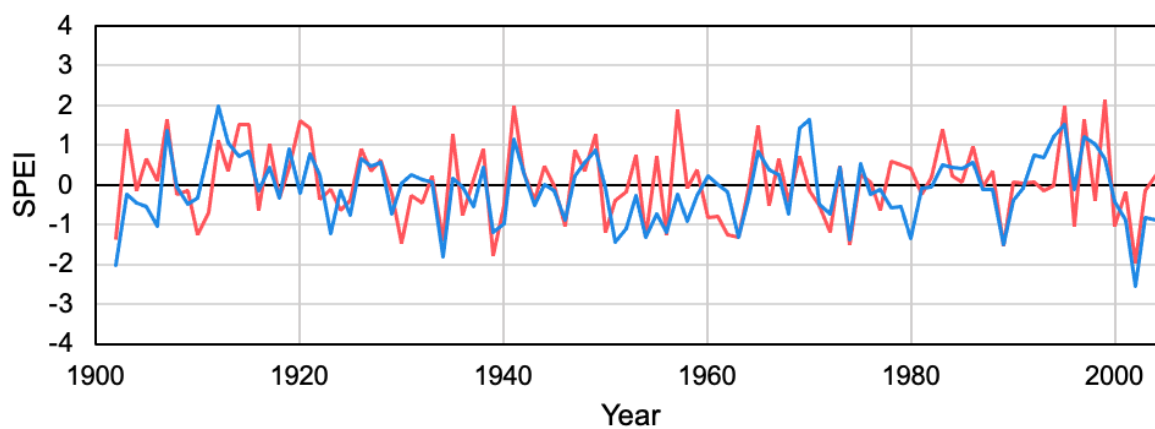

Figure C.S2. Comparison between the observed spring SPEI (red) and the spring SPEI reconstruction constructed with standard chronologies (blue) over the common interval of 1902-2004.
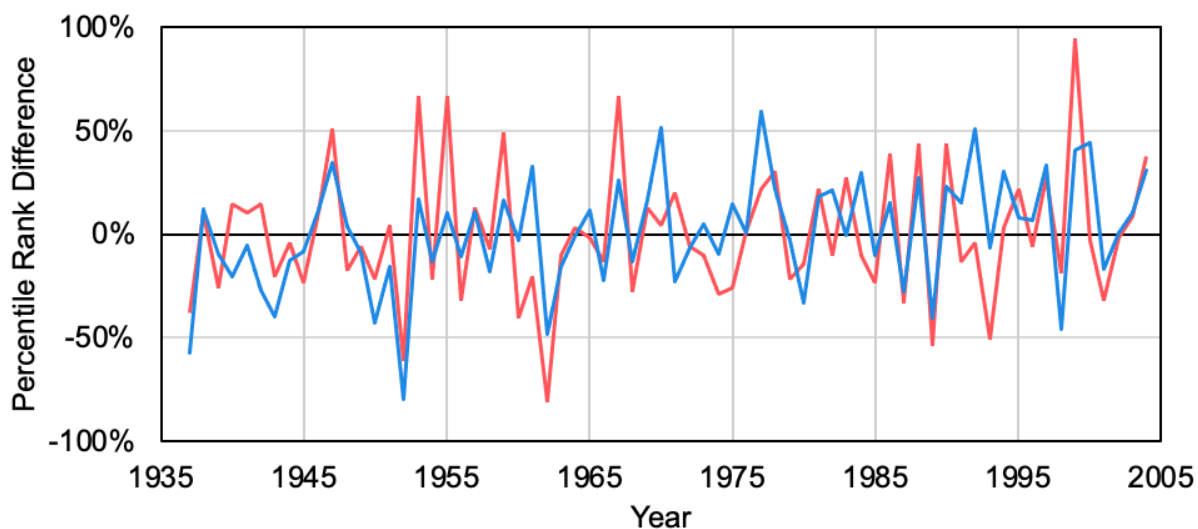
Figure C.S3. Comparison of the percentile rank difference between observed SWE and SPEI (red) and the percentile rank difference between reconstructed SWE and spring SPEI reconstruction (blue) over the common interval of 1937-2004. For both time series the SWE percentile rank was subtracted from the SPEI percentile rank to produce a percentile difference value. The spring SPEI reconstruction used in this figure is the reconstruction developed from residual chronologies.

C.11.S5   Supplemental Works Cited

Alfons, A. (2012). *cvTools: Cross-validation tools for regression models.* R Package Version 0.3, 2(5).

Bunn, A. G. (2008). A dendrochronology program library in R (dplR). *Dendrochronologia*, 26(2), 115–124. https://doi.org/10.1016/j.dendro.2008.01.002

Cook, E. R., & Kairiukstis, L. A. (2013). *Methods of dendrochronology: applications in the environmental sciences*. Springer Science & Business Media.

Cook, E. R., & Peters, K. (1997). Calculating unbiased tree-ring indices for the study of climatic and environmental change. *The Holocene*, 7(3), 361–370.

Meko, D. (1997). Dendroclimatic Reconstruction with Time Varying Predictor Subsets of Tree Indices. *Journal of Climate*, 10(4), 687–696. https://doi.org/10.1175/1520-0442(1997)010<0687:DRWTVP>2.0.CO;2

Tintor, W. L., & Woodhouse, C. A. (2021). The variable climate response of Rocky Mountain bristlecone pine (*Pinus aristata* Engelm.). *Dendrochronologia*, 68, 125846. https://doi.org/10.1016/j.dendro.2021.125846

Woodhouse, C. A., & Pederson, G. T. (2018). Investigating Runoff Efficiency in Upper Colorado River Streamflow Over Past Centuries. *Water Resources Research*, 54(1), 286–300. https://doi.org/10.1002/2017WR021663